

**Copyright**

**By**

**Joshua Stephen Black**

**2005**

**Design and Construction of Small-Scale Bridge Bents on Drilled  
Shaft Foundations**

by

**Joshua Stephen Black, B.S.**

**Thesis**

Presented to the Faculty of the Graduate School of

The University of Texas at Austin

in Partial Fulfillment

of the Requirements

for the Degree of

**Master of Science in Engineering**

**The University of Texas at Austin**

**December 2005**

**The Thesis Committee for Joshua S. Black certifies that this is the approved  
version of the following thesis:**

**Design and Construction of Small-Scale Bridge Bents on Drilled  
Shaft Foundations**

**Committee:**

---

**Sharon L. Wood**

---

**Ellen M. Rathje**

## **Dedication**

To Julie, my love, my life, my partner

To my Mother and Father, who always made me feel that  
I was special and could accomplish anything

## **Acknowledgements**

The research described in this thesis was sponsored by the National Science Foundation through grant CMS-0324326 to the University of Texas at Austin. The land used for the test site was provided by Capitol Aggregates, Inc., in Austin. Capital Aggregates designed concrete mixtures specifically for the test specimens and helped with issues related to security at the site. The drilling was graciously donated by McKinney Drilling Company, in Buda. Neal Howard helped us with practical issues prior to drilling and Ed Beers oversaw the drilling.

Many thanks go out to everyone at the Ferguson Laboratory for their help and support on this project. Many undergraduates worked long hours on the project including, Hong Loan Bui, Joel Santos-Shepherd, Royce Owens, Larua Wendling, and Kyle Steuck. Their hard work and cheerful attitudes were much appreciated.

To the graduate students who helped with the transportation of the shafts, concrete formwork, and concrete placement, I am particularly indebted since all took time from their own research to help me with mine. Many thanks to Matthew Bean, Michael Brown, Jun Ki Lee, Justin Brown, Fernando Torrealva, and Puneet Agarwal. In addition to helping out at the site, Mike Brown also helped me with just about every phase of the project, including instrumentation, test equipment, concrete construction methods, and writing. Sunjin Bae provided very valuable advice regarding some critical connection details. I am also very

grateful to Puneet Agarwal who took over testing for me when it was time to start writing.

The laboratory technicians at the Ferguson Laboratory were a constant source of help and expertise. Thanks to Dennis Phillip for his help with fabrication of various components and his desire to teach me about the process, to Eric Schell who wrote the software for the project and dealt with all the bugs and hardware defects with determined effort, to Mike Wason for his input and efforts during the fabrication of the electronic components, to Blake Stasney for every miscellaneous problem I encountered, and to Mike Bell for teaching me to weld.

I'm grateful to the FSEL staff including Hortensia Peoples, Barbara Howard, Regina Forward, and Michelle Santos for taking care of the business aspects of the project, and the administrative details of my graduate appointment and thesis submission.

Ensoft, Inc. provided a copy of the LPILE software for use on this project. I am grateful for technical support and much more. Jose Arrellaga helped me with analysis issues and documentation and Bill Isenhower was always ready with advice and insight regarding specimen design, construction methods, and soil analysis parameters.

Many aspects of the project were aided by the hard work and dedication of the NEES staff at the University of Texas Equipment Site: Cecil Hoffpauir, Farn-Yuh Menq, and Christopher Stanton. In addition to managing and running the NEES equipment, they were never afraid to get their hands dirty and always ended up helping out during various stages of construction.

This project involved a lot of close work with the Geotechnical Department at the University of Texas. Faculty members Kenneth H. Stokoe II, and Ellen M. Rathje provided valuable input in the design and construction of the specimens and were always present to help out during the construction process. I am also indebted to Asli Kurtulus who was the primary graduate student from the geotechnical department on the project. She put in many long hours and her meticulous research has provided valuable data for this thesis.

The advisory committee on this project is composed of Professors Sharon L. Wood and Ellen M. Rathje, both of whom were non-wavering in their commitment to good research and analytical writing. I'd like to thank Dr. Wood for her patience and help in finding solutions to the many problems, both technical and personal, which were encountered along the way. She helped me to think like an engineer and take pride in my work.

August 25, 2005

# **Design and Construction of Small-Scale Bridge Bents on Drilled Shaft Foundations**

Joshua Stephen Black, M.S.E.

The University of Texas at Austin, 2005

Supervisor: Sharon L. Wood

The response of structures with deep foundations subjected to dynamic loading is of key interest in areas of high seismicity and is not well understood. This lack of understanding has resulted in design practices which may be overly conservative or inadequate in describing complex structural systems. As part of an experimental program sponsored by the National Science Foundation, two quarter-scale bridge bents on drilled shaft foundations were constructed to investigate soil-foundation-structure interaction under dynamic loading. The bents represent supporting elements in typical highway bridge construction.



# Table of Contents

<b>CHAPTER 1 INTRODUCTION</b>	<b>1</b>
1.1 Overview .....	1
1.2 Experimental Program.....	3
1.2.1 Shaking Table Tests .....	3
1.2.2 Centrifuge Tests .....	5
1.2.3 Field Tests .....	7
1.2.4 Structural Component Tests .....	8
1.3 Research Objectives .....	9
1.4 Scope .....	10
1.5 Research Team .....	10
<b>CHAPTER 2 CONCEPTUAL DESIGN OF FIELD SPECIMENS</b>	<b>12</b>
2.1 Overview .....	12
2.2 Specimen Geometry .....	12
2.3 Loading Protocols .....	15
2.3.1 Passive Excitation .....	16
2.3.2 Active Excitation.....	18
2.3.3 Pull-over Tests.....	19
2.4 Test Site and Site Layout .....	22
2.5 Preliminary Soil Properties .....	26
2.6 Assumed Structural Material Properties .....	31

<b>CHAPTER 3 CALCULATED RESPONSE OF TEST SPECIMENS</b>	<b>33</b>
3.1 Overview .....	33
3.2 Notation and Terminology .....	34
3.3 Lateral Analysis of Drilled Shafts .....	36
3.3.1 Overview .....	36
3.3.2 Cross-Sectional Analysis of Reinforced Concrete Shafts .....	37
3.3.3 Lateral Response of Shaft .....	40
3.3.4 Calculated Response of Shafts .....	44
3.4 Modal Analyses .....	61
3.5 Beam Design .....	68
3.5.1 Overview .....	68
3.5.2 Design for Flexure .....	68
3.5.3 Design for Shear .....	69
3.5.4 Connection to Hydraulic Shaker .....	71
3.5.5 Connection for Pull-Over Tests .....	72
<b>CHAPTER 4 SPECIMEN CONSTRUCTION</b>	<b>74</b>
4.1 Introduction .....	74
4.2 Fabrication of Reinforcement Cages .....	74
4.3 Construction of Vertical Elements .....	79
4.3.1 Overview .....	79
4.3.2 Drilling .....	79
4.3.3 Placement of Reinforcement Cages .....	82
4.3.4 Formwork .....	82
4.3.5 Concrete Placement .....	88

4.4	Construction of Horizontal Elements .....	92
4.5	Measured Properties of Concrete .....	97
4.6	Measured Soil Properties .....	97
4.7	Weather Patterns .....	102
4.8	Summary .....	105
<b>CHAPTER 5 CALCULATED FREQUENCY RESPONSE OF AS-BUILT SPECIMENS</b>		<b>107</b>
5.1	Overview .....	107
5.2	Revised Soil Parameters .....	108
5.3	Revised Properties of Shafts and Columns .....	110
	5.3.1 Arrangement of Longitudinal Reinforcement .....	110
	5.3.2 Structural Material Properties .....	111
5.4	Modal Hammer Tests .....	112
5.5	Calculated Response of As-Built Specimens .....	114
5.6	Sensitivity Analyses .....	117
	5.6.1 Overview .....	117
	5.6.2 Range of Parameters Considered .....	118
	5.6.3 Results of Sensitivity Studies for Bent 1 .....	124
	5.6.4 Bounding the Measured Frequency Response of Bents .....	128
5.7	Summary .....	131
<b>CHAPTER 6 LATERAL CAPACITY OF AS-BUILT SPECIMENS</b>		<b>133</b>
6.1	Overview .....	133
6.2	Soil and Specimen Properties .....	134
	6.2.1 Shaft Diameter .....	134
	6.2.2 Concrete Material Properties .....	135

6.2.3 Soil Properties .....	135
6.3 Moment-Curvature Relationships .....	137
6.4 Lateral Response of the Specimens.....	139
6.4.1 Overview .....	139
6.4.2 Calculated Deflected Shapes and Moment Diagrams .....	142
6.4.3 Calculated Load-Deflection Response .....	149
6.5 Summary .....	152
<b>CHAPTER 7 CONCLUSION</b>	<b>153</b>
7.1 Overview .....	153
7.2 Conclusions .....	153
<b>APPENDIX A MATERIAL PROPERTIES</b>	<b>156</b>
A.1 Properties of Concrete .....	156
A.2 Properties of Reinforcing Steel .....	162
<b>APPENDIX B PROCEDURES USED TO INSTALL STRAIN GAGES</b>	<b>164</b>
B.1 Overview .....	164
B.2 Strain Gage Description .....	164
B.3 Surface Preparation .....	165
B.4 Strain Gage Application .....	166
B.5 Diagnostics .....	166
B.6 Protection and Waterproofing .....	166
<b>APPENDIX C IDENTIFICATION LABELS FOR STRAIN GAGES</b>	<b>168</b>
C.1 Overview .....	168

<b>APPENDIX D SHAKER CONNECTION DETAILS</b>	<b>177</b>
D.1 Overview .....	177
<b>APPENDIX E DESIGN OF THREADED RODS</b>	<b>182</b>
E.1 Design Calculations.....	182
<b>REFERENCES</b>	<b>184</b>
<b>VITA</b>	<b>186</b>

## List of Tables

<b>Table</b>		<b>Page</b>
1.1	Research team members from other universities .....	11
2.1	Soil classification and fines content from preliminary soils investigation .....	27
2.2	Corrected and uncorrected blow counts from preliminary soils investigation .....	29
2.3	Values of subgrade modulus, $k$ , recommended for sands .....	31
2.4	Summary of soil parameters used for preliminary design.....	31
2.5	Assumed structural material properties.....	32
3.1	Summary of input parameters for analysis of shafts .....	44
3.2	Calculated critical length of shafts .....	47
3.3	Summary of strain gage locations for Shafts 1E, 1W, 2N, and 2S .....	54
3.4	Summary of strain gage locations for Shafts C and D .....	57
3.5	Soil spring constants used for modal analyses .....	62
3.6	Calculated natural frequencies of bents .....	65
3.7	Weight of hydraulic shaker and connection assembly .....	72
4.1	Measured concrete material properties .....	97
4.2	Summary of soil index properties .....	99
4.3	Soil classification and fines content .....	99
4.4	Results from standard penetration tests.....	100
4.5	Summary of weather data in Austin, TX.....	103

<b>Table</b>	<b>Page</b>
5.1 Soil parameters used to analyze the as-built specimens.....	108
5.2 Measured natural frequencies of specimens during modal hammer tests .....	114
5.3 Soil spring constants used for modal analyses of as-built specimens .....	115
5.4 Calculated frequencies of as-built specimens .....	117
5.5 Soil spring constants used in sensitivity studies to evaluate influence of subgrade modulus .....	119
5.6 Soil spring constants used in sensitivity studies to evaluate influence of vertical distribution of soil stiffness .....	123
5.7 Sensitivity of calculated natural frequencies for Bent 1 to modulus of elasticity of concrete .....	124
5.8 Sensitivity of calculated natural frequencies for Bent 1 to subgrade modulus.....	125
5.9 Sensitivity of calculated natural frequencies for Bent 1 to diameter of shaft.....	126
5.10 Sensitivity of calculated natural frequencies for Bent 1 to vertical distribution of soil stiffness .....	127
5.11 Combinations of parameters used to bound the measured natural frequencies for modes 1 and 2 for Bent 1 and mode 1 for Bent 2.....	129
5.12 Measured natural frequencies of specimens during ground excitation tests with T-Rex .....	131
6.1 Soil and specimen properties used for as-built lateral analysis.....	135
6.2 Calculated limiting moments in columns and shafts.....	138
6.3 Calculated response of individual shafts corresponding to cracking of shaft .....	142

<b>Table</b>	<b>Page</b>
6.4 Calculated response of individual shafts corresponding to capacity of bent .....	145
6.5 Lateral Capacity of Bents .....	149
A.1 Measured compressive strength of concrete .....	157
A.2 Measured load and displacement data for three concrete cylinders .....	158
A.3 Values of stress and strain used to determine modulus of elasticity of concrete.....	159
A.4 Measured dynamic modulus of concrete cylinders .....	161
A.5 Measured properties of longitudinal reinforcement.....	163
B.1 Strain gage specifications.....	165
C.1 Identification labels for strain gages in Bent 1.....	170
C.2 Identification labels for strain gages in Bent 2.....	173
C.3 Identification labels for strain gages in Shafts C and D.....	176
E.1 Calculations to check the shear capacity of threaded rods used for pull-over tests. ....	183



## List of Figures

<b>Figure</b>	<b>Page</b>
1.1 Prototype structure .....	1
1.2 Central role of computational models .....	3
1.3 Bents positioned on the shaking tables at the University of Nevada, Reno .....	4
1.4 Shaking table specimen with deck and masses in place.....	5
1.5 Aluminum specimens used in first series of centrifuge tests at the University of California, Davis .....	6
1.6 Shafts and soil in place during the construction of the first series of centrifuge tests .....	6
1.7 T-Rex was used to excite the ground surface in the vicinity of the field specimens.....	7
1.8 Shaker from Thumper was positioned at midspan of the beam .....	8
1.9 Structural component test specimens at Purdue University .....	9
2.1 Field test specimens .....	14
2.2 Shaft cross section used for design .....	15
2.3 Theoretical force output for T-Rex mobile ground shaker .....	17
2.4 Example test grid for testing with T-Rex .....	17
2.5 Active excitation of the bent specimens.....	18
2.6 Theoretical force output for the hydraulic shaker from Thumper.....	19
2.7 Pull-over mechanism and resulting moment diagram.....	21
2.8 Location of the Capitol Aggregates test site in Austin, TX .....	23

<b>Figure</b>	<b>Page</b>
2.9	Relative locations of preliminary and final test sites ..... 24
2.10	Site layout for field test specimens ..... 25
2.11	Corrected SPT blow count profile for preliminary site investigation ..... 28
2.12	Effective friction angle from SPT $N_{60}$ values ..... 30
3.1	Notation used to represent the response of a multi-column bent supported on drilled shaft foundations ..... 35
3.2	Idealized stress-strain relationship for concrete ..... 38
3.3	Calculated moment-curvature relationship for shaft ..... 39
3.4	Calculated relationship between flexural stiffness and moment ..... 39
3.5	Family of $p$ - $y$ curves for sand ..... 41
3.6	Calculated $p$ - $y$ curves for medium dense sand ..... 43
3.7	Calculated $p$ - $y$ curves for loose sand ..... 43
3.8	Influence of embedment length on behavior of shaft ..... 46
3.9	Representative relationship between shaft embedment depth and lateral deflection of column ..... 47
3.10	Sensitivity of critical length of shaft to soil density and rotational restraint at top of columns ..... 49
3.11	Variation in depth of maximum moment for zero rotational restraint at the top of the column ..... 50
3.12	Variation in depth of maximum moment full rotational restraint at the top of the column ..... 51
3.13	Layout of strain gages ..... 53
3.14	Moment envelope and strain gage stations for Shafts 1E, 1W, 2N, and 2S ..... 55

<b>Figure</b>	<b>Page</b>
3.15 Moment envelope and strain gage stations for Shafts C and D .....	58
3.16 Locations of geophones in shafts .....	60
3.17 Mode shapes associated with fundamental modes of vibration .....	63
3.18 Calculated natural frequencies .....	66
3.19 Beam reinforcement details.....	70
3.20 Schematic view of connection between hydraulic shaker and concrete beam .....	72
3.21 Embedded rods for pullover tests.....	73
4.1 Reinforcement cages .....	76
4.2 Arrangement of reinforcing bars and vinyl tubes.....	77
4.3 Shaft instrumentation details.....	78
4.4 Drill rig.....	80
4.5 Partial caving of soil in holes for Bent 2.....	81
4.6 Crane used to lift reinforcing cage for Shaft 2N .....	83
4.7 Position of reinforcing cages in holes .....	84
4.8 Typical formwork for shaft at ground surface .....	86
4.9 Formwork for bents.....	87
4.10 Concrete placement methods .....	90
4.11 Columns prior to construction of bent caps .....	91
4.12 Completed single shafts specimens.....	92
4.13 Construction of bent caps .....	94
4.14 Completed test specimens .....	95

<b>Figure</b>	<b>Page</b>
4.15 Test site after construction of bent specimens .....	96
4.16 Location of boreholes used to determine soil properties.....	98
4.17 Corrected blow count profile.....	101
4.18 Weather data recorded at Austin–Bergstrom International Airport .....	104
5.1 Effective friction angle from SPT $N_{60}$ values.....	109
5.2 Column cross section used to analyze the as-built specimens .....	110
5.3 Shaft cross section used to analyze the as-built specimens.....	111
5.4 Modal hammer tests on Bent 2.....	113
5.5 Comparison of calculated and measured natural frequencies .....	116
5.6 Measured shear wave velocity profiles for test site .....	121
5.7 Variation of initial soil stiffness with depth .....	122
5.8 Calculated variation in natural frequencies with concrete modulus.....	125
5.9 Calculated variation in natural frequency with subgrade modulus .....	126
5.10 Calculated variation in natural frequency with diameter of shaft .....	127
5.11 Calculated variation in natural frequency with vertical distribution of soil stiffness .....	128
5.12 Combinations of parameters used to bound the measured natural frequencies for modes 1 and 2 for Bent 1 .....	129
5.13 Combinations of parameters used to bound the measured natural frequency for mode 1 for Bent 2 .....	130
6.1 Representative $p$ - $y$ curves for pull-over analyses.....	137
6.2 Calculated moment-curvature response of columns and shafts .....	138

<b>Figure</b>	<b>Page</b>
6.3 Calculated relationship between flexural stiffness and moment for columns and shafts.....	139
6.4 Possible mechanisms for specimen pullover tests.....	141
6.5 Calculated deflections corresponding to cracking of shafts.....	143
6.6 Moment distributions corresponding to cracking of shafts.....	144
6.7 Calculated deflections corresponding to capacity of bent.....	147
6.8 Moment distributions corresponding to capacity of bent.....	148
6.9 Calculated load-deflection curves for Bent 1 .....	150
6.10 Calculated load-deflection curves for Bent 2.....	151
A.1 Representative stress-strain curve for concrete cylinder.....	160
A.2 Representative stress-strain curve for steel reinforcement.....	162
D.1 Dimensions of embedded plate .....	178
D.2 Dimensions of adapter plate .....	178
D.3 Shaker oriented along transverse axis of bridge.....	179
D.4 Shaker oriented along longitudinal axis of bridge .....	180
D.5 Shaker oriented 45° from transverse axis of bridge .....	181

# CHAPTER 1

## Introduction

### 1.1 OVERVIEW

The design and construction of two quarter-scale, reinforced concrete bridge bents are described in this thesis. These specimens were constructed at a field site in Austin, TX on drilled shaft foundations. The activities related to these bents are part of a coordinated research project to study soil-foundation-structure interaction. The research team includes structural and geotechnical engineers at eight universities and three NEES Equipment Sites were used in the experimental phases of the project.

The prototype structure selected for investigation in this project is a continuous, reinforced concrete bridge with drilled shaft foundations (Figure 1.1). This type of structure is common in regions of high and moderate seismicity throughout the US. Although the seismic response of ductile reinforced concrete structural elements is well understood, the extent to which nonlinear behavior of the soil and foundation influences the performance of the complete system is not well defined.

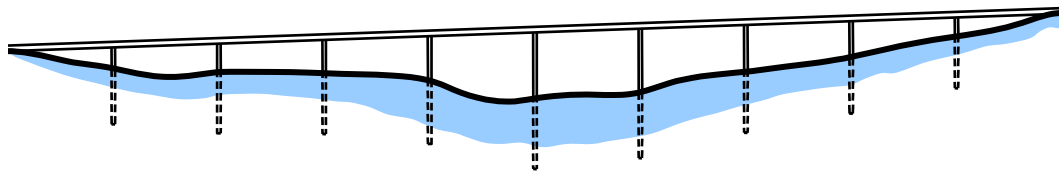


*Figure 1.1 Prototype structure*

Due to the size and complexity of the prototype system, it is impossible to test a single physical model and reproduce all key aspects of the system performance. Therefore, four complementary experimental programs were

developed to investigate the response of critical components: centrifuge tests were selected to evaluate the nonlinear response of the soil-foundation system, field tests were selected to evaluate the linear response of the soil, foundation, and structure in situ, shaking table tests were selected to evaluate the nonlinear structural response, and structural tests were selected to evaluate the sensitivity of the structural response to size effects and modes of failure expected in older structures.

Computational simulations play a central role in the project (Figure 1.2). The computational models will be used to interpret the response of the individual test specimens, relate the specimen response to the performance of the prototype system, and understand the limitations of the boundary conditions inherent in each experiment. In addition, the simulations will be used to determine the complexity of the analytical model that is needed to capture key aspects of the system response.

The goals of the coordinated research project are: (1) to develop computational models that are capable of representing the seismic response of the complete soil-foundation-structure system, and (2) develop appropriate models for design of continuous concrete bridges considering the soil-foundation system.

Details of each of the experiments associated with this project are described in Section 1.2. The specific objectives and scope for the field testing portion of the project are described in Sections 1.3 and 1.4, respectively. The members of the research team are listed in Section 1.5.

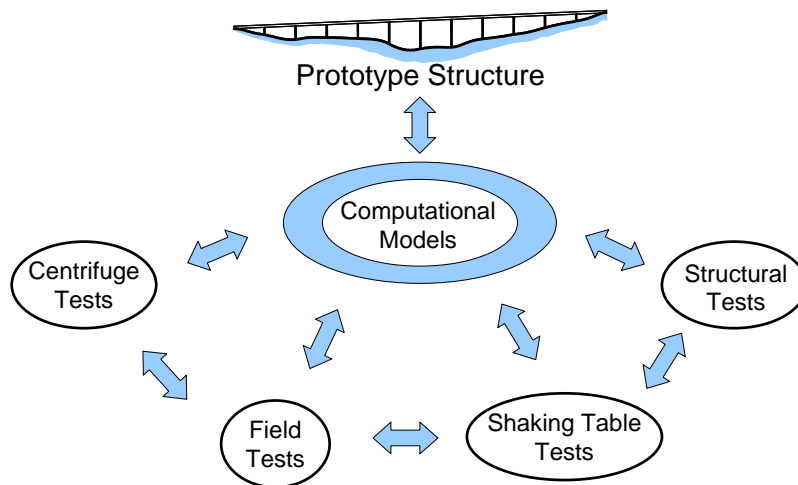


**Figure 1.2 Central role of computational models**

## **1.2 EXPERIMENTAL PROGRAM**

Scale models of key components of the prototype structure (Figure 1.1) will be tested at four universities. The methods of loading, boundary conditions, and scales of the specimens vary depending on the unique characteristics of each of the experimental facilities. Shaking table tests were conducted at one-quarter scale using the NEES facilities at the University of Nevada, Reno; the field tests were conducted at one-quarter scale using the mobile field shakers that comprise the NEES facilities at the University of Texas at Austin; the centrifuge tests were conducted at approximately one-fiftieth scale using the NEES facilities at the University of California, Davis; and the structural tests are being performed at one-quarter and one-half scale at Purdue University. The characteristics of the specimens for each phase of the experimental program are described briefly below.

### **1.2.1 Shaking Table Tests**

Shaking table tests were performed to investigate the inelastic response of a two-span section of the prototype bridge. The effects of soil and foundation



flexibility were not considered explicitly in the experiment and the columns were fixed at their bases. To represent variations in ground surface elevation, the three bents have column heights of five, six, and eight feet (Figure 1.3). All reinforced concrete columns were circular in cross section with a diameter of 12 in.



***Figure 1.3 Bents positioned on the shaking tables at the University of Nevada, Reno***

The deck was post-tensioned to the individual bents and additional masses were positioned on the deck before the specimen was tested (Figure 1.4). The two-span assembly was tested in January and February 2005. During low amplitude tests, incoherent, bidirectional ground motion was used to excite the specimen. Coherent ground motion in the transverse direction of the bridge was used during the larger amplitude tests.



*Figure 1.4 Shaking table specimen with deck and masses in place*

### **1.2.2 Centrifuge Tests**

The centrifuge tests at the University of California, Davis featured 1/52-scale tests of individual shafts, full bents, and a complete bridge. Aluminum tubes were used to model the shafts. The diameter of the tubes was approximately 1 in. Aluminum blocks were used to represent a rigid bent cap and provide additional mass for the specimens. The specimens used in the first of three test series are shown in Figure 1.5.

The centrifuge soil was dry Nevada sand, placed at a relative density of 80% in a flexible shear beam model container. A V-shaped groove was constructed along the soil surface such that bents with different height columns could be tested (Figure 1.6). Stiff plates were used to model the bridge deck. Ground motions were applied at the base of the soil container in the transverse direction of the bridge.

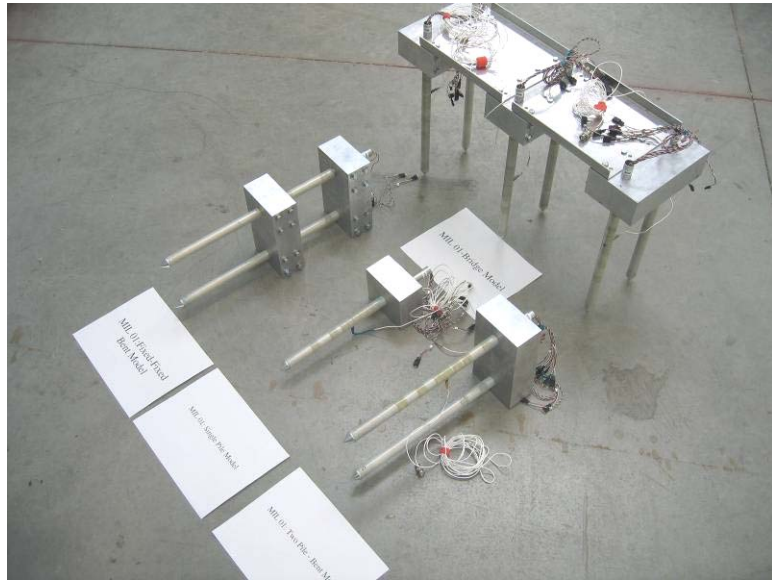


*Figure 1.5 Aluminum specimens used in first series of centrifuge tests at the University of California, Davis*

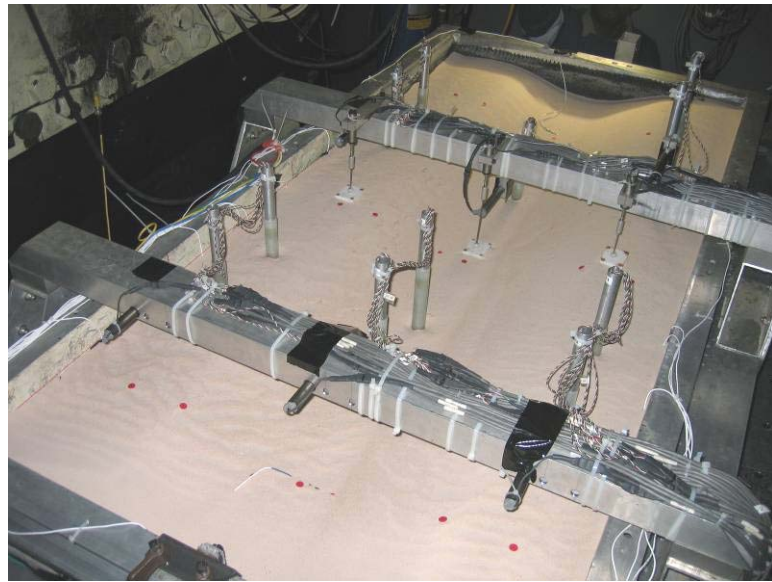


*Figure 1.6 Shafts and soil in place during the construction of the first series of centrifuge tests*

The first series of centrifuge tests were completed in January 2005 and the second series was completed in April 2005. A third series is planned for late 2005 or early 2006.

### 1.2.3 Field Tests

The field tests were designed to provide a means of understanding the linear response for the complete soil-foundation-structure system. Specimen scale and shaft cross-sectional properties are comparable to those from the tallest and shortest bents tested on the shaking tables. However, additional mass was not attached to the specimens. The bents were supported on drilled shaft foundations.



*Figure 1.7 T-Rex was used to excite the ground surface in the vicinity of the field specimens*

The NEES mobile shaker, T-Rex, was used to excite the specimens indirectly by shaking the surrounding soil (Figure 1.7). The hydraulic shaker from another NEES shaker, Thumper, was attached to the bent at midspan and excited the specimens directly (Figure 1.8). The specimens were tested

dynamically in June and July 2005, although the interpretation of the measured response is beyond the scope of this thesis.



*Figure 1.8 Shaker from Thumper was positioned at midspan of the beam*

#### **1.2.4 Structural Component Tests**

The structural component tests will be conducted at Purdue University. Their purpose is to compliment the other tests and provide some information on size effects as well as the effect of varying transverse reinforcement. Three, half-scale, single shaft specimens and two, quarter-scale bent specimens (Figure 1.9) will be tested using static loads. Testing is scheduled to begin in August 2005.



*Figure 1.9 Structural component test specimens at Purdue University*

### **1.3 RESEARCH OBJECTIVES**

During the design of typical highway bridges, the flexibility of the drilled shaft foundations is often approximated by increasing the clear height of the columns. The column is assumed to be fixed at the depth at which the maximum moment occurs in the shaft. As a further simplification, the depth of the maximum moment is assumed to be two to three shaft diameters below the ground surface for drilled shafts. This approach was taken in the design of the shaking table tests at the University of Nevada, Reno. Therefore, the clear heights of the columns in the tallest and shortest bents in the shaking table specimen are 24 in. longer than the column heights in the field specimens.

The objectives of the field testing portion of this research project are to: (1) understand the dynamic response of the complete soil-foundation-structure system, (2) evaluate if simple design approaches should be used to represent the flexibility of drilled shaft foundations, and (3) monitor the movement of the

location of maximum moment in the shaft as the intensity of the applied loading increases.

#### **1.4 SCOPE**

The design and construction of the field specimens are presented in this thesis. Chapter 2 presents the conceptual design of the specimens, describes the field site, and summarizes the proposed loading protocols. Chapter 3 contains the calculated response of the specimens using common design methods and software. The analysis relies on approximate soil and material properties and model geometry is based on the conceptual design in Chapter 2. The layout of the shaft instrumentation is then selected based on the results of the analyses. The construction of the specimens is described in Chapter 4. Changes in cross-sectional, soil, and material properties are considered in Chapter 5 and the impact of these changes on the expected frequency response of the specimens is evaluated. Frequency data obtained during hammer tests of the bent specimens are also presented in Chapter 5 and the models are calibrated to bound the measured response. Chapter 6 contains the expected response for the static pull-over tests with revised parameters. Conclusions are presented in Chapter 7. The majority of the experimental data associated with the field test research objectives will be reported by subsequent researchers at the University of Texas at Austin.

#### **1.5 RESEARCH TEAM**

The research team associated with this project is large and many individuals contributed valuable comments during the design and construction phase of the field tests. The name and primary responsibility of each researcher outside the University of Texas are listed in Table 1.1.

**Table 1.1 Research team members from other universities**

<b>University</b>	<b>Researcher</b>	<b>Primary Responsibility</b>
University of California, Berkeley	Matthew Dryden Gregory Fenves	Computational models of prototype structure
University of California, Davis	Boris Jeremic	Computational models of soil-foundation systems
	M. Ilankatharan Bruce Kutter Daniel Wilson	Centrifuge tests
University of Kansas	Will Kritikos Adolfo Matamoros	Data Models
University of Nevada, Reno	Nathan Johnson M. Saiidi David Sanders	Shaking table tests
Purdue University	Akira Makido Julio Ramirez	Structural tests
San Jose State University	Thalia Anagnos Kurt McMullin	Educational modules for SFSI interaction
University of Washington	Marc Eberhard Tyler Ranf	Computational models of shaking table specimen
	Pedro Arduino Steven Kramer Hyung-Suk Shin	Computational models of centrifuge specimens



## **CHAPTER 2**

### **Conceptual Design of Field Specimens**

#### **2.1 OVERVIEW**

The two field specimens were modeled on two bents from the shaking table specimen. The tallest and the shortest of the three bents tested on the shaking table were selected for testing in the field. The cross-sectional dimensions and reinforcement in the columns and shafts were nominally identical to those tested at the University of Nevada, Reno. An initial depth of embedment for the drilled shafts was assumed for the conceptual design. The specimens were later analyzed to verify that the depth of the drilled shaft was sufficient to ensure that the lateral capacity of the bents could be developed.

This chapter introduces the preliminary geometry of the test specimens. Target dimensions of the columns/shafts and overall specimen dimensions are presented in Section 2.2. The planned testing protocol for the two bents is described in Section 2.3. Section 2.4 provides a description of the field site in southeast Austin. The soil properties used to design the specimens are presented in Section 2.5 and Section 2.6 summarizes the assumed material properties for the concrete and reinforcement.

#### **2.2 SPECIMEN GEOMETRY**

The target dimensions of the two field specimens are shown in Figure 2.1. The columns in the shorter bent have a clear height of 3 ft and the columns in the taller bent have a clear height of 6 ft. As discussed in Chapter 1, the clear height of the columns is less for the field specimens than for the bents used to construct the shaking table specimen. This is because the plastic hinge will form at the base

of the column for the shaking table specimen, but is expected to form below grade for the field specimens.

All shafts are assumed to extend a distance of 12 ft below the ground surface. The preliminary design was based on the assumption that the diameter of the shaft was 12 in. both above and below grade. The actual diameter of the shafts is larger below the ground surface, as discussed in Chapter 4. The influence of the larger shaft on the calculated response of the specimens will be discussed in Chapter 5.

The dimensions of the shaft cross-section used during design are shown in Figure 2.2. Sixteen, #3 deformed reinforcing bars are distributed uniformly around the perimeter. The transverse reinforcement in the shaft consists of annealed W2.9 wire spirals with an outside diameter of 10.5 in. and a pitch of 1.25 in.

The bent cap was assumed to be rigid during the preliminary design. Based on this assumption, the pile head was assumed to be fixed for motion in the transverse direction of the bridge. In contrast, the pile head was assumed to be free for motion in the longitudinal direction of the bridge. The design of the bent cap is described in Chapter 3.

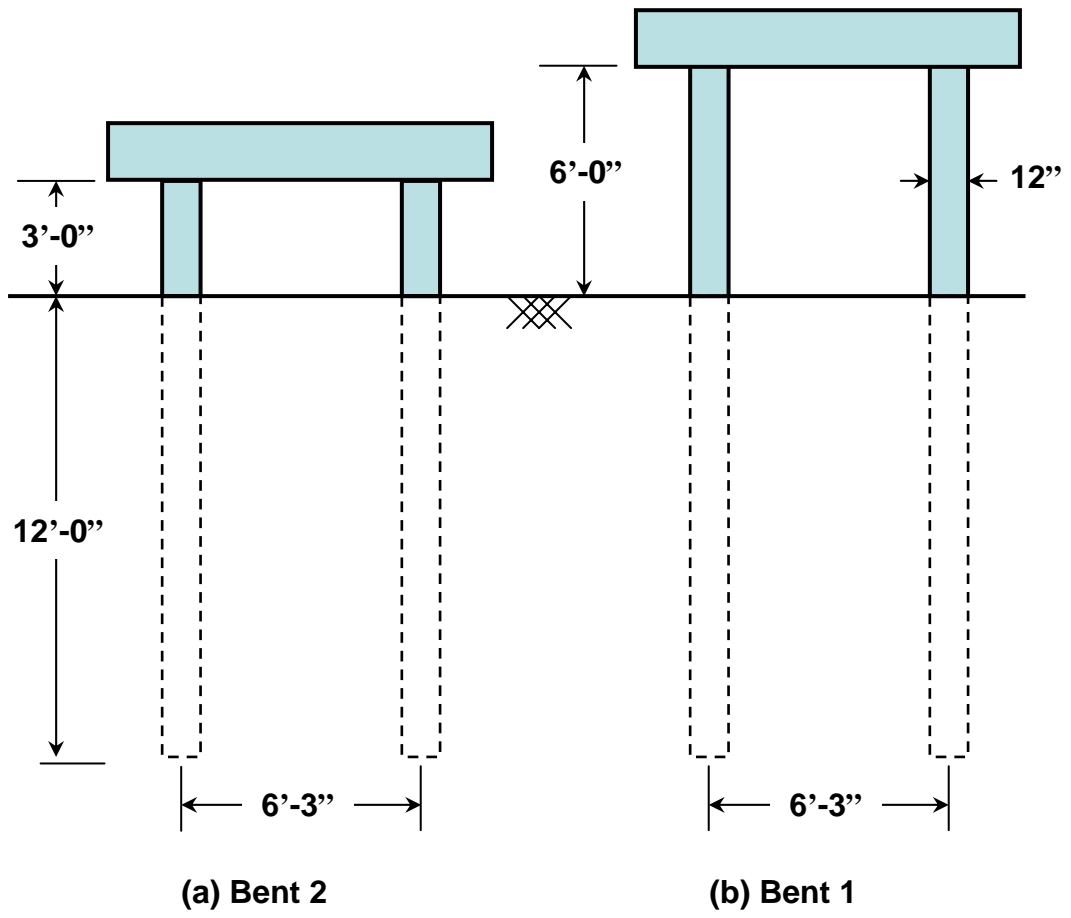


*Figure 2.1 Field test specimens*

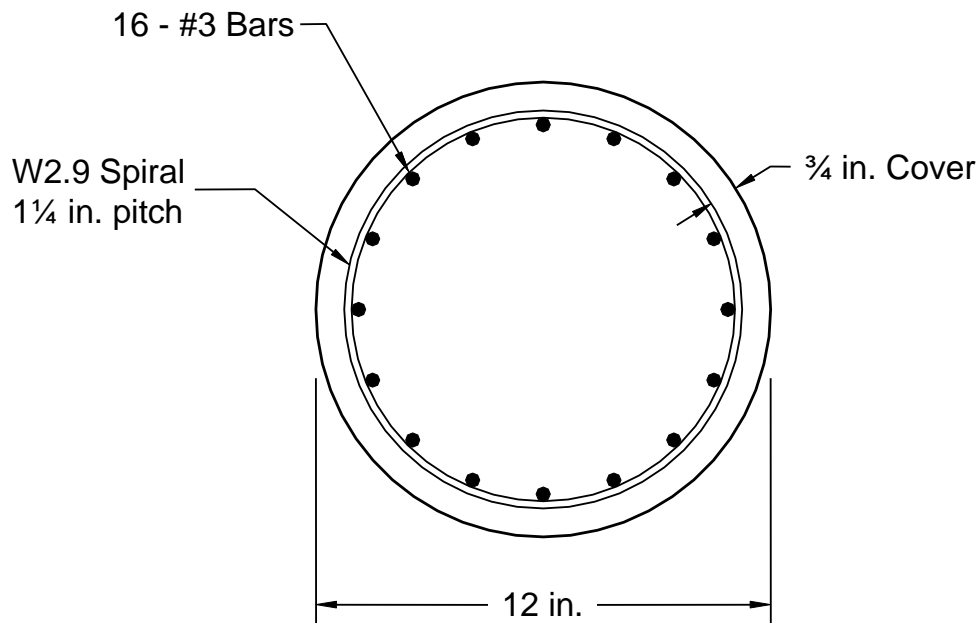


*Figure 2.2 Shaft cross section used for design*

### 2.3 LOADING PROTOCOLS

The two bents will be subjected to dynamic loading and then tested statically to failure. The NEES shaker, T-Rex, will be used to excite the specimens by shaking the ground. The shaker from the NEES shaker, Thumper, will be attached to the top of the bent caps and will excite the bents directly. The dynamic tests are expected to produce strains in the shafts that are well within the linear range of response. All of the dynamic tests will use sinusoidal input motions to determine the dynamic properties of the field specimens. Following the dynamic tests, static pull-over tests will be conducted to study the nonlinear behavior of the bents and determine their nominal lateral capacity in the transverse direction of the bridge. Each type of test is described in the following sections.

### **2.3.1 Passive Excitation**

T-Rex (Figure 1.5) will be used to excite the specimens indirectly by applying sinusoidal forcing functions to the surface of the ground. T-Rex is capable of shaking in three directions (vertical, horizontal in the transverse direction, and horizontal in the longitudinal direction) although force can only be applied in one direction at any given time. The theoretical force output for T-Rex is shown in Figure 2.3. For horizontal excitation, the maximum force output is 30 kip within a frequency range of 5 to 180 Hz. The maximum force output for vertical excitation is 60 kip within a frequency range of 12 to 180 Hz. Additional mass was not added to the bents in the field to ensure that the frequencies of the specimens were within the range of maximum force response.

T-Rex will be positioned around the specimens in a radial pattern, an example of which is shown in Figure 2.4. Experimental variables include T-Rex location, orientation of shaking, and frequency of input motion. Although the force level applied to the ground appears to be high, the actual force that can be transmitted to the specimen through surrounding soil is expected to be quite low. The specimens are not expected to crack under passive excitation.

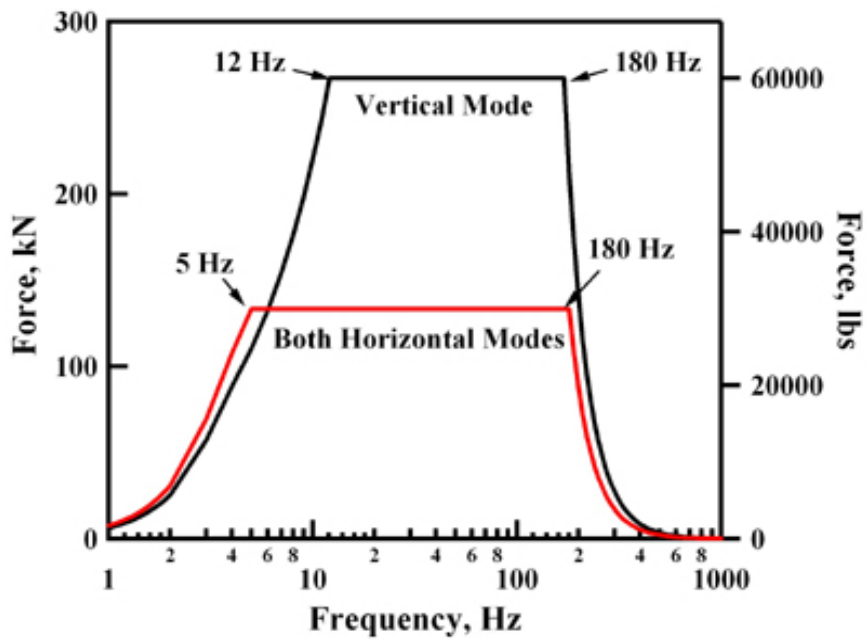


Figure 2.3 Theoretical force output for T-Rex mobile ground shaker (nees.utexas.edu, 2005)

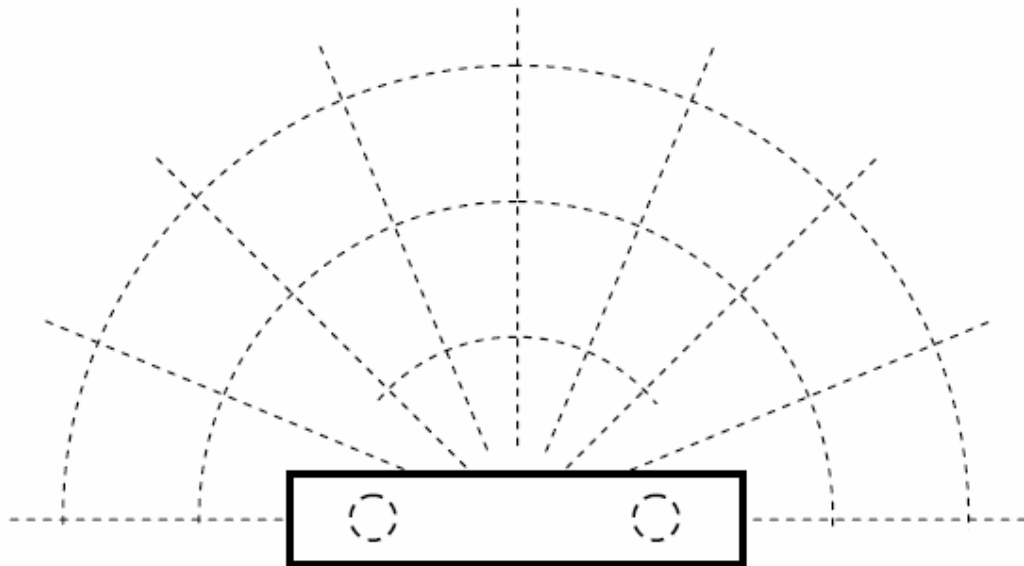
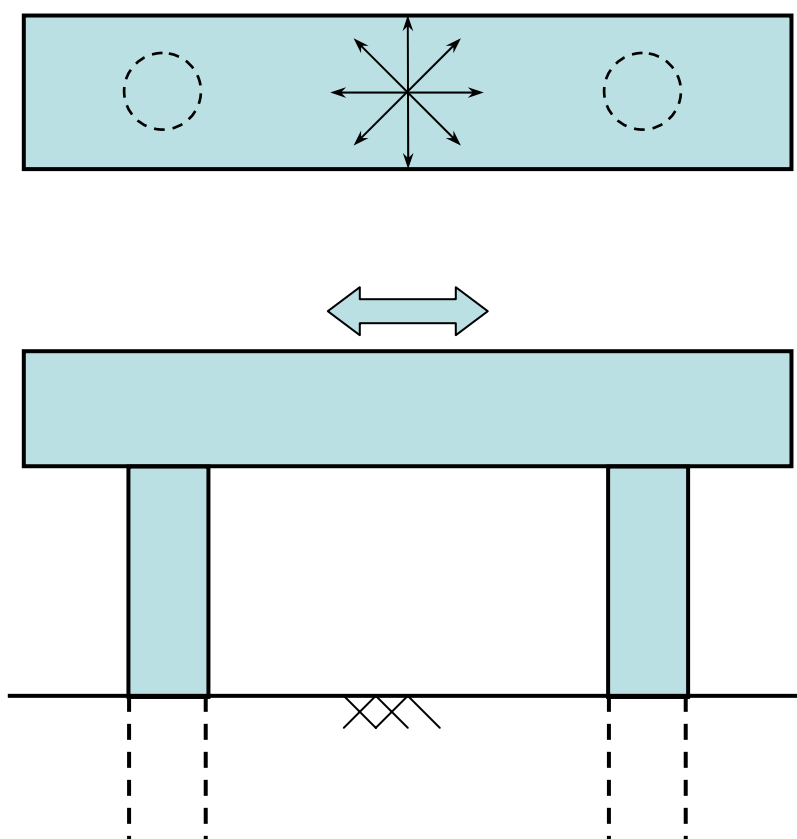


Figure 2.4 Example test grid for testing with T-Rex

### 2.3.2 Active Excitation

Following the tests with T-Rex, the bent specimens will be tested by attaching the hydraulic shaker from Thumper to the midspan of the bent cap. This shaker is capable of applying the sinusoidal forces in one direction, and will be rotated to excite the specimen in 45-degree increments (Figure 2.5).



*Figure 2.5 Active excitation of the bent specimens*

The theoretical force output for the Thumper shaker is shown in Figure 2.6. Although the forces are lower than those from T-Rex, the forces will be

transmitted directly to the structure and the levels of response are expected to be much greater. The active excitation is expected to cause cracking in the columns at the beam-column interface and possibly in the shafts below grade.

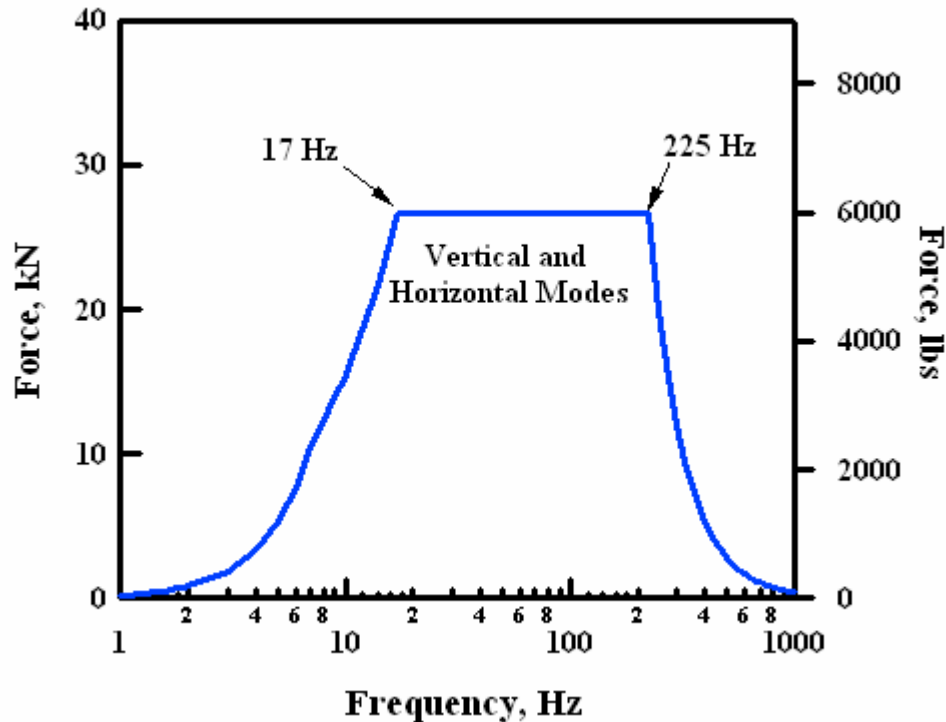


*Figure 2.6 Theoretical force output for the hydraulic shaker from Thumper (nees.utexas.edu, 2005)*

### 2.3.3 Pull-over Tests

After completing the dynamic tests, static pullover tests will be conducted by applying a lateral force in the plane of the bent at mid-height of the bent cap. This force will be sufficient to form flexural hinges in the shafts, which will cause a mechanism to develop in the bent (Figure 2.7). These pullover tests will establish the complete load deflection curve for each bent. The data will also be used to determine the moment diagram along the shafts when the bent reaches its



nominal lateral capacity. The length and depth of the flexural hinges below grade will also be reported.

The behavior of a drilled shaft under lateral loads depends on the boundary conditions at the top of the shaft. In the analyses described in Chapter 3, these boundary conditions are modeled as either allowing unlimited rotation at the shaft head (free head condition) or zero rotation at the shaft head (fixed head condition). To facilitate the comparison of the measured bent response with these idealized models, the flexural stiffness of the bent cap needs to be sufficient such that negligible rotations occur at the beam-column interface when lateral forces are applied to the specimens.

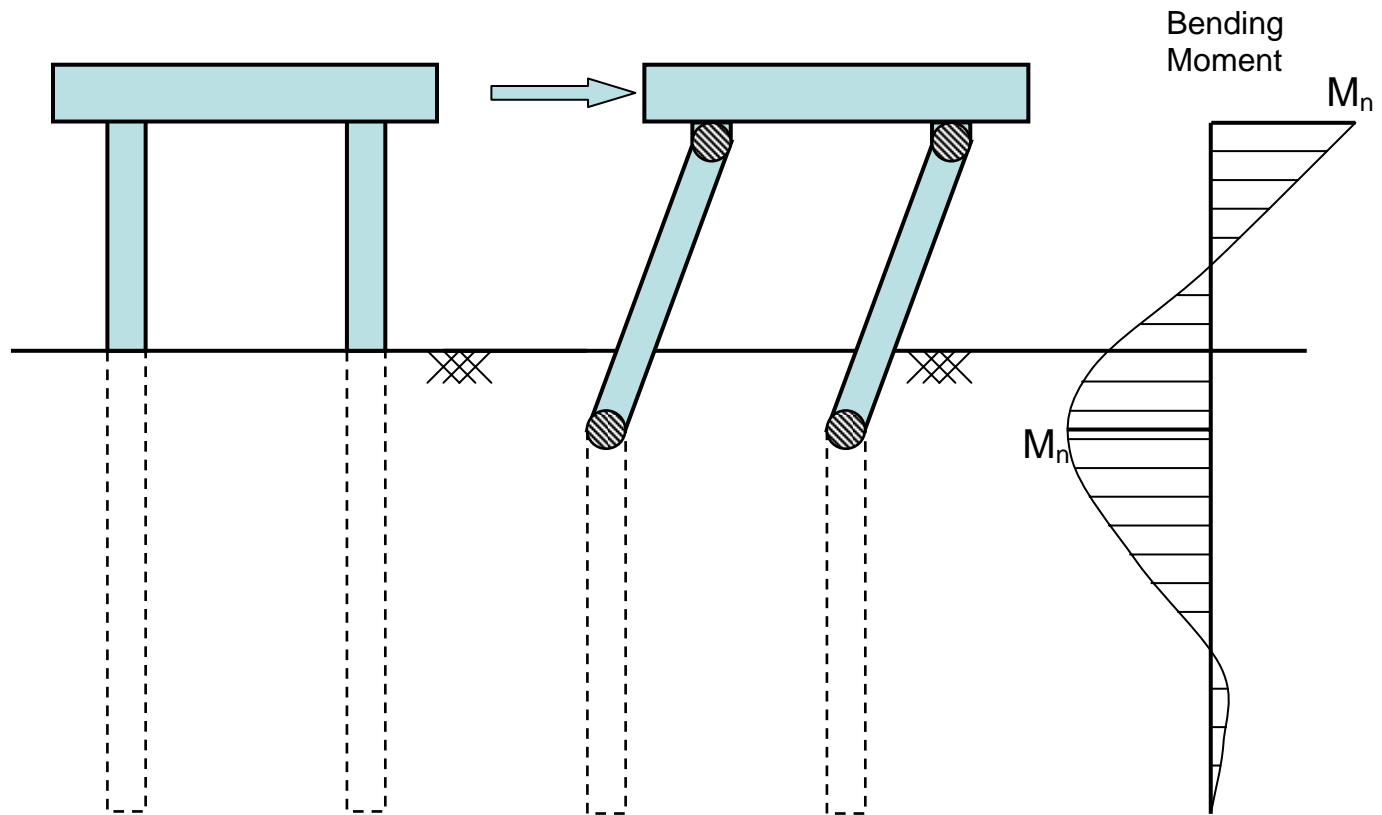


*Figure 2.7 Pull-over mechanism and resulting moment diagram*

## **2.4 TEST SITE AND SITE LAYOUT**

The test site is located in southeast Austin on private land leased and mined by Capitol Aggregates, Inc., a local aggregates and ready-mix concrete supplier. An area map is shown in Figure 2.8. A preliminary site was selected near the Colorado River, and geotechnical tests were performed to characterize the soil properties. These results are reported in Section 2.5.

The design of the shafts was based on these soil properties. This preliminary site was later abandoned because the soil at the surface was believed to be fill. The final site is located about 200 ft west of the preliminary site (Figure 2.9), and the soil at this location is believed to be less disturbed by heavy equipment. A soil characterization report for the final site was completed in March 2005 (Kurtulus, et al.). The effects of the new soil properties on the expected specimen response are discussed in detail in Chapter 5.

The test site dimensions and layout of the specimens are shown in Figure 2.10. The term “Bent 1” is used to identify the taller specimen (6-ft clear height) and the term “Bent 2” is used to identify the shorter specimen (3-ft clear height). Individual shaft designations are based on the bent number and location relative to the Project North direction, also shown in Figure 2.10.

Shafts A-D are isolated single shaft specimens that were built for additional geotechnical tests at the site. All four single shafts contain geophones and shafts C and D also contain strain gages. Instrumentation details for the single shafts can be found in Appendix D.

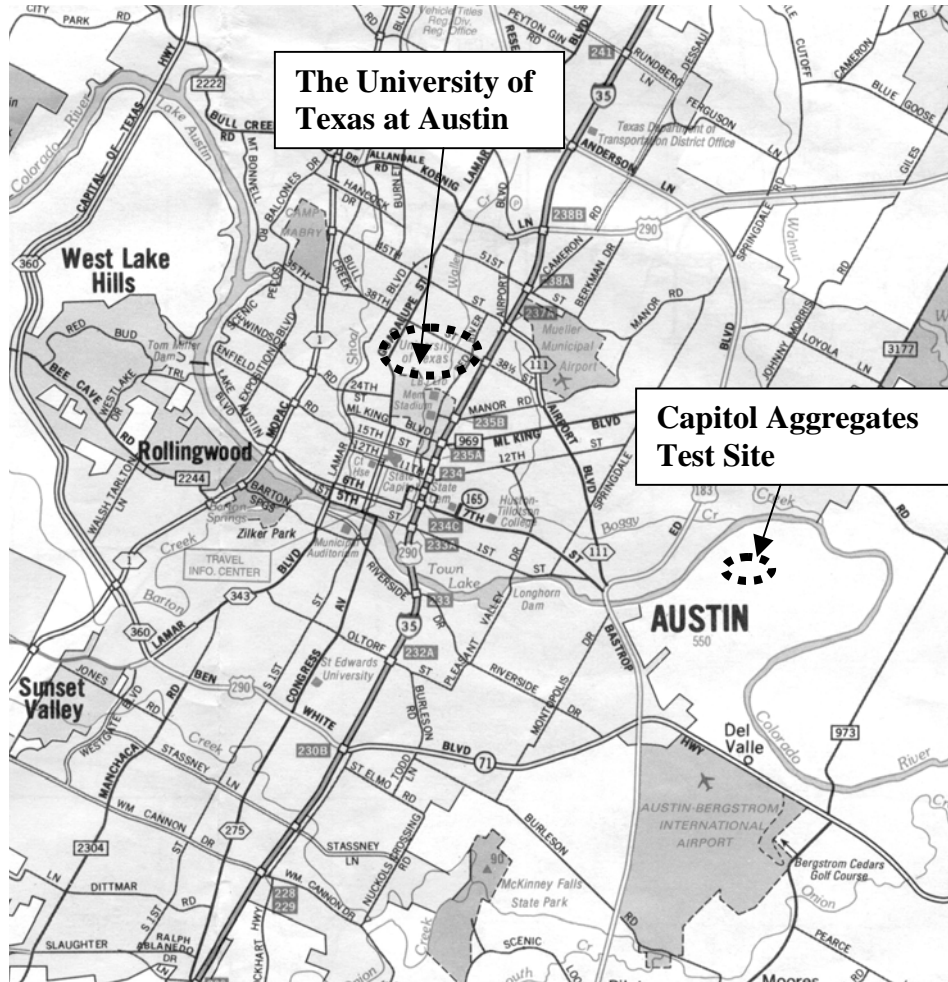


*Figure 2.8 Location of the Capitol Aggregates test site in Austin, TX (Kurtulus, et al., 2005)*

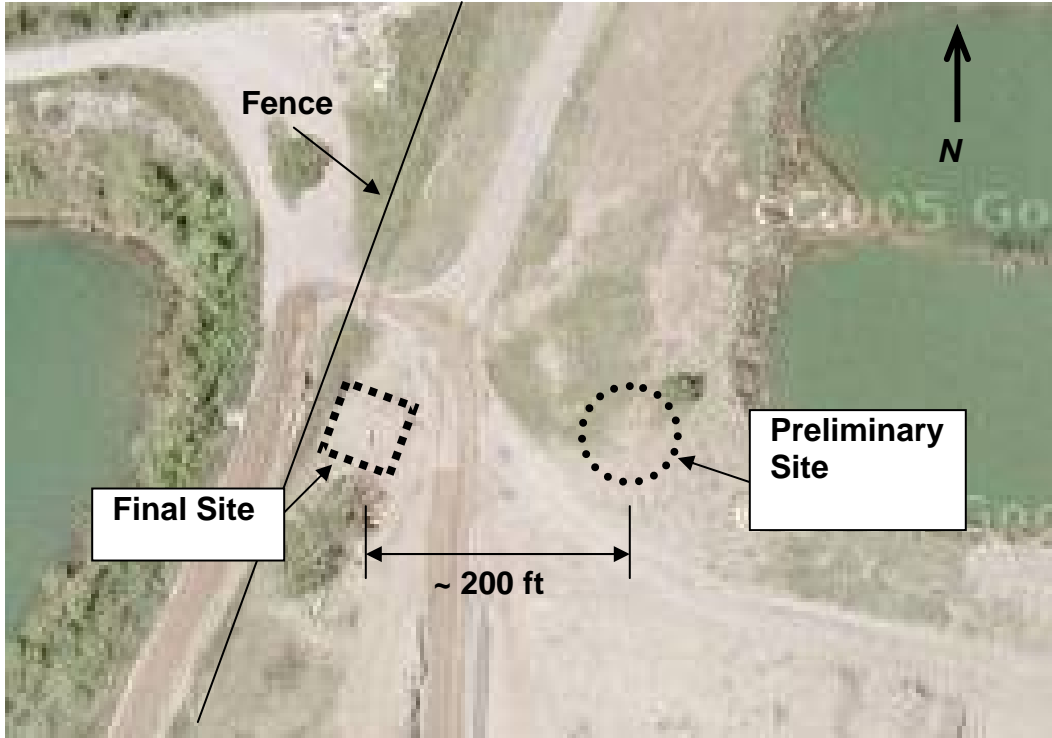


*Figure 2.9 Relative locations of preliminary and final test sites (Google.com, 2005)*



## 2.5 PRELIMINARY SOIL PROPERTIES

A preliminary site investigation was performed by Kurtulus in 2004. The soil profile from standard penetration tests (Figure 2.11) suggests the presence of a dense crust near the ground surface. The analyses discussed in Chapter 3 are based on the assumption that this crust would be removed prior to the construction of the specimens. Therefore, the SPT values for depths between 0 and 6 ft were not considered when choosing representative soil parameters for design of the specimens. Soil classification and fines content are shown in Table 2.1. The soil was classified as silty sand (SM). The silt was observed to be nonplastic, meaning that although the fines content was significant, little or no cohesive strength was observed. Therefore, the cohesion,  $c$ , was taken as zero. The soils investigation also indicated that the location of the water table was 21 ft below the ground surface.

The corrected and uncorrected blow counts from the standard penetration tests are shown in Table 2.2. The  $N_{60}$  values represent the standard penetration test blow counts corrected for equipment and energy. These values were correlated to friction angles,  $\phi$ , using Figure 2.1212 (DeMello, 1971). First, the overburden stress for each depth was estimated based on an assumed unit weight of 90 lb/ft<sup>3</sup>. These values were then paired with the corresponding values of  $N_{60}$ . Finally, the friction angle was estimated by linear interpolation between the diagonal lines. A friction angle of 30 degrees, corresponding to two of the data points, was taken as a conservative lower bound for the soil. A friction angle of 36 degrees was taken as the upper bound based on the remaining points. At the time the upper bound values for soil strength were chosen, the research team determined that it would be better to slightly underestimate the strength of the soil

for design purposes. Therefore, the first data point shown for Borehole 3 in Figure 2.12 was not used in the selection of the upper-bound friction angle.

Based on this range of assumed friction angles and assumed values of relative density, values of the subgrade modulus,  $k$ , were then selected from the suggested values shown in Table 2.3. The two values for loose and medium sand above the water table were chosen to represent a reasonable range of subgrade moduli for the analyses. To simplify the preliminary analyses, the soil profile was assumed to be either entirely loose soil or entirely medium soil. The soil parameters used in the preliminary analyses are summarized in Table 2.4.

**Table 2.1 Soil classification and fines content from preliminary soils investigation (Kurtulus, et al., 2004)**

<b>Borehole</b>	<b>Depth Range (ft)</b>	<b>Soil Classification</b>	<b>Fines Content (%)</b>
B1	0- 1.5	SC/SM	41
	2.5-4.0	Fine Grained	54
	5.0- 6.5	Fine Grained	77
	7.5- 9.0	SC/SM	18
	10.0- 11.5	Fine Grained	88
	12.5- 14.0	Fine Grained	81
	15.0-16.5	Fine Grained	78
	17.5- 19.0	SC/SM	21
	20.0-21.5	SC/SM	38
	22.5-24.0	SW-SC/SW-SM	6
B3	0- 1.5	SW-SC/ SW-SM	10
	5.0- 6.5	Fine Grained	59
	7.5- 9.0	SC/ SM	18
	10.0- 11.5	SC/ SM	35
	12.5- 14.0	Fine Grained	64
	15.0-16.5	Fine Grained	72
	17.5- 19.0	SC/ SM	34
	20.0-21.5	SP-SC/ SP-SM	6
	22.5-24.0	SC/ SM	40



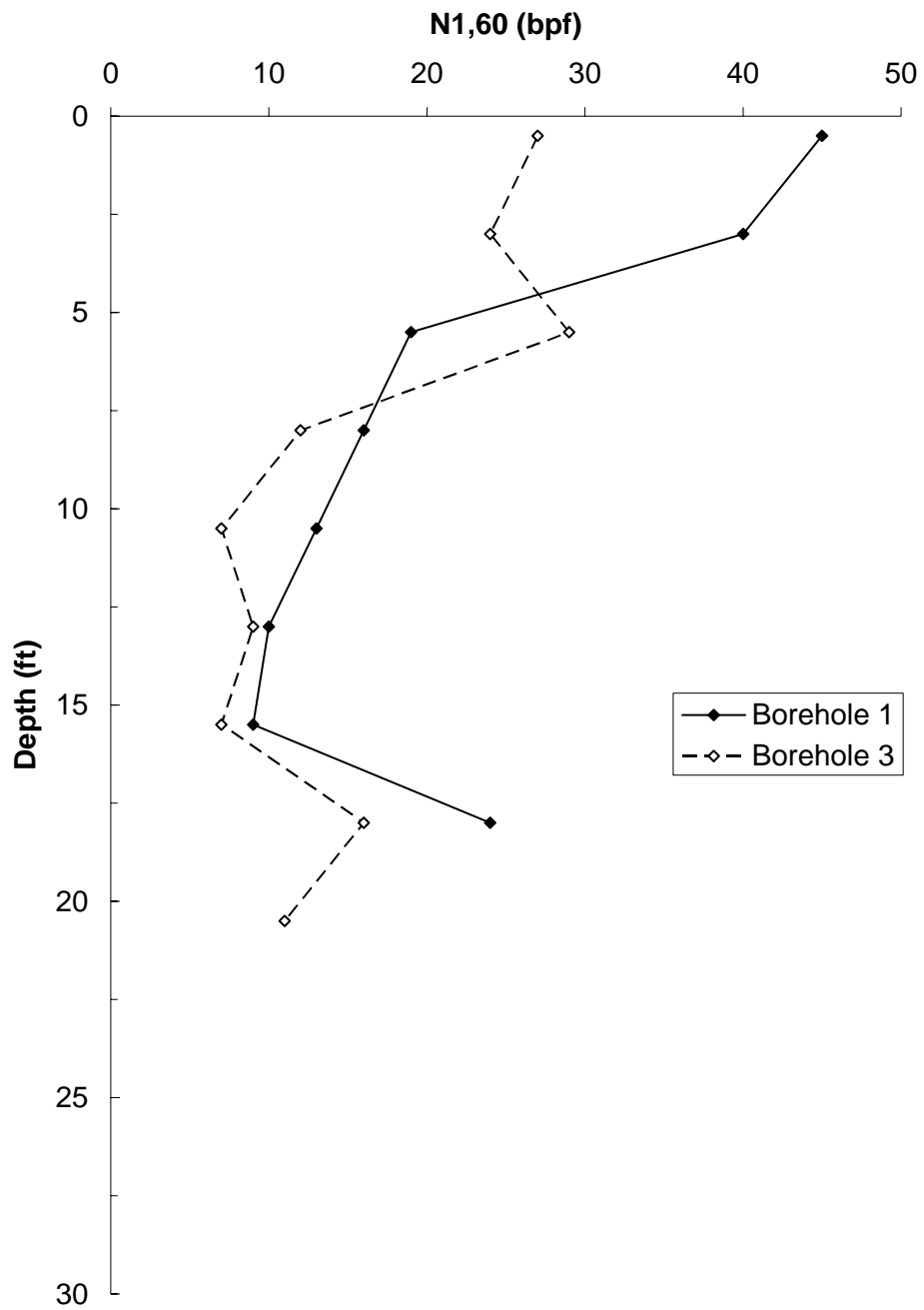


**Figure 2.11** Corrected SPT blow count profile for preliminary site investigation (Kurtulus, et al., 2004)

**Table 2.2 Corrected and uncorrected blow counts from preliminary soils investigation (Kurtulus, et al., 2004)**

<b>Borehole</b>	<b>Depth (ft)</b>	<b><math>N_{SPT}</math> (bpf)</b>	<b><math>N_{60}</math> (bpf)</b>	<b><math>N_{1,60}</math> (bpf)</b>
<b>B1</b>	0.5	35	26	45
	3	31	23	40
	5.5	15	11	19
	8	13	10	16
	10.5	11	9	13
	13	10	9	10
	15.5	9	8	9
	18	24	23	24
<b>B3</b>	0.5	21	16	27
	3	19	14	24
	5.5	23	17	29
	8	10	8	12
	10.5	6	5	7
	13	9	8	9
	15.5	7	6	7
	18	16	15	16
	20.5	11	10	11

Where:

$N_{SPT}$  = Uncorrected blow counts from a standard penetration test

$N_{60}$  = Blow counts corrected for equipment and energy

$N_{1,60}$  = Blow counts corrected for equipment, energy and overburden

bpf = Blow counts per foot depth

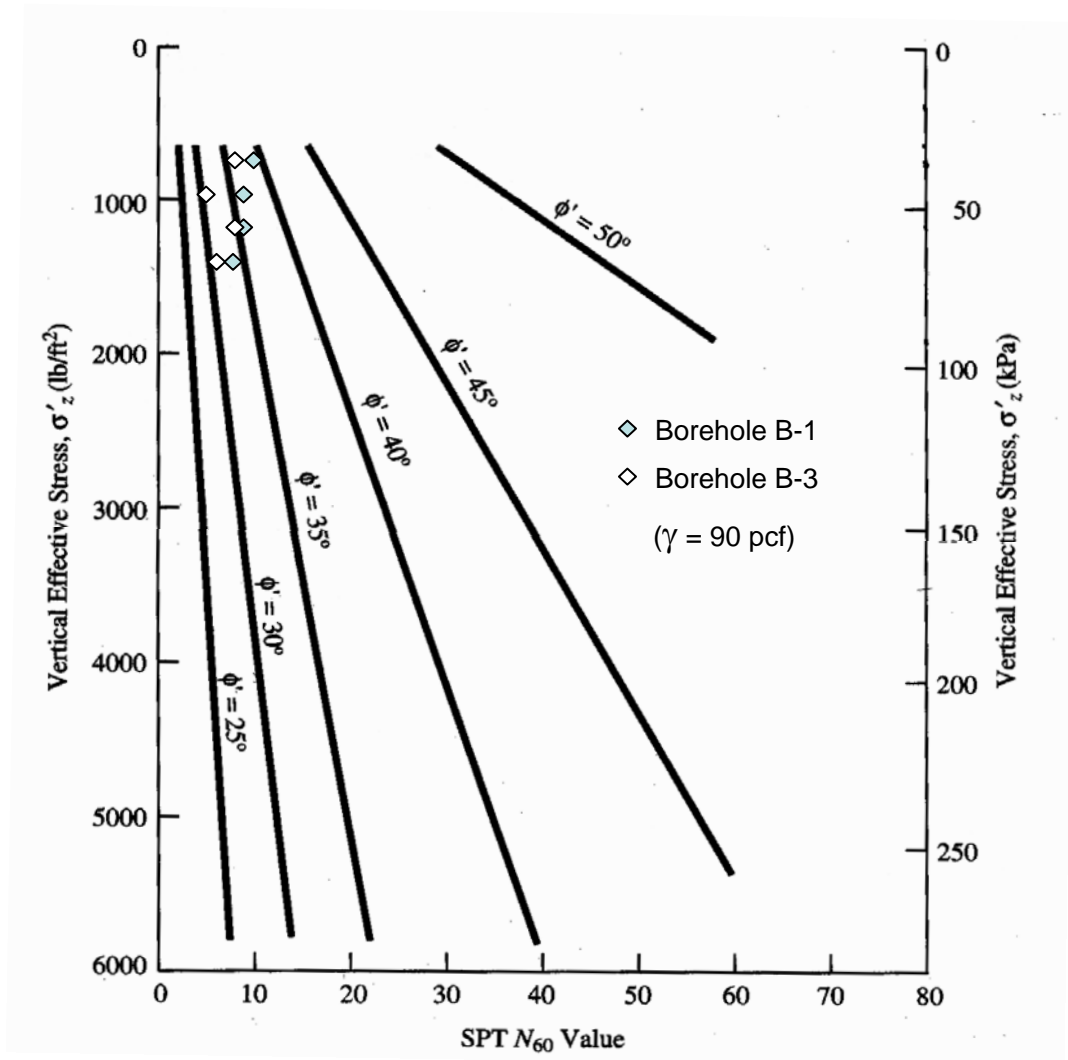


Figure 2.12 Effective friction angle from SPT  $N_{60}$  values (DeMello, 1971)

**Table 2.3** Values of subgrade modulus,  $k$ , recommended for sands (Reese, et al., 2004)

Relative Density	Loose	Medium	Dense
Submerged Sand	20 lb/in. <sup>3</sup>	60 lb/in. <sup>3</sup>	125 lb/in. <sup>3</sup>
Sand Above WT	25 lb/in. <sup>3</sup>	90 lb/in. <sup>3</sup>	225 lb/in. <sup>3</sup>

**Table 2.4** Summary of soil parameters used for preliminary design

Relative Density	Loose	Medium
Subgrade Modulus, $k$	25 lb/in. <sup>3</sup>	90 lb/in. <sup>3</sup>
Friction Angle, $\phi$	30°	36°
Unit Weight, $\gamma$	90 lb/ft <sup>3</sup>	90 lb/ft <sup>3</sup>
Cohesion, $c$	0	0
Soil Classification	SM—Silty Sand	SM—Silty Sand

## 2.6 ASSUMED STRUCTURAL MATERIAL PROPERTIES

Structural material properties used for the preliminary design of the test specimens are reported in Table 2.5. Measured properties of the concrete and concrete mixture proportions are given in Appendix A.

***Table 2.5 Assumed structural material properties***

Compressive Strength of Concrete, $f'_c$	4000 psi
Modulus of Elasticity for Concrete, $E_c$	3,600 ksi
Yield Stress of Reinforcing Steel, $f_y$	60 ksi
Modulus of Elasticity for Steel, $E_s$	29,000 ksi

## **CHAPTER 3**

### **Calculated Response of Test Specimens**

#### **3.1 OVERVIEW**

This chapter presents the results of the preliminary analyses of the test specimens. Specimen geometry, material properties, and loading protocols are based on the conceptual design presented in Chapter 2. Two commercial analysis programs were used to evaluate the response of the specimens:

- LPILE Plus 5.0 (Ensoft, Inc., 2004) was used to calculate the nonlinear response of the soil and shafts under lateral loads. The response of the soil was represented using a predefined, nonlinear model for sand (Reese, et al., 1974). LPILE also evaluates the moment-curvature response of the reinforced concrete shaft, so that the lateral response of the soil-foundation system may be limited by either the capacity of the soil or the flexural capacity of the shaft.
- SAP 2000 Nonlinear 8.2.7 (Computers and Structures, Inc., 2003) was used to estimate the natural frequencies of the bents. The soil was modeled using discrete, linear springs and the shafts were represented using elastic members.

The LPILE analyses were used to ensure that the depth of the shafts was sufficient to develop the flexural capacity of the bents under lateral loads in the transverse direction of the bridge and to calculate the variation of moment along the length of the shafts. The results of these analyses were used to select the instrumentation plan for the shafts. The LPILE analyses are discussed in Section 3.3.

The results of the SAP analyses were used to determine if the geotechnical shakers (T-Rex and Thumper) were sufficient to excite the test specimens. These analyses are summarized in Section 3.4. The design of the bent beams, including the connection to the hydraulic shaker and placement of the threaded rods for the pull-over tests, is described in Section 3.5.

### 3.2 NOTATION AND TERMINOLOGY

Before discussing the details of the analyses, it is helpful to define the notation and terminology that will be used throughout this thesis. The notation used to discuss the lateral response of a multi-column bent supported on drilled shafts is given in Figure 3.1 and defined below. Terms are similar to those used by Chai (2002).

- $L_a$  = distance from ground surface to point of zero moment in shaft.
- $L_c$  = distance from ground surface to top of column (bottom of bent cap).  $L_c$  is also called the clear height of the column.
- $L_d$  = distance from ground surface to bottom of drilled shaft.  $L_d$  is also called the depth of embedment of the shaft.
- $L_m$  = distance from ground surface to location of maximum moment in shaft;
- $L_t$  = distance from top of column to location of maximum moment in shaft.  $L_t = L_c + L_m$ .
- $V$  = inertial shear force induced during dynamic response of bent.

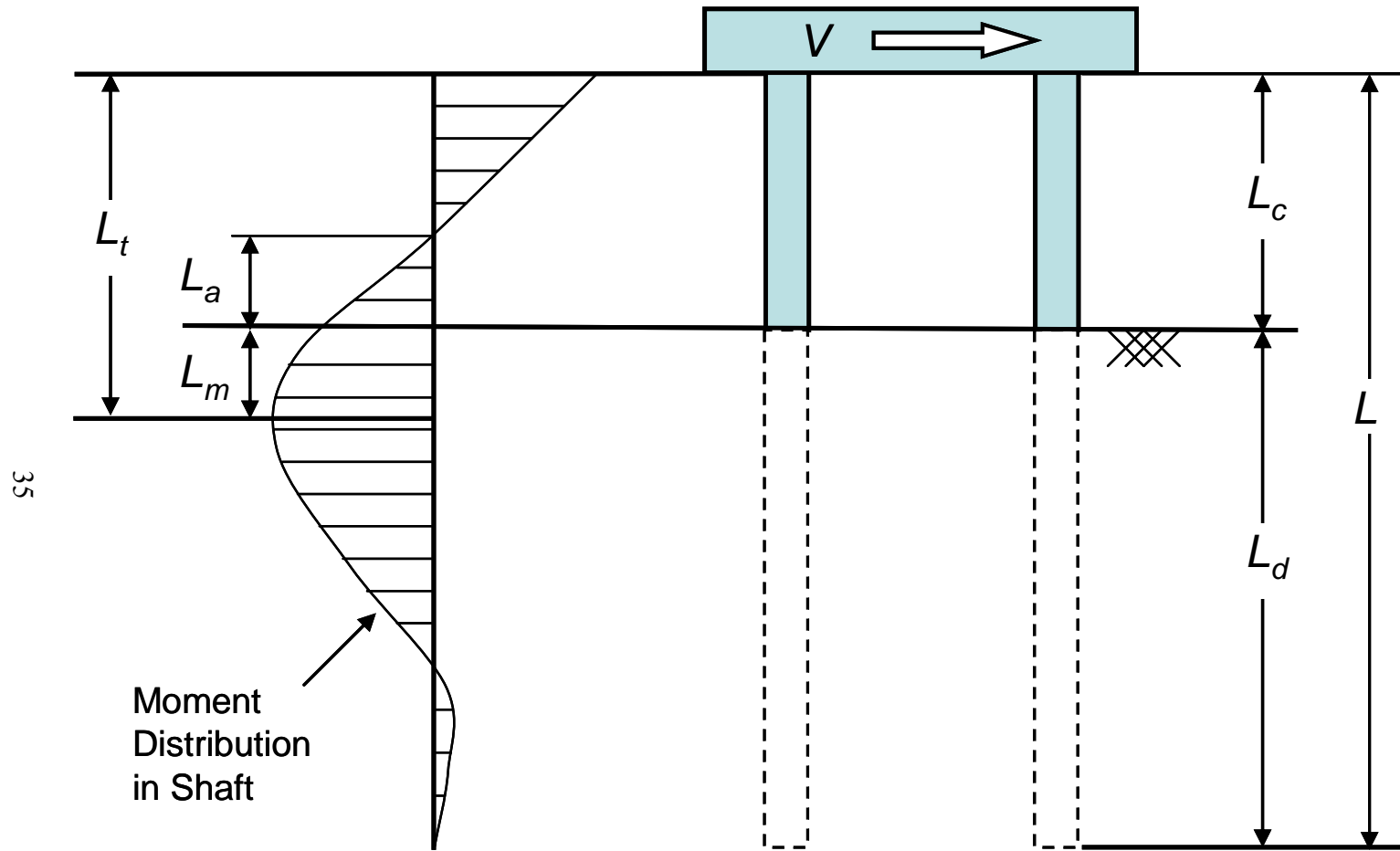


Figure 3.1 Notation used to represent the response of a multi-column bent supported on drilled shaft foundations



The term “shaft” refers to the below-grade portion of the vertical elements in the bents, while the term “column” refers to the above-grade portion of the vertical elements. When referring to the entire vertical element, the term “column-shaft” may also be used. The terms “bent cap,” “bent beam,” and “beam” are used interchangeably and all refer to the horizontal elements in the bents.

The boundary conditions assumed at the top of the columns have a significant influence on the calculated response of the specimens. Because the beam was assumed to be much stiffer and stronger than the columns, the top of the columns was assumed to be fixed against rotation when the transverse response of the bridge was considered. Translation of the top of the columns was not restrained. In contrast, the top of the columns was assumed to be free to rotate and translate when the longitudinal response of the bridge was considered.

### **3.3 LATERAL ANALYSIS OF DRILLED SHAFTS**

#### **3.3.1 Overview**

As discussed in Section 3.1, the commercial analysis program LPile (Ensoft, Inc., 2004) was used to analyze the response of the drilled shafts. Critical parameters in the analyses were the embedded depth of the shaft,  $L_d$ ; the clear height of the column,  $L_c$ ; the relative density of the soil; the boundary conditions at the top of the column; and the magnitude of the maximum moment along the shaft.

Two sets of soil properties were defined in Table 2.4 and those parameters were used in all analyses. All calculations were based on the shaft cross section shown in Figure 2.2 and the assumed structural material properties given in Table 2.5.

Three different column clear heights were used: 0 ft, 3 ft, and 6 ft. The clear height of 0 ft was selected to model shafts A through D, the clear height of 3 ft was selected to model shafts 2N and 2S in the shorter bent, and the clear height of 6 ft was selected to model shafts 1E and 1W in the taller bent.

Only a single shaft was considered in each analysis. Therefore, the variation of axial load in the shafts, which is expected when a multi-column bent is subjected to lateral loads in the transverse direction of the bridge, was not included in the analyses.

### **3.3.2 Cross-Sectional Analysis of Reinforced Concrete Shafts**

L-Pile was used to evaluate the moment-curvature response of the shafts. The calculations are based on a linear variation of strain over the depth of the cross section. The values of moment and curvature correspond to equilibrium within the cross section and the maximum compressive strain at the extreme fiber of the concrete was varied between 0 and 0.003.

The stress-strain relationships used for the concrete and steel are predefined in L-Pile. The curve for concrete is based on the relationship proposed by Hognestad (1951). A parabolic relationship between stress and strain is used to define the loading portion of the curve and a linear relationship is used to define the post-peak response (Figure 3.2). The maximum compressive stress that can be achieved in the shaft,  $f_c''$ , is equal to 85% of the specified compressive strength of the concrete,  $f_c'$ . The model does not consider the increase in concrete compressive strength observed in confined concrete.

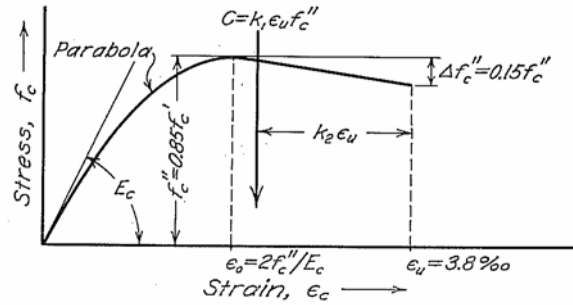


**Figure 3.2 Idealized stress-strain relationship for concrete (Hognestad, 1951)**

The tensile strength of the concrete was assumed to be equal to the modulus of rupture. The values of the modulus of rupture,  $f_r$ , and modulus of elasticity,  $E_c$ , are calculated using the relationships in ACI 318 (2005) for normal weight concrete:

$$f_r = 7.5\sqrt{f'_c} \quad (3.1)$$

$$E_c = 57,000\sqrt{f'_c} \quad (3.2)$$

where  $f'_c$ ,  $f_r$ , and  $E_c$  are expressed in units of psi.

The calculated moment curvature response is shown in Figure 3.3. The flexural capacity of the cross-section is approximately equal to 470 kip-in. The moment versus bending stiffness diagram is shown in Figure 3.4. Both diagrams indicate an instantaneous change in stiffness when the concrete cracks. This transition is expected to be more gradual in the actual shafts (Reese, et al., 2004).

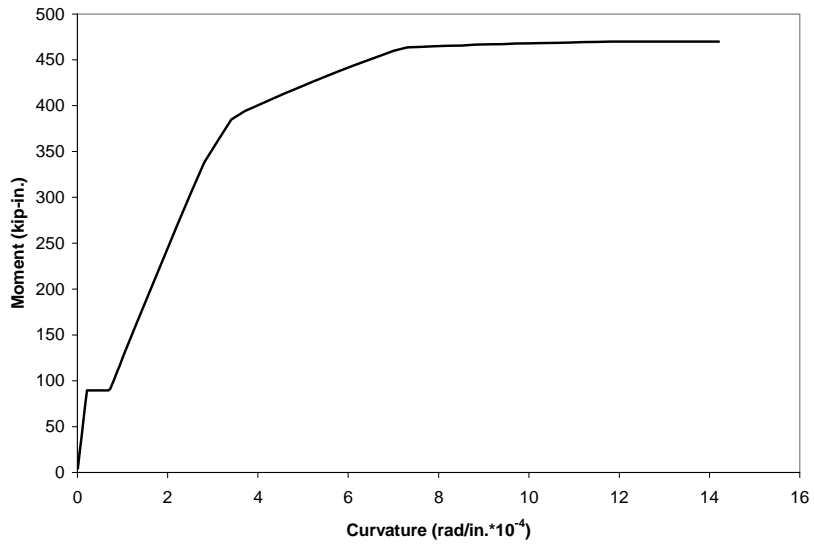


**Figure 3.3** *Calculated moment-curvature relationship for shaft*

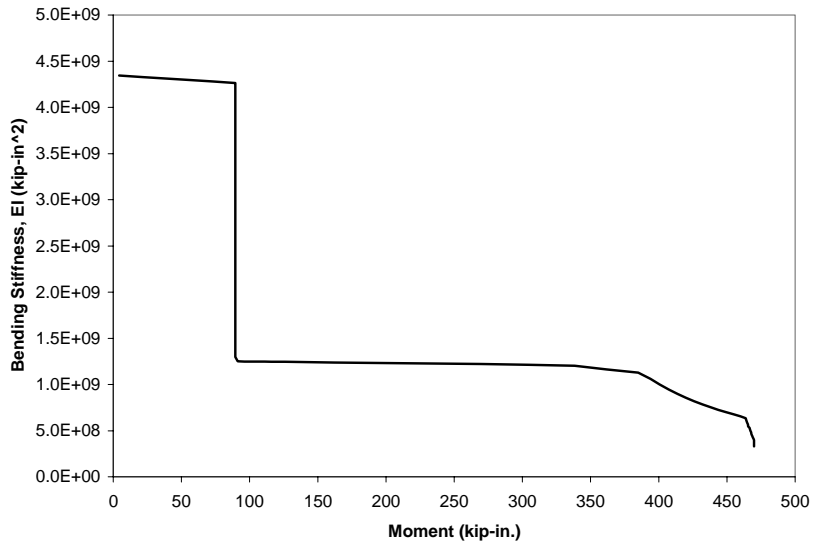


**Figure 3.4** *Calculated relationship between flexural stiffness and moment*

### 3.3.3 Lateral Response of Shaft

#### 3.3.3.1 Governing Differential Equation

L-Pile idealizes the shaft as a continuous beam supported on a Winkler foundation (Reese, et al., 2004). Therefore, the lateral resistance of the foundation is modeled using discrete springs. The governing differential equation for this system is given in Eq. 3.3.

$$EI(x) \frac{d^4 y}{dx^4} + Q(x) \frac{d^2 y}{dx^2} - p(x) + w(x) = 0 \quad (3.3)$$

where:

$EI(x)$  = bending stiffness of shaft, psi

$y(x)$  = lateral deflection of the shaft, in.

$Q(x)$  = axial load on shaft, lb

$p(x)$  = soil reaction per unit length of shaft, lb/in.

$w(x)$  = distributed lateral load along the above-grade portion of the shaft, lb/in.

Equation 3.3 is solved using a finite difference approach. Both the bending stiffness,  $EI(x)$ , and the soil reaction per unit length,  $p(x)$ , are represented using nonlinear relationships. The calculated relationship between moment and bending stiffness for the shafts is shown in Figure 3.4. The lateral response of the soil is described in the next section.

#### 3.3.3.2 Calculated Response of Soil

The soil is modeled as nonlinear springs in the lateral load analysis. The soil resistance versus deflection curve for one of these springs is called the  $p$ - $y$

curve. A family of these curves is needed to describe the variation of soil resistance with depth.

L-Pile includes ten predefined models for developing  $p$ - $y$  curves, two of which may be used to represent sand: the model introduced by Reese, et al. (1974) and the approach recommended by the American Petroleum Institute (1987).

The model developed by Reese, et al. (1974) was selected for the design of the specimens. Input parameters for this model include the subgrade modulus,  $k$ ; the angle of internal friction,  $\phi$ ; the unit weight of the soil,  $\gamma$ ; and the depth of the water table. The user must also designate if the lateral loads are applied statically or cyclically. A set of  $p$ - $y$  curves calculated using this model is shown in Figure 3.5. The parameter  $x$  is used in Figure 3.5 to define the depth below grade at which the  $p$ - $y$  curve is calculated.

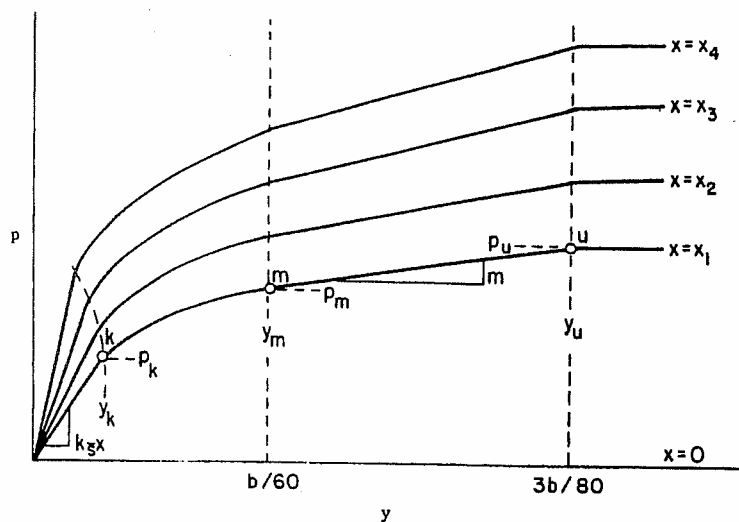


**Figure 3.5 Family of  $p$ - $y$  curves for sand (Reese, et al., 1974)**

The basic shape of the curves does not vary with depth, but the strength and stiffness of the soil increases with increasing depth. The  $p$ - $y$  curves are

divided into four regions. The initial straight line portion of the curves is defined by the expression:

$$p(x) = k \cdot x \cdot y(x) \quad (3.4)$$

Where

$p(x)$  = soil reaction per unit length of shaft, lb/in.

$x$  = distance below grade, in.

$k$  = soil subgrade modulus, lb/in.<sup>3</sup>

$y(x)$  = lateral deflection of the shaft, in.

The value of  $k$  is assumed to be a constant for a given sand density (Table 2.4). Equation 3.4 is valid for displacements less than  $y_k$ , as defined in Figure 3.5.

A transition region is defined between this initial linear response and the ultimate soil resistance per unit length,  $p_u(x)$ . A parabolic relationship is used between displacement levels  $y_k$  and  $y_m$ , while a linear relationship is used between displacement levels  $y_m$  and  $y_u$  (Figure 3.5). Plastic deformation is assumed once the capacity of the soil is reached. Details of the procedures used to determine the soil reaction and displacement at each of the limiting values are presented in the LPILE Technical Manual (Reese, et al., 2004).

The soil parameters used to analyze the test specimens are given in Table 2.4. As discussed in Chapter 2, two soil profiles were assumed in an attempt to bound the response of the specimens. Three  $p$ - $y$  curves are shown in Figure 3.6 for medium dense sand, and similar curves are shown in Figure 3.7 for loose sand. Lateral loads were assumed to be applied statically in all analyses.

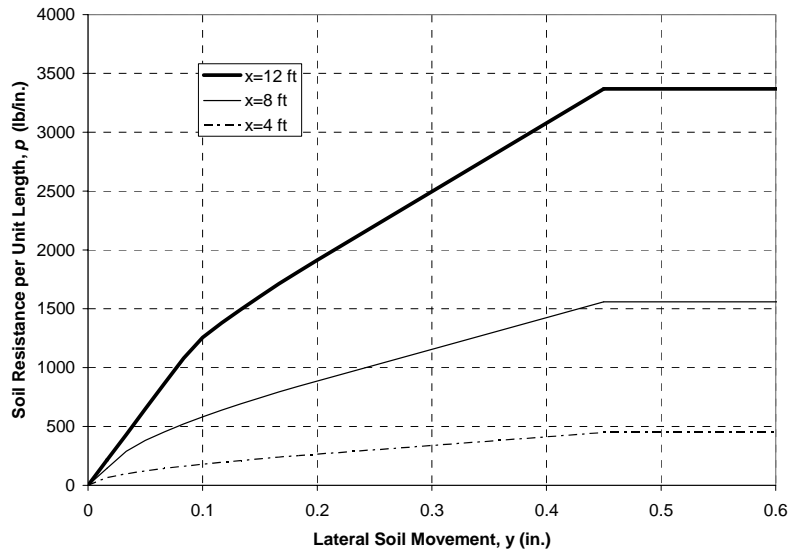


**Figure 3.6** *Calculated p-y curves for medium dense sand*

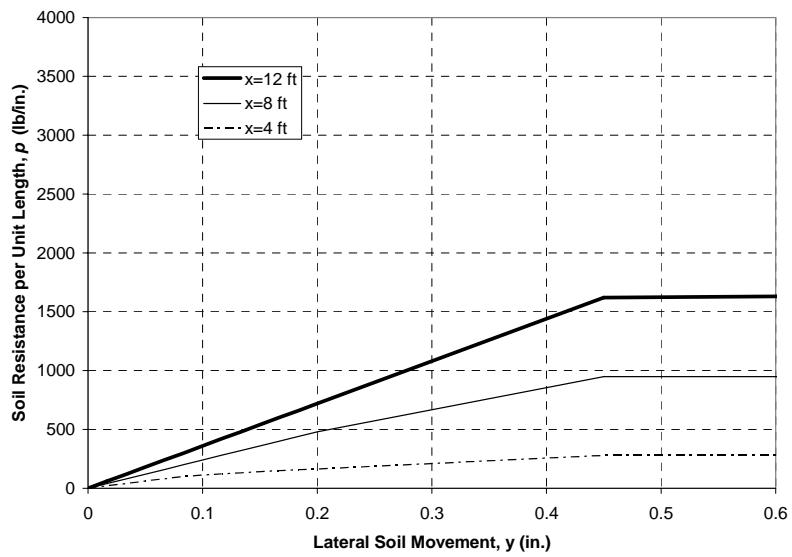


**Figure 3.7** *Calculated p-y curves for loose sand*



### 3.3.4 Calculated Response of Shafts

The results of the initial analyses of the shafts are described in this section. For each analysis, the total length of the shaft was divided into 100 increments of equal length. The resulting increments varied between 1.5 in. for the shafts with  $L_c$  equal to 0 ft and 2.25 in. for the shafts with  $L_c$  equal to 6 ft. The  $p$ - $y$  curves were calculated every increment along the length of the shaft. A convergence tolerance of 0.001 in. was used for all analyses.

Eight different analyses were conducted for each type of shaft and the key input parameters for each analysis are listed in Table 3.1. Analyses A through D are based on the soil properties for medium dense sand, while Analyses E through H are based on the properties for loose sand. In all cases, the water table was assumed to be located below the bottom of the shafts.

**Table 3.1 Summary of input parameters for analysis of shafts**

Analysis ID	Relative Density of Soil	Rotational Restraint at Top of Column	Magnitude of Maximum Moment Below Grade
A	Medium	Free	$M_n$
B			$M_{cr}$
C		Fixed	$M_n$
D			$M_{cr}$
E	Loose	Free	$M_n$
F			$M_{cr}$
G		Fixed	$M_n$
H			$M_{cr}$

Analyses A, B, E, and F correspond to lateral forces applied in the longitudinal direction of the bridge, and therefore, the top of the column is free to rotate. Lateral loads were applied in the transverse direction of the bridge in Analyses C, D, G, and H. In these cases, the top of the column was restrained against rotation.

Two values of maximum moment in the shafts were considered. Because the shafts were expected to respond linearly during the dynamic tests, the maximum moment was taken as the cracking moment of the cross section,  $M_{cr}$ . The nominal flexural capacity of the shaft,  $M_n$ , was selected to represent the response during the pull-over tests.

Section 3.3.4.1 summarizes the analyses used to determine if the assumed embedment depth of 12 ft was sufficient to develop a mechanism in the bent. A parametric study to determine the depth of the maximum moment is summarized in Section 3.3.4.2, and these results are used as a basis for selecting the shaft instrumentation in Section 3.3.4.3.

#### **3.3.4.1 Embedment Depth of Shaft**

The depth of the drilled shaft has a significant impact on the lateral response of the test specimens. If the drilled shaft is too short, it is possible that the lateral capacity of the soil will be exceeded before a mechanism forms in the bents (Figure 3.8a). The shafts need to be sufficiently long to ensure formation of a flexural hinge below the ground surface (Figure 3.8b). It is also desirable to keep the shaft length to a minimum to prevent caving of the soil along the sides of the hole after the hole is drilled and before the concrete is placed. A shorter shaft length also minimizes logistical problems associated with transporting and positioning the continuous, instrumented reinforcement cages.

The assumed shaft embedment length of 12 ft was checked by completing a pile length versus lateral deflection analysis using LPile. This type of analysis is used for shafts with low axial loads and high lateral loads, such as those in the test specimens. LPile calculates the lateral deflection at the top of the column for the embedment depth and lateral force specified by the user. The same lateral force is then applied to the top of nine shafts with shorter embedment depths. Representative results for medium dense sand, a column shear height of 3 ft, and rotational restraint at the top of the column are shown in Figure 3.9. As expected, the calculated lateral deflections increase as the embedded depth decreases.

LPile defines the critical length,  $L_{cr}$ , as the total length of the shaft at which a selected shear can no longer be carried due to global soil failure. The critical length for the example shown in Figure 3.9 is 11.5 ft (embedded depth of 8.5 ft). The algorithm will not converge for shorter lengths, indicating unacceptably large deformations in the soil.

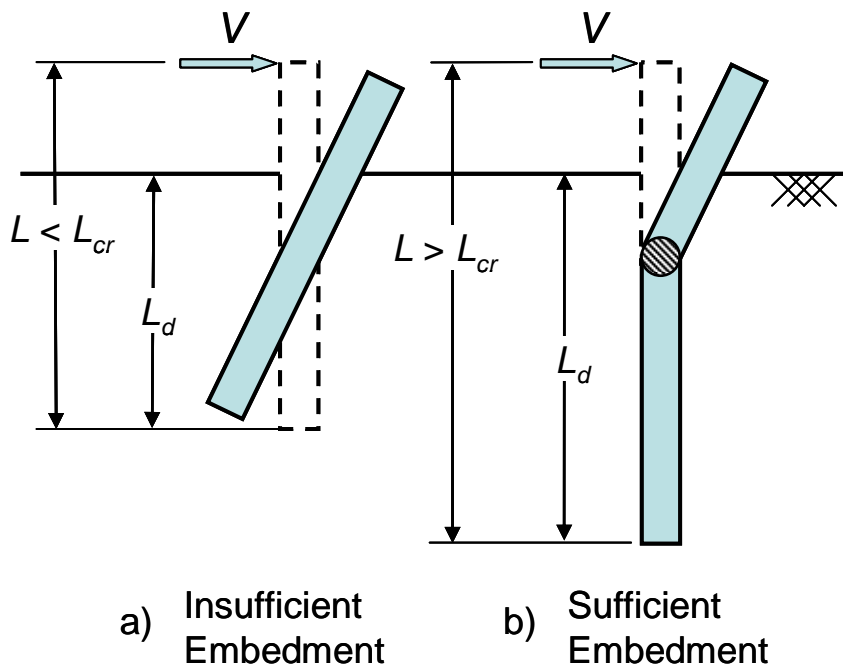


**Figure 3.8 Influence of embedment length on behavior of shaft**

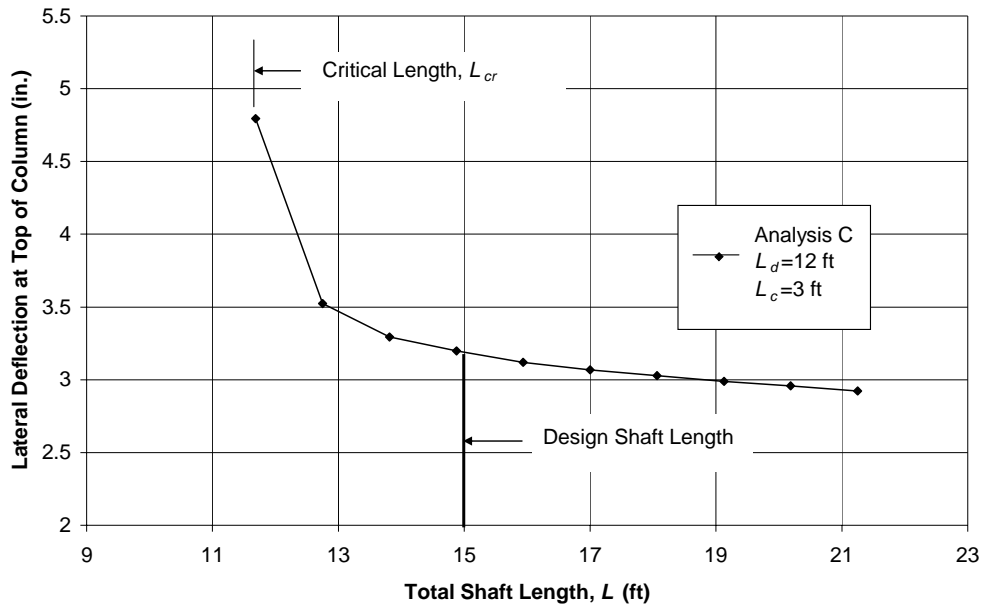


**Figure 3.9** Representative relationship between shaft embedment depth and lateral deflection of column

The results of the analyses are summarized in Table 3.2. In each case the shear applied at the top of the column,  $V$ , corresponds to the shear required to form a plastic mechanism in a shaft with  $L_d = 12$  ft. The analysis ID listed in Table 3.2 corresponds to the combination of input parameters listed in Table 3.1.

**Table 3.2** Calculated critical length of shafts

Analysis ID	$L_c = 3$ ft		$L_c = 6$ ft	
	$V^*$ (kip)	$L_{cr}$ (ft)	$V^*$ (kip)	$L_{cr}$ (ft)
A	7.4	10.6	5.0	13.3
C	13.3	11.7	9.3	13.9
E	6.9	11.7	4.7	14.5
G	12.2	12.7	8.8	15.0

\* Shear required to form a plastic hinge below grade when  $L_d=12$  ft

The results shown in Table 3.2 for analyses C and G correspond to the response of the bents in the transverse direction of the bridge. Because plastic hinges must form at the top of the column and within the shaft for a mechanism to form in this direction, the applied shear,  $V$ , is larger than the applied shear in the longitudinal direction of the bridge (analyses A and E). The top of the column is not restrained in the longitudinal direction, and therefore, a mechanism develops when the first plastic hinge develops in the shaft.

A comparison of the critical lengths in Table 3.2 and the design lengths of the shafts is presented in Figure 3.10. The results indicate that the assumed embedment depth of 12 ft is sufficient to develop a mechanism in the test specimens before failure occurs in the soil. This embedment depth was also considered to be reasonable with respect to the stability of the hole and the constructability of the reinforcement cages.

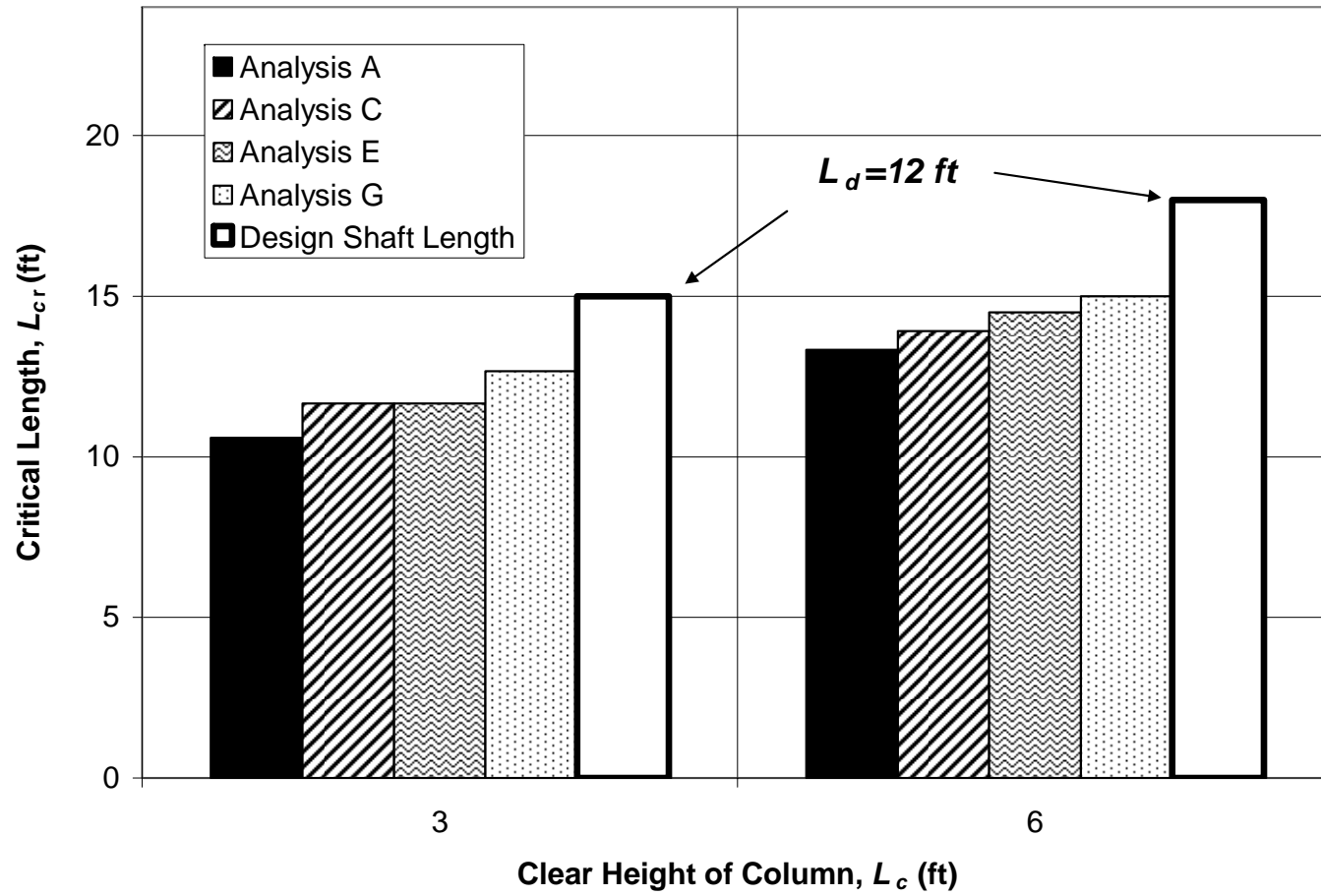
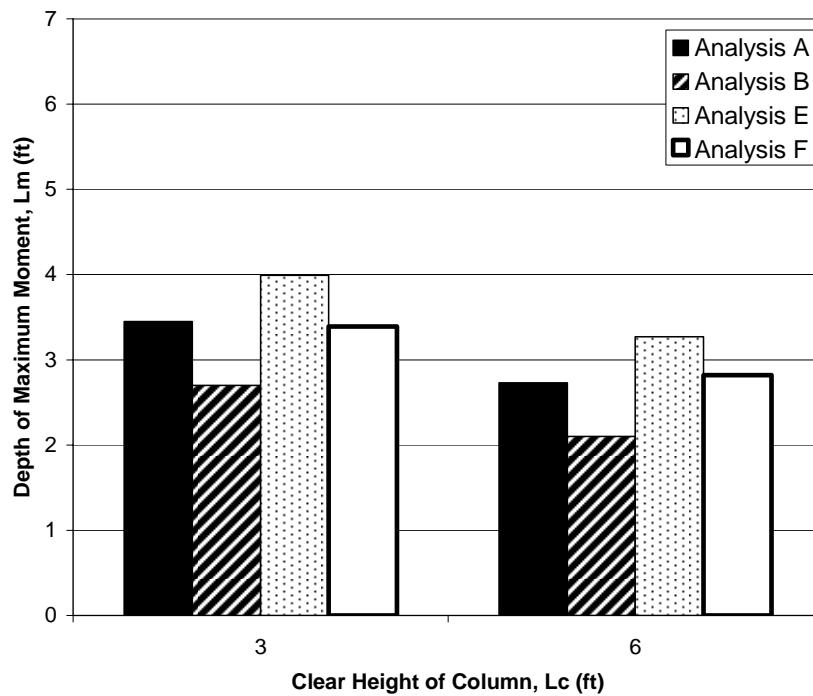


Figure 3.10 Sensitivity of critical length of shaft to soil density and rotational restraint at top of columns

### 3.3.4.2 Location of Maximum Moment

A parametric study was performed to estimate the locations of the maximum moment along the shafts. The results were used to select the shaft instrumentation. Results are shown in Figure 3.11 for response in the longitudinal direction of the bridge and in Figure 3.12 for response in the transverse direction.



*Figure 3.11 Variation in depth of maximum moment for zero rotational restraint at the top of the column*

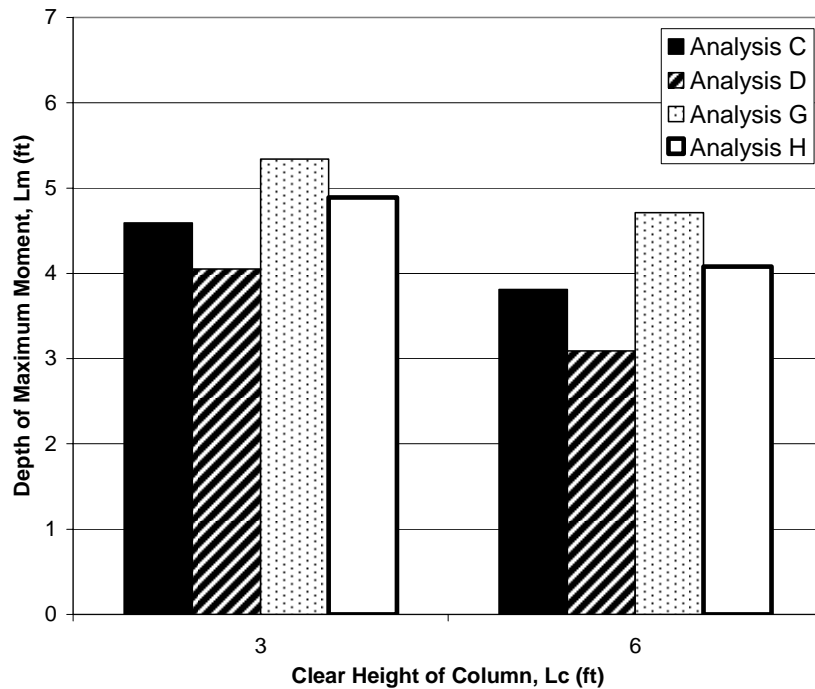


**Figure 3.12** Variation in depth of maximum moment full rotational restraint at the top of the column

The results of the parametric study indicate that the depth of the maximum moment in the shaft,  $L_m$ , increases with:

- Decreasing clear height of the column,  $L_c$
- Decreasing soil density
- Increasing maximum moment in the shaft
- Increasing rotational restraint at the top of the column

The maximum moment was closest to the ground surface for medium dense soil with a maximum moment in the shaft equal to the cracking moment and no rotational restraint at the top of the column. Conversely, the combination of loose soil, full rotational restraint at the top of the column, and a maximum moment in



the shaft equal to the nominal capacity lead to the deepest location for the maximum moment in the shaft.

#### **3.3.4.3 Instrumentation Embedded in Shafts**

Because the shafts are below grade, all instrumentation must be attached to the reinforcement cages before the concrete is placed for the shafts. Therefore, the locations for the instruments must be selected based on the results of the preliminary analyses. As discussed in Chapter 2, the as-built dimensions of the shafts did not match those assumed during design. The implications of these changes will be presented in Chapter 5.

Two sets of geophones were embedded in each shaft, but this distribution was too coarse to determine the profile of shaft response with depth. Strain gages were attached to the longitudinal reinforcement for this purpose. The number and distribution of strain gages was selected based on the calculated variations of moment along the length of the shaft.

A moment envelope was developed by superimposing the moment diagrams from the analyses with the shallowest and deepest values of  $L_m$ . The envelope was then divided vertically into zones of relative importance. For example, a region where the maximum moment is expected below grade would be considered to be of high importance, while the base of the shaft, where essentially no response was expected, was considered to be of low importance. A higher density of strain gages was located in zones of greater importance.

To accommodate the limitations of the data acquisition system that would be used to collect data in the field, a total of 92 strain gages were attached to the longitudinal reinforcement in the two shafts that formed each bent. The number of gages was not divided equally between the shafts, however. Each bent has one heavily instrumented shaft and one shaft with moderate instrumentation. Fifty-six

strain gages were attached to the reinforcement in Shafts 1E and 2S, while only 36 strain gages were attached to the reinforcement in Shafts 1W and 2N.

The locations of the strain gages for the shafts in Bents 1 and 2 are defined in Table 3.3. Vertical stations were defined along the length of the shafts with a typical spacing of 12 in. The vertical datum was taken at the ground surface. The station numbers correspond to the depth of the gages in inches. Stations above the ground surface are indicated with a negative sign.

At each station, one of three strain gage layouts was used (Figure 3.13). A local coordinate system was assigned to each bent with the local North-South direction in the plane of the bent (transverse direction of the bridge) and the East-West direction in the perpendicular direction (longitudinal direction of the bridge). Reinforcing bar and gage layouts for the individual shafts utilize this local bent coordinate system.

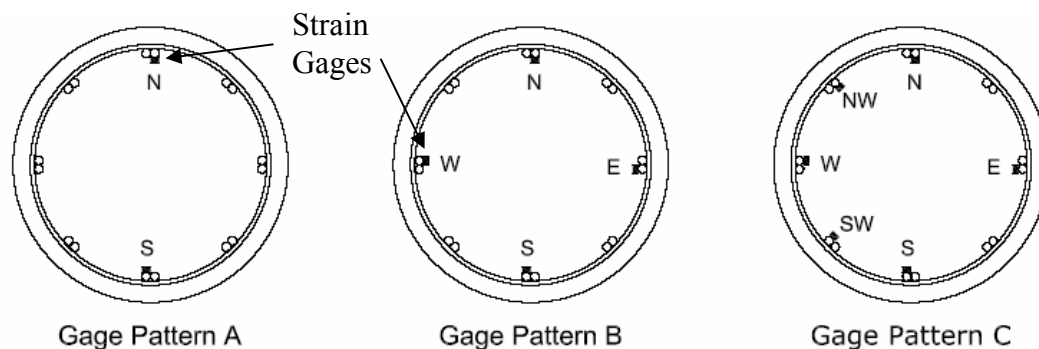


**Figure 3.13** *Layout of strain gages*

Shafts 1E and 2S have identical instrumentation as do Shafts 1W and 2N (Table 3.3). Above the ground surface, both bents have gage stations at the beam-column interface and six in. below the interface. The moment diagram envelope with zones of importance and gage stations is shown in Figure 3.14.

**Table 3.3 Summary of strain gage locations for Shafts 1E, 1W, 2N, and 2S**

Station Number	Importance Level	Shafts 1E and 2S		Shafts 1W and 2N	
		Gage Pattern	# Gages	Gage Pattern	# Gages
-72 or -36	medium	B	4	A	2
-66 or -30	medium	B	4	A	2
0	low	A	2	A	2
12	medium	B	4	A	2
24	high	C	6	B	4
36	high	C	6	B	4
48	high	C	6	B	4
60	high	C	6	B	4
72	high	C	6	B	4
84	medium	B	4	A	2
96	medium	B	4	A	2
108	low	A	2	A	2
120	low	A	2	A	2
		<b>Total</b>	<b>56</b>	<b>Total</b>	<b>36</b>

As discussed in the previous section, the depth of the maximum moment is shallowest for the shaft with a column clear height of 6 ft, no rotational restraint at the top of the column, medium dense soil, and linear response of the shaft (Analysis B). The depth of the maximum moment is deepest for the shaft with a column clear height of 3 ft, loose soil, full rotational restraint at the top of the column, and nonlinear response of the shaft (Analysis G). The depths of the maximum moment calculated in both of these analyses were within the region where six strain gages were positioned at each station (Gage Pattern C).

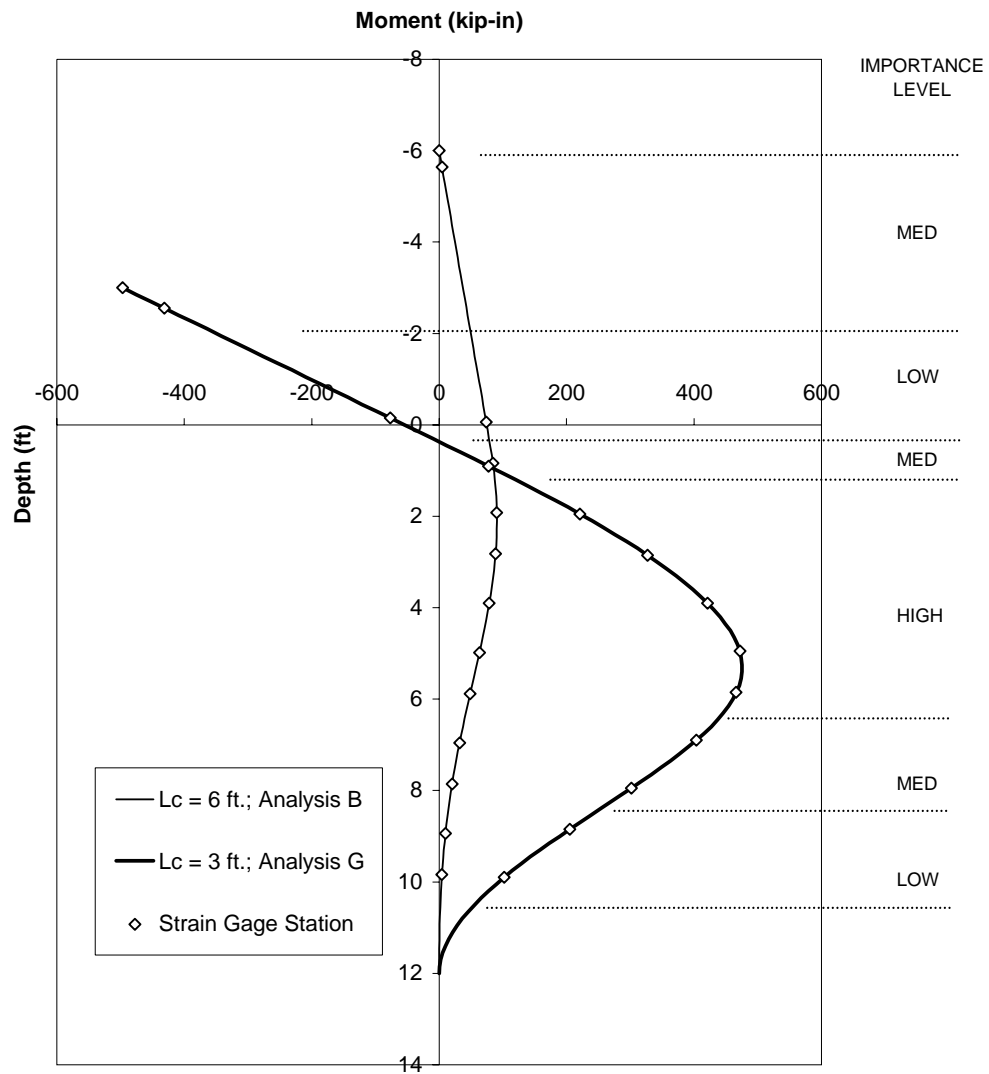


*Figure 3.14 Moment envelope and strain gage stations for Shafts 1E, 1W, 2N, and 2S*

It should be noted that the strain gages are oriented to capture the maximum and minimum response of the shafts for response in the longitudinal and transverse directions within regions of medium and high importance. However, the response of the bent in the longitudinal direction of the bridge will not be captured for stations of low importance, because only two strain gages were positioned at each station.

Two of the isolated shafts, Shafts C and D, were also instrumented with strain gages. The strain gage locations for these shafts were selected using the same procedure that was used for the shafts in the bents. However, the strain gage stations were not spaced equally for the isolated shafts.

Two zones of importance were assigned to the isolated shafts (Table 3.4). The gage patterns correspond to those in Figure 3.13. The limiting moment diagrams with zones of importance and strain gage stations indicated are shown in Figure 3.15. Because static, pull-over tests are not planned for these shafts, the moment envelopes used to determine the instrumentation layout were based on the linear response of the shafts. In addition, the top of the column was assumed to be free to rotation in these analyses.

**Table 3.4 Summary of strain gage locations for Shafts C and D**

Station Number	Importance Level	Gage Pattern	# Gages
0	medium	B	4
6	medium	B	4
18	low	A	2
26	low	A	2
34	medium	B	4
42	medium	B	4
50	medium	B	4
58	low	A	2
70	low	A	2
82	low	A	2
100	low	A	2
118	low	A	2
136	low	A	2
		<b>Total</b>	<b>36</b>

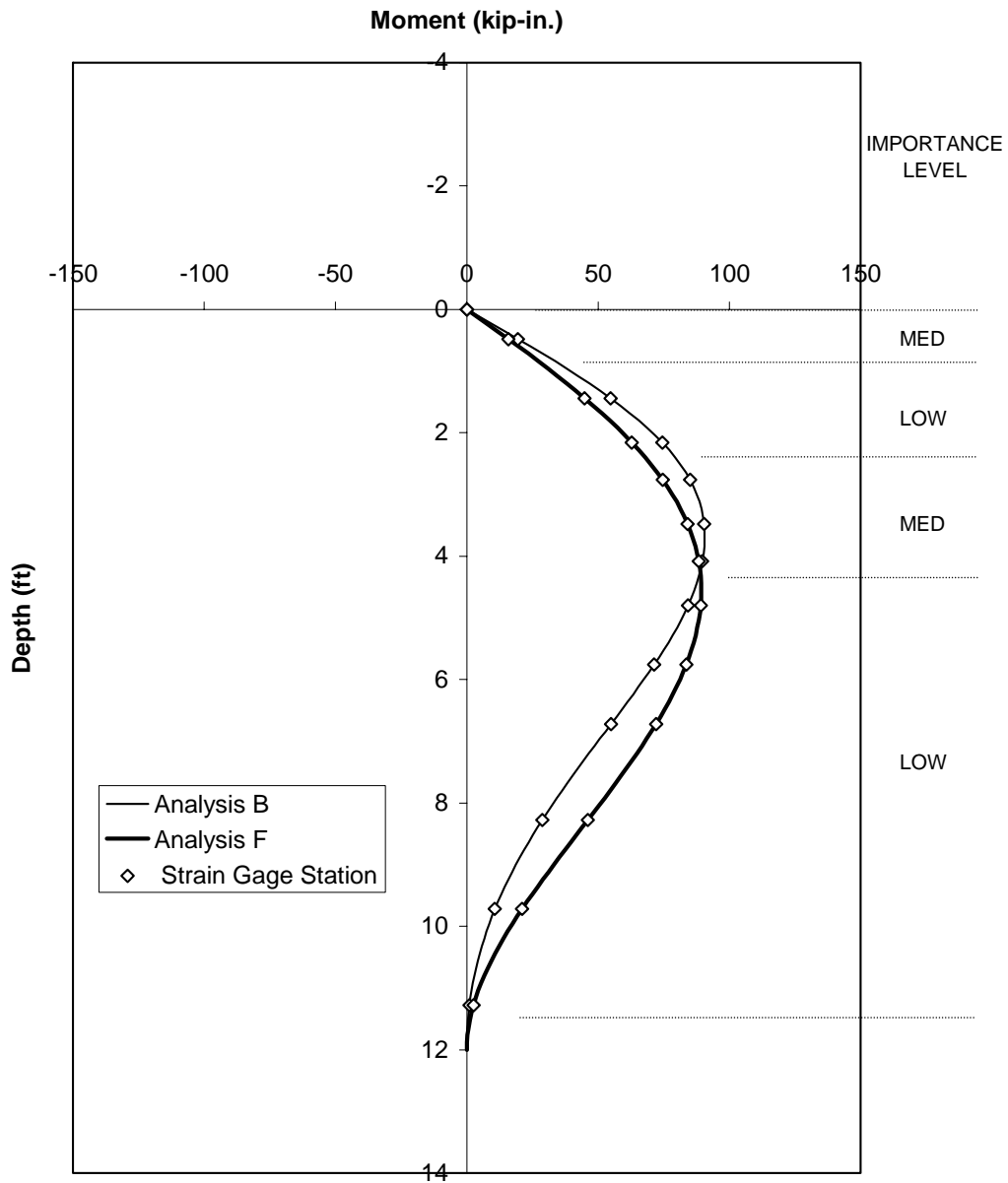


**Figure 3.15** *Moment envelope and strain gage stations for Shafts C and D*

The geophones locations were selected by Kurtulus and Stokoe (2004) are presented in Figure 3.16. Two sets of geophones were positioned in each shaft. Single-component geophones, which measure response in the vertical direction

only, were used in Shaft A (**Error! Reference source not found.**Figure 3.16a). Two-component geophones, which measure response in the vertical and one horizontal direction, were used in Shafts B, C, and D (Figure 3.16b). Three-component geophones, which measure response in the vertical and two horizontal directions, were used in Shafts 1E, 1W, 2N, and 2S (Figure 3.16c).

The geophones were housed in an acrylic cylinder. Holes were machined along perpendicular axes, and the geophones were positioned in these holes. This approach ensured that the axes of the geophones were oriented along perpendicular axes. In all eight shafts, the geophones were positioned near, or slightly below, the depth of the maximum moment and near the base of the shaft.



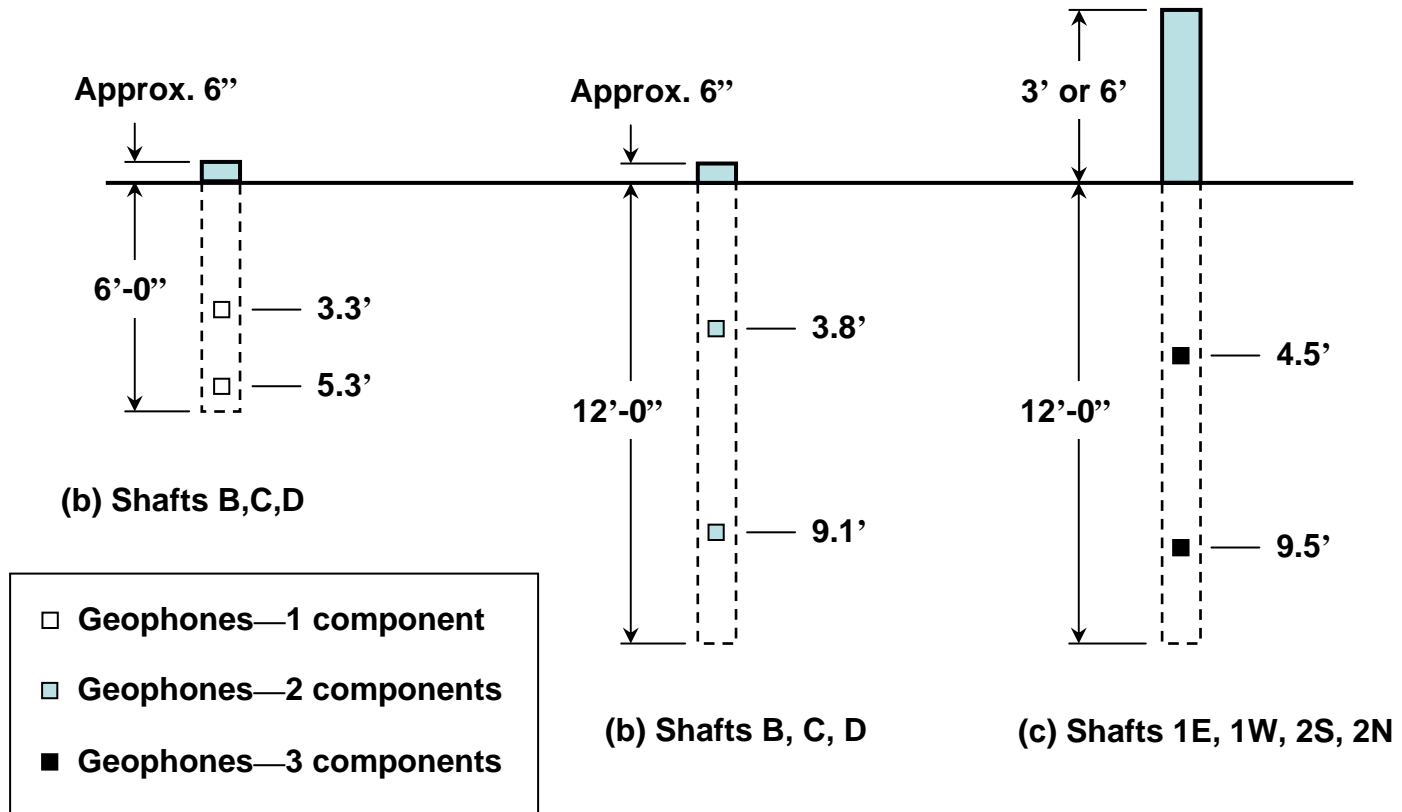


Figure 3.16 Locations of geophones in shafts

### 3.4 MODAL ANALYSES

The modal analyses were used to estimate the natural frequencies of the specimens. These results were then compared with the frequency ranges of the NEES shakers T-Rex and Thumper. The model was based on the specimen geometries shown in Figures 2.1 and 2.2, the structural material properties given in Table 2.5, and assumed bent cap dimensions of 24 in. wide by 18 in. deep. The unit weight of the concrete was assumed to be 150 lb/ft<sup>3</sup>. No additional mass was considered in the analyses.

The soil resistance was modeled using linear springs spaced at 12 in. on center along the length of the shafts in both the transverse and longitudinal directions. The spring constants represented the initial, linear portion of the  $p$ - $y$  curves (Figures 3.4 and 3.5) and were calculated by multiplying the subgrade modulus,  $k$ , by the depth of the spring,  $x$ , by the tributary length of 12 in. The values of these soil spring constants are reported in Table 3.5.

Three fundamental modes of vibration were considered in the modal analyses: response in the longitudinal direction of the bridge, response in the transverse direction of the bridge, and torsional response of the bent. The physical significance of these mode shapes is shown in Figure 3.17.

**Table 3.5 Soil spring constants used for modal analyses**

Depth below Grade (ft)	Spring Constant (k/in.)	
	Loose Sand*	Medium Dense Sand†
0.5	1.8	6.5
1.5	5.4	19.4
2.5	9.0	32.4
3.5	12.6	45.4
4.5	16.2	58.3
5.5	19.8	71.3
6.5	23.4	84.2
7.5	27.0	97.2
8.5	30.6	110.2
9.5	34.2	123.1
10.5	37.8	136.1
11.5	41.4	149.0

Notes:

\* Subgrade modulus,  $k_s = 25 \text{ lb/in.}^3$

† Subgrade modulus,  $k_s = 90 \text{ lb/in.}^3$

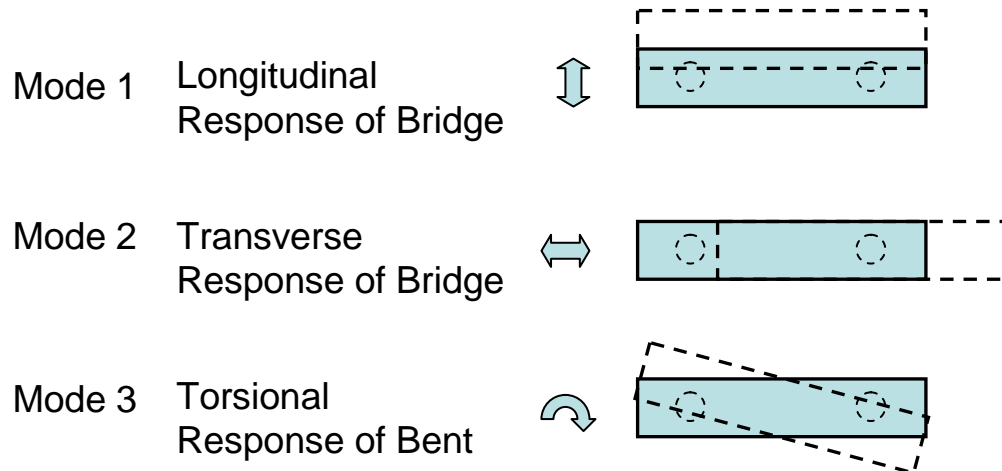


**Figure 3.17 Mode shapes associated with fundamental modes of vibration**

The calculated frequencies for each of the fundamental modes of vibration are reported in Table 3.5. Three analyses were conducted for each bent. Analyses 1A and 2A correspond to loose sand, while Analyses 1B and 2B correspond to medium dense sand.

Analyses 1C, 1D, 2C, and 2D provide frequencies based on the common design assumption of ignoring the soil and fixing the base of the shaft at the depth of maximum moment from the lateral analysis. Because the depth to maximum moment is dependent on the direction of loading, two analyses per bent were necessary to test the assumption: one for the longitudinal direction of the bridge and one for the transverse direction of the bridge.

As expected, the calculated natural frequencies (Figure 3.18) were higher for denser soil, and for shorter columns. Higher frequencies were also calculated when the tops of the columns were restrained against rotation. Hence, the frequencies in the transverse direction of the bridge were nearly twice those in the longitudinal direction of the bridge for all analyses considered.

Analyses 1C, 1D, 2C, and 2D produced frequencies from 30% to 90% greater than those calculated with soil springs, with an average increase of about 60% as shown in Figure 3.18. These results indicate the design assumption generally underestimates foundation flexibility. The fact that two analyses are necessary also indicates that the method may not be appropriate for three-dimensional models where only one support length can be specified.

**Table 3.6 Calculated natural frequencies of bents**

Analysis ID	$L_c$ (ft)	$L_t^*$ (ft)	Support Conditions	Natural Frequencies (Hz)		
				Mode 1	Mode 2	Mode 3
1A	6	-	Loose Soil	3.1	6.0	10.1
1B	6	-	Medium Soil	3.8	7.6	11.0
1C	6	8.46 <sup>†</sup>	Fixed Base	5.5	—	—
1D	6	9.59 <sup>‡</sup>	Fixed Base	—	9.8	—
2A	3	-	Loose Soil	4.6	8.5	13.8
2B	3	-	Medium Soil	6.0	11.5	15.6
2C	3	6.05 <sup>†</sup>	Fixed Base	8.9	—	—
2D	3	7.47 <sup>‡</sup>	Fixed Base	—	15.3	—

Notes:

\* Distance from top of column to the depth of maximum moment (Figure 3.1), used as the length of the fixed-base columns for analyses 1C, 1D, 2C, and 2D.

<sup>†</sup>  $L_t=L_c+L_m$ , where  $L_m$ = the average depth to maximum moment in the longitudinal direction of the bridge from Section 3.3.4.2 (analyses B and F)

<sup>‡</sup>  $L_t=L_c+L_m$ , where  $L_m$ = the average depth to maximum moment in the transverse direction of the bridge from Section 3.3.4.2 (analyses D and H)

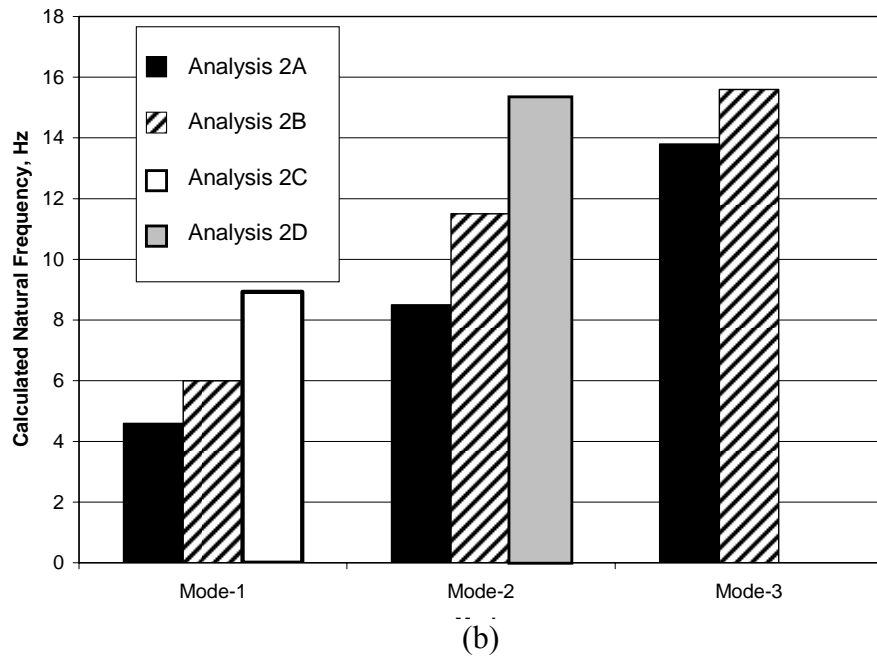
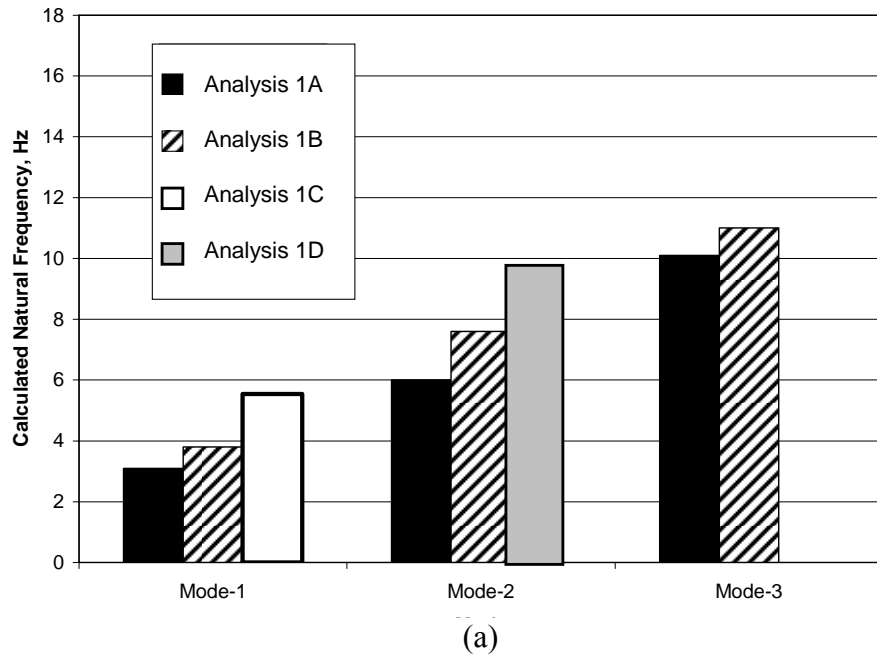


**Figure 3.18** Calculated natural frequencies: (a) Bent 1 (b) Bent 2

The results of the preliminary modal analyses indicate that the natural frequencies of the test specimens are likely to be less than the lowest frequency at which the maximum force can be achieved using either T-Rex or Thumper (Figure 2.4 and Figure 2.6).

As will be discussed in Chapter 5, the concrete compressive strengths were higher, the diameters of the shafts were larger, and the stiffness of the soil was higher than assumed in these analyses. Therefore, the measured natural frequencies were considerably higher than those indicated in Table 3.6 and Figure 3.18.



## 3.5 BEAM DESIGN

### 3.5.1 Overview

Four issues were considered during the design of the beams: (1) the beams must have sufficient flexural strength such that flexural hinges develop in the columns before the beams, (2) the beams must have sufficient shear strength such that the nominal flexural capacity of the beams exceeds the nominal shear capacity, (3) the beams must be designed with an embedded plate to accommodate attachment of the linear shaker from Thumper, and (4) the beams must be designed with attachment points such that the static pull-over tests can be conducted after the completion of the dynamic tests. Each of these issues is discussed in the sections below.

The cross section selected for the beam is 18 in. deep and 24 in. wide. The depth matches the depth of the cap beams in the shaking table specimen, while the width was selected to accommodate the linear shaker. The final beam reinforcement details are shown Figure 3.19. All calculations were based on the assumed material properties for the concrete and steel given in Table 2.5.

### 3.5.2 Design for Flexure

Equal amounts of top and bottom reinforcement were provided in the beams to resist the positive and negative moments that will occur during the static pull-over tests. The longitudinal reinforcement ratio is 0.6% along each face. The calculated cracking moment for the cross section,  $M_{cr}$ , is 615 kip-in. and the nominal flexural capacity,  $M_n$ , is 2350 kip-in.

The calculated flexural capacity of the columns is 470 kip-in.; therefore, the longitudinal reinforcement in the columns is expected to yield before the concrete in the beam cracks. The response of the beam is expected to be

controlled by gross cross-sectional properties for all levels of response, and the assumption that the tops of the columns are restrained against rotation is appropriate.

### **3.5.3 Design for Shear**

Transverse reinforcement, in the form of #3 hoops and cross ties, was provided in the beam. The hoops were made using two pieces of reinforcement to facilitate construction.

The transverse reinforcement was designed to carry all the shear in the beam, while the concrete not assumed to contribute to the shear strength. As indicated in Figure 3.19, the spiral reinforcement was continuous throughout the beam-column joint.

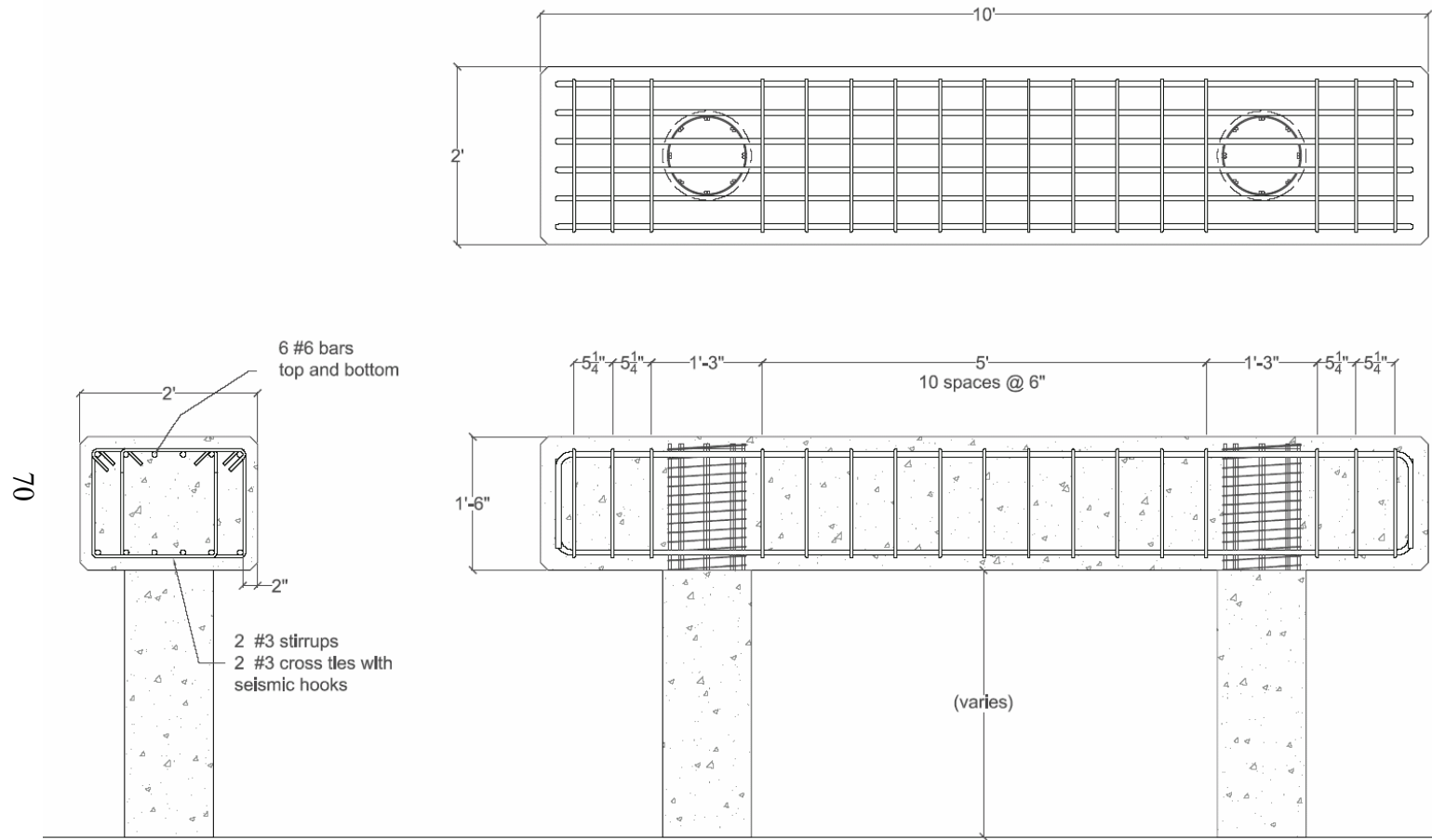


**Figure 3.19** *Beam reinforcement details*

### 3.5.4 Connection to Hydraulic Shaker

For active excitation of the test specimens, the hydraulic shaker from Thumper will be attached to beams at midspan. Two  $\frac{3}{4}$ -in. steel plates were designed to facilitate this connection. The plates were designed to transfer the horizontal forces from the shaker into the confined concrete and to allow the shaker to be rotated in 45-degree increments to permit multiple loading directions (Figure 2.5).

A schematic representation of the shaker-beam connection is shown in Figure 3.20. The bottom plate was embedded in the concrete in the beam. Shear is transferred from the plate to the concrete through eight shear studs welded to the bottom of the plate and through bearing along the edges of the plate. The shear studs were 4 in. long and had a diameter of  $\frac{1}{2}$  in.

The shaker is attached to the embedded plate using an adapter plate. The two plates are connected using eight,  $\frac{1}{2}$ -in. bolts. The hole pattern in the embedded plate was designed to permit the shaker to be oriented along the longitudinal and transverse axes of the bent and at 45 degrees to these axes (Figure 2.5).

The shaker is positioned vertically when attached to Thumper. However, a cradle is available to support the shaker horizontally. The shaker is attached to the cradle using six,  $\frac{1}{2}$ -in. bolts. Details of the cradle and the two plates are presented in Appendix E. The weight of each of the components is listed in Table 3.7.

**Table 3.7 Weight of hydraulic shaker and connection assembly**

Component	Weight (lb)
Linear Shaker	311
Cradle	73.6
Adapter Plate	45.2

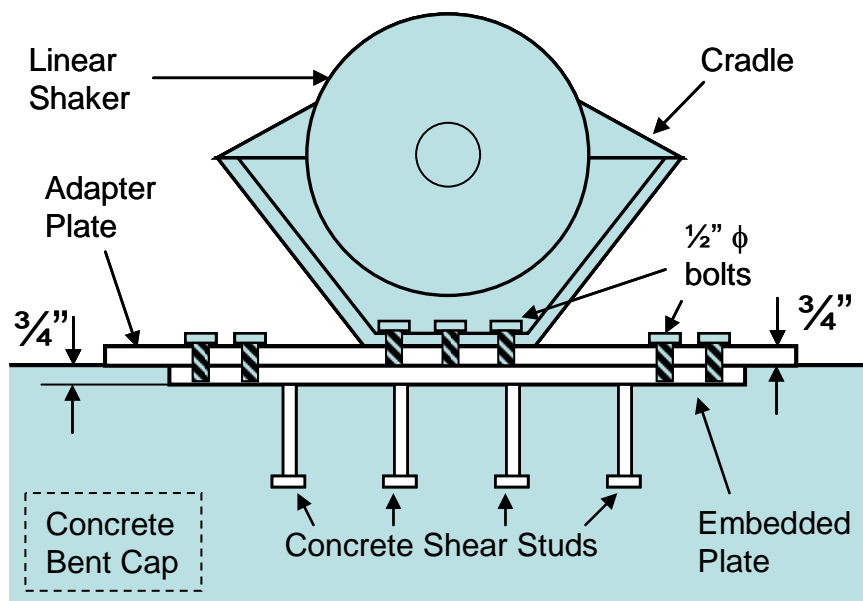


**Figure 3.20 Schematic view of connection between hydraulic shaker and concrete beam**

### 3.5.5 Connection for Pull-Over Tests

A 1-in. threaded rod was embedded at mid-height of each beam near the centroid of each column (Figure 3.21). The rods extend approximately 6 in. beyond the beam faces on either side. During the pull-over tests, cables will be attached to the rods, and the lateral force will be applied equally to the columns such that no tension will be induced in the beam.

The size of the rods was estimated conservatively by assuming that the columns were fixed at the surface of the ground. Flexural hinges were then assumed to form in the column at the ground surface and at the bottom of the beam. The shear strength of the rods exceeds the shear required to develop a mechanism in the bents. These calculations associated with the design of the rods are summarized in Appendix G.

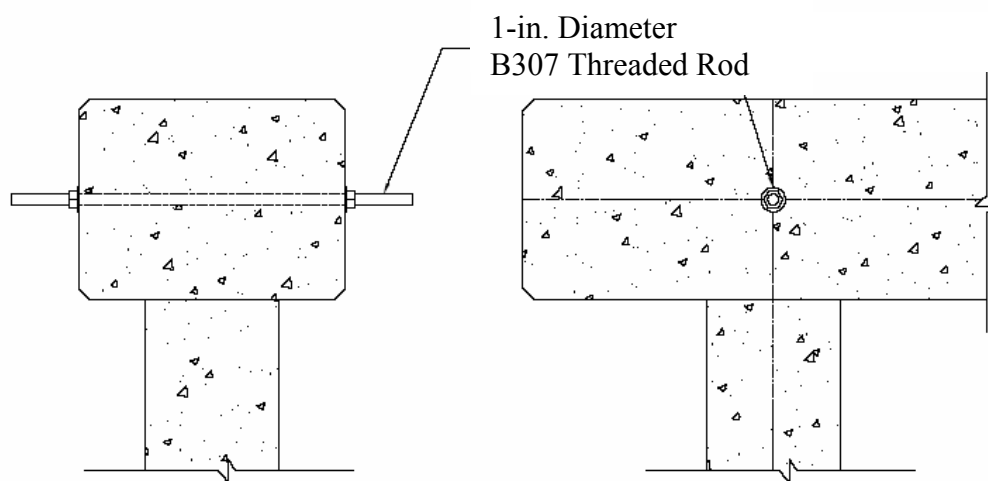


*Figure 3.21 Embedded rods for pullover tests*

## **CHAPTER 4**

### **Specimen Construction**

#### **4.1 INTRODUCTION**

The construction of the test specimens is described in this chapter. Shafts A, B, C, and D were cast on 17 December 2004. These shafts extend approximately 6 in. above the ground surface and will be used primarily for geotechnical testing. The shafts and columns that form the bent specimens were cast on 25 February 2005. The bent specimens were completed on 22 May 2005 when the beams were cast. All specimens were constructed at the Capitol Aggregates site in southeast Austin (Figures 2.9 and 2.10)

The construction process is presented in three sections. Section 4.2 summarizes the fabrication of the reinforcement cages, Section 4.3 describes the construction of the shafts and columns, Section 4.4 presents the construction of the beams. Measured concrete material properties are discussed in Section 4.5 and measured soil properties at the test site are presented in Section 4.6. Section 4.7 summarizes temperature and rainfall data for Austin during the past year.

As discussed in Chapter 2, the as-built dimensions of the test specimens and measured strength of the concrete exceeded those assumed during design. These differences are presented in this chapter, but the influence of these changes on the calculated response of the specimens is discussed in Chapter 5.

#### **4.2 FABRICATION OF REINFORCEMENT CAGES**

The reinforcing cages were constructed using #3 deformed reinforcing bars as the longitudinal reinforcement and annealed W2.9 wire as the transverse

reinforcement. The wire was fabricated into spirals with an outside diameter of 10.5 in. and a pitch of 1.25 in. The same wire was used to construct the columns for the shaking table specimen at the University of Nevada, Reno and the bent specimens at Purdue University. Measured material properties for the longitudinal reinforcement are presented in Appendix A.

The spirals were shipped to Austin as continuous coils (Figure 4.1a). Each spiral was sufficiently long that the reinforcement cages could be constructed from a single spiral (Figure 4.1b) without splices. The longitudinal reinforcement was also continuous within each reinforcing cage.

Each longitudinal bar was cut to the desired length and the strain gages were attached to the surface of the bars at the locations indicated in Chapter 3. The process used to attach the strain gages to the reinforcement is described in Appendix B. The strain gages had a gage length of 3 mm, a resistance of 120 Ohm, and a gage factor of  $2.13 \pm 1\%$ .

The longitudinal bars were then tied to the spiral to form the reinforcement cages. Because the strain gages were installed before the cages were assembled, slight misalignments were observed in the locations of the strain gages that were intended to be positioned the same station. These differences were typically less than  $\frac{1}{2}$  in. Photographs of the completed reinforcement cages prior to installation are shown in Figure 4.1(c) for shafts A, B, C, and D and Figure 4.1(d) for shafts 1E, 1W, 2N, and 2S.





(a)



(b)



(c)



(d)

**Figure 4.1 Reinforcement cages: (a) Spiral Reinforcement, (b) Cage during fabrication, (c) Cages for shafts A, B, C, and D at site prior to installation, (d) Cages for shafts 1E, 1W, 2N, and 2S at site prior to installation**

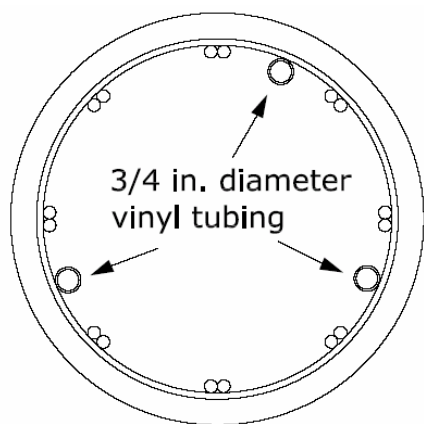


**Figure 4.2** *Arrangement of reinforcing bars and vinyl tubes*

As described in Chapter 2, the longitudinal reinforcement was bundled to provide sufficiently large gaps within the cages for the concrete to flow uniformly during placement (Figure 4.2). Because the reinforcing cages were heavily instrumented, the wires from the strain gages and geophones had to be protected to prevent damage during construction. The wires were grouped and positioned within  $\frac{3}{4}$ -in. diameter vinyl tubes (Figure 4.2 and Figure 4.3c). The tubes extended beyond the concrete formwork. Three tubes were used in Shafts 1E and 2S, while two tubes were used in Shafts 1W and 2N.

Photographs of the strain gages and geophones attached to the longitudinal bars are shown in Figures 4.3(a) and 4.3(c), respectively.



(a)



(b)



(c)

**Figure 4.3** Shaft instrumentation details: (a) Strain gage, (b) Set of two geophones, (c) Vinyl tubing to protect wires

## **4.3 CONSTRUCTION OF VERTICAL ELEMENTS**

### **4.3.1 Overview**

The construction of the shafts and columns is described in this section. An auger was used to drill the holes for the shafts and cardboard tubes were used to form the columns. Preliminary design assumed that the columns and shafts had the same diameter, unfortunately the diameter of the as-built shafts was considerably larger than the diameter of the columns.

### **4.3.2 Drilling**

The holes were drilled by McKinney Drilling Company from Buda, TX using a light-duty drill rig and a double slight (double helix) auger (Figure 4.4a). The holes for shafts A, B, C, and D were drilled on 17 December 2004. A 12-in. diameter auger was used, but the nominal diameter of the holes near the ground surface was approximately 15 in. due to drilling tolerances. The holes for shafts 1E, 1W, 2N, and 2S were drilled on 25 February 2005. On this occasion a larger auger was brought to the site by the contractors by mistake and the nominal diameter of the holes near the ground surface was approximately 18 in.

During the drilling process, the crew monitored the depth of the hole each time that the auger was withdrawn. All of the holes were at least the target depth of 12 ft (6 ft for shaft A) and most were 1 to 3 in. deeper.

Once drilling was completed, the sides of the holes were stable. However, caving of the soil was observed near the surface. The holes for shafts 2S and 2N are shown in Figure 4.5. The extent of the caving, which may have been aggravated by the placement of the reinforcing cages and concrete, will not be known until after the tests are completed and the specimens are removed.



(a)

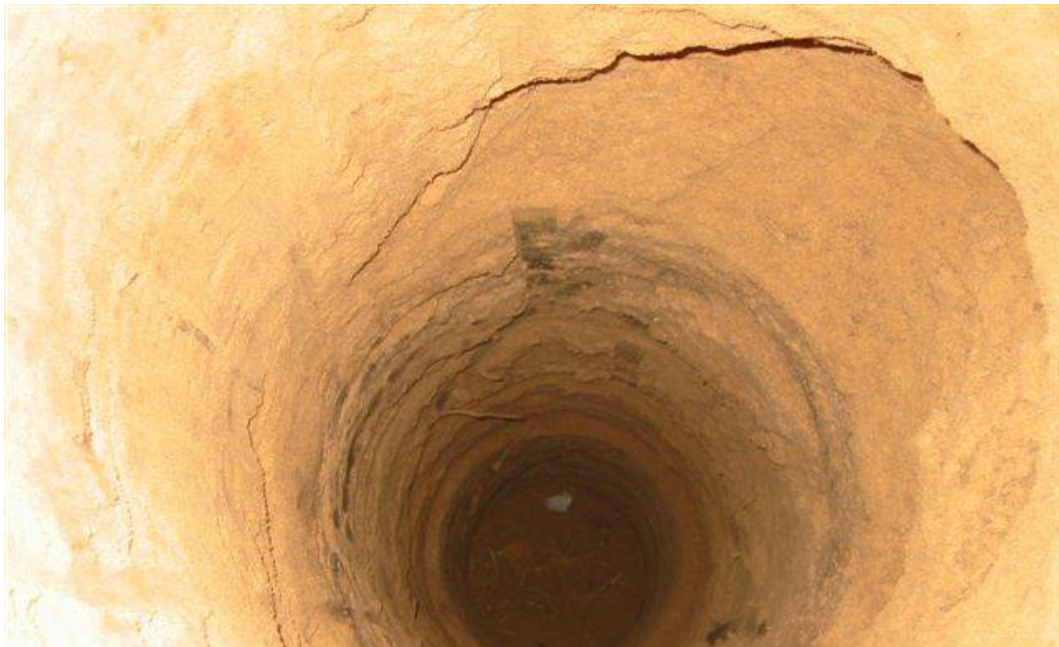


(b)

**Figure 4.4 Drill rig: (a) Light-duty drill rig used to drill holes for shafts, (b) Twelve-in. auger used during construction of shafts A, B, C, and D**



(a)



(b)

***Figure 4.5 Partial caving of soil in holes for Bent 2: (a) Shaft 2N, (b) Shaft 2S***

### **4.3.3 Placement of Reinforcement Cages**

After the holes were drilled, the reinforcement cages were positioned in the holes. Due to the length of the cages required for the bents, a crane was used to lift the cages (Figure 4.6). Although centering devices had been attached to the cages prior to installation, the devices were not in contact with the sides of the holes because the holes were larger than anticipated (Figure 4.7). Therefore, the research team attempted to center the cages within the holes.

During lifting, the vertical positions of the longitudinal reinforcing bars shifted slightly. While this did not influence the integrity of the reinforcing cage, the locations of the strain gages were affected. Based on the relative positions of the tops of the bars, it is estimated that the locations of the strain gages shifted less than ½ in. during this process.

### **4.3.4 Formwork**

The formwork for shafts A, B, C, and D was relatively modest. A 12-in. section of tube form was placed around the top of the reinforcement cage. The tube extended approximately 2 in. above the top of the longitudinal reinforcement and approximately 6 in. below the ground surface (Figure 4.2 and Figure 4.7b). The reinforcement cages were supported only at the bottom of the holes (Figure 4.7a).



(a)



(b)



(c)

***Figure 4.6 Crane used to lift reinforcing cage for Shaft 2N***





(a)



(b)



(c)



(d)

**Figure 4.7** Position of reinforcing cages in holes: (a-b) Isolated shafts (hole diameter of approximately 15 in., (c-d) Shafts in bents (hole diameter of approximately 18 in.)

A similar approach was used for shafts 1E, 1W, 2N, and 2S, but more elaborate formwork was required because the concrete was placed in the shafts and columns at the same time. After orienting and centering the reinforcement cages within the holes, a wooden collar was placed on the ground surface around each reinforcing cage (Figure 4.7c). The collar was constructed using sections of 2x4 lumber and a 22 by 22-in. piece of plywood. A circle had been cut in the plywood to accommodate the cylindrical cardboard tube form. The plywood portion of the collar was placed against the ground surface, and this was used as the datum for setting the elevation of the reinforcement for each shaft. The collars were held in place using four grade stakes.

The cardboard tubes were then placed over the reinforcing bars and positioned such that the bottom was approximately 7 in. below grade (**Error! Reference source not found.**). These sections of plywood were sufficiently large to cover the majority of the hole, even though the holes were larger than expected. Each cardboard tube was set at the correct elevation and tied to the collar using screws. A second collar was placed near the top of the cardboard tubes (Figure 4.9). These collars were also screwed to the tubes and then supported laterally using four braces. Each tube was plumbed by adjusting the length of the braces. This formwork helped to center and align the reinforcing cages in the holes.

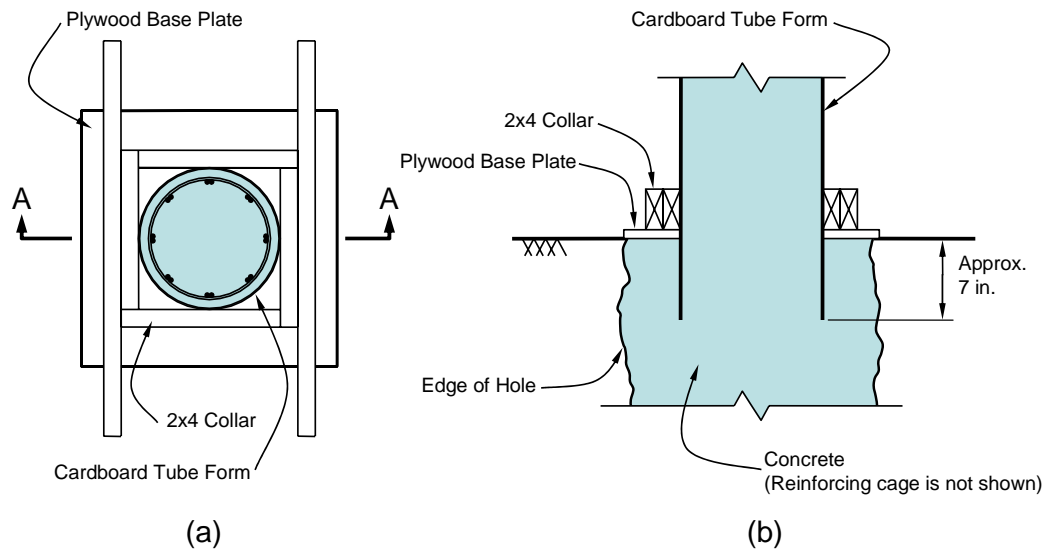


**Figure 4.8 Typical formwork for shaft at ground surface: (a) Plan, (b) Section A-A**

The formwork was preassembled such that the top of the tube form would be at the correct elevation relative to the ground surface when the collar and base plate were bearing on the soil. Due to slight variations in ground elevation, formwork for shafts of the same bent were leveled relative to each other by first setting the shaft form at the lower elevation and then matching the elevation at the second shaft location by removing up to 1 in. of topsoil.



(a)



(b)

**Figure 4.9 Formwork for bents: (a) Bent 2, (b) Bent 1**

After the formwork was secured around the reinforcement cages, the elevations of the cages were set by lifting the cages to the desired height relative to the top of the formwork. Short sections of reinforcing bars were placed on top of the upper collars and the longitudinal reinforcement was secured to these bars. These bars were removed after placement of the concrete.

Significant twist of the reinforcement cage was noted for shaft 1W after the formwork was secured. The angle of twist at the top of the reinforcement cage was approximately 15 degrees in a counter-clockwise direction. The twist was believed to have occurred during placement of the formwork when screws used to attach the cardboard tubes to the collars penetrated through the cardboard. The distribution of twist along the length of the shaft is not known.

Bundled instrumentation leads were passed through the formwork via oversized holes drilled in the cardboard tubes near the ground surface. After the instrumentation leads were pulled to the outside of the forms and protected, the size of the holes was reduced by using cardboard wraps secured with hose clamps.

#### **4.3.5 Concrete Placement**

The concrete used to cast the shafts had a maximum aggregate size of 3/8 in. and a target slump of 7 to 9 in. The measured properties of the fresh and hardened concrete are reported in Section 4.5 and Appendix A.

For shafts A, B, C, and D, concrete was placed by free-fall. The ready-mix truck deposited the concrete directly into the hole (Figure 4.10a). An internal vibrator was used to consolidate the concrete near the surface. Due to the height of the formwork, a concrete pump was used to place the concrete for shafts 1E, 1W, 2N, and 2S (Figure 4.10b). The hose on the pump was lowered inside the reinforcement cage and then raised as the concrete filled the hole. Because the

holes were irregularly shaped at the ground surface, it was possible to use the internal vibrator at grade in a few locations by positioning the head between the side of the hole and the plywood in the collar. The vibrator was also used to consolidate concrete within the column from the top of the reinforcement and along the sides of the cardboard forms.

The columns are shown in Figure 4.11 after the above-grade portion of the cardboard forms were removed, and the completed single shafts are shown in Figure 4.12. Slight honeycombing was observed in the column concrete at locations where the instrumentation wires extended out of the forms.



(a)

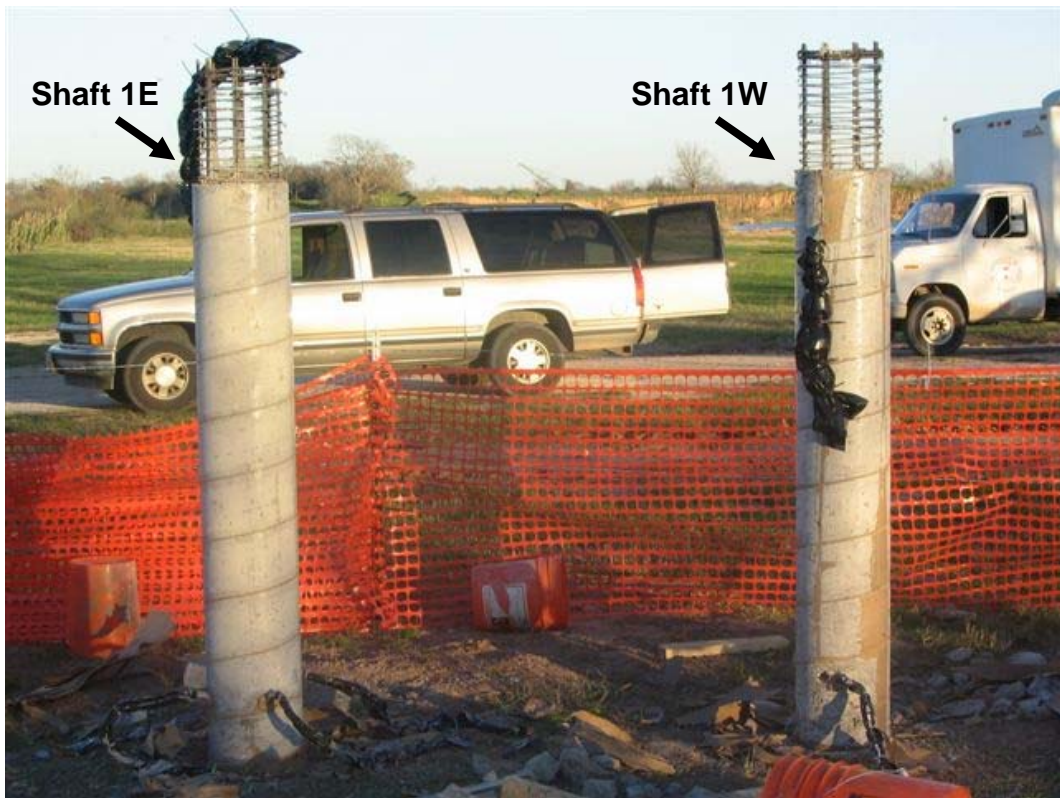


(b)

**Figure 4.10 Concrete placement methods: (a) Free-fall with funnel for shafts A, B, C, and D, (b) Pumping for bents**



(a)



(b)

**Figure 4.11** Columns prior to construction of bent caps: (a) Bent 2, (b) Bent 1



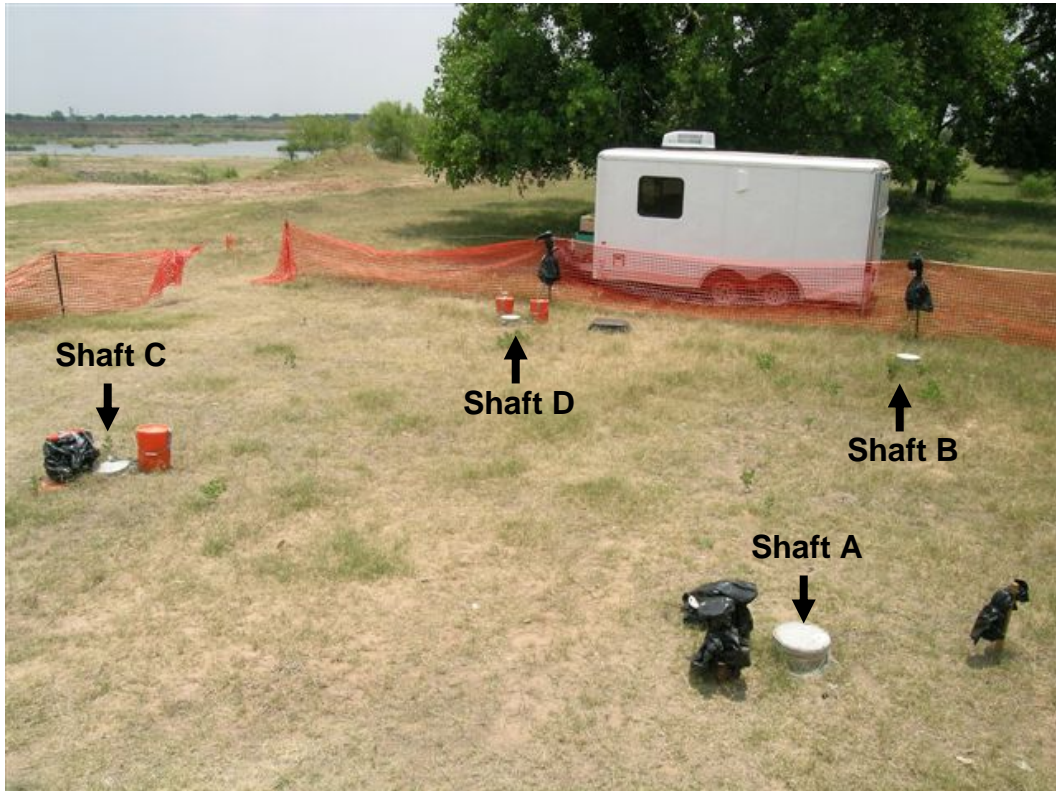


*Figure 4.12 Completed single shafts specimens*

#### **4.4 CONSTRUCTION OF HORIZONTAL ELEMENTS**

The beams for the bent specimens were cast on 17 May 2005. Scaffolding was set up around the shafts, and a platform was constructed on 4x4 lumber which spanned between the scaffold supports. The reinforcement cages were assembled on site, and formwork was supported on the platforms. Beam formwork and reinforcement are shown in Figure 4.13. The concrete mixture design was revised to reduce the target slump to 6 in., but the target compressive strength was the same as that used for the columns. The measured properties of the fresh and hardened concrete are reported in Section 4.5 and Appendix A.

The elevations of the beams were determined by the height of the columns supporting them. The elevations of the beam forms were set low enough that the tops of the hardened concrete in the columns were embedded in the beams, but the embedment depth of the concrete columns had to be small enough that the concrete did not interfere with the placement of the bottom steel in the beam reinforcement cages. The beam elevations were within ½ in. of the target heights, which is approximately equal to the variations in the elevation of the surrounding ground surface.

The concrete was placed in the beams using a front-end loader provided by Capital Aggregates (Figure 4.13c). The finished beams are shown in Figures 4.14 and 4.15.

The embedded steel plates, which were designed to permit the hydraulic shaker from Thumper to be attached to the beams, were positioned before the concrete was placed. The embedded plate in Bent 2 is shown in Figure 4.14(d). As discussed in Chapter 3, threaded rods were also cast in the beams. These are also shown in Figure 4.14.



(a)



(b)



(c)

**Figure 4.13 Construction of bent caps: (a) Beam reinforcement, (b) Shoring and formwork for Bent 2, (c) Placement of concrete for Bent 1**



(a)



(b)



(c)



(d)

**Figure 4.14 Completed test specimens: (a) Bent 1, (b) Bent 2, (c) Rod for pull-over test, (d) Embedded plate for connection to hydraulic shaker**

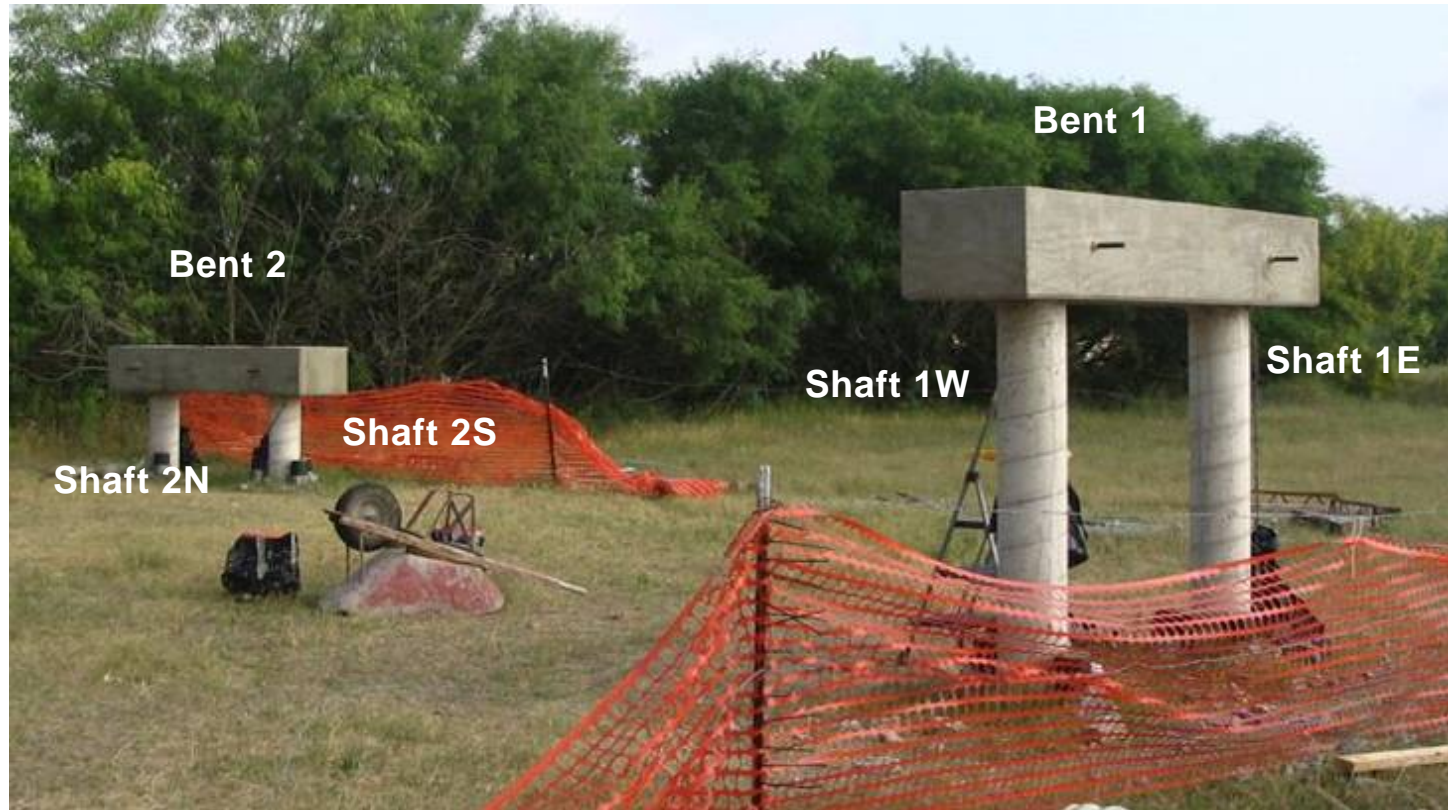


*Figure 4.15 Test site after construction of bent specimens*

#### 4.5 MEASURED PROPERTIES OF CONCRETE

Three batches of concrete were used to construct the test specimens. Concrete cylinders were cast from the same batches of concrete as the test specimens. The cylinders were stored in a fog room at 73 °F and tested approximately 28 days after casting. The average compressive strengths of each batch of concrete are reported in Table 4.1.

The compressive strengths were determined using the procedures in ASTM C39 (2005). The elastic modulus was determined using two techniques. The procedures in ASTM C 469 (2005) were used to determine the static modulus. Nondestructive tests (Malhotra and Sivasundaram, 1990) were used to assess the dynamic modulus of the concrete cylinders.

*Table 4.1 Measured concrete material properties*

Batch	Slump (in.)	Average Compressive Strength (psi)	Elastic Modulus (ksi)	
			Static	Dynamic*
Isolated Shafts	8	4820	3810	4480
Bents – Shafts	10	7190	NA	5850
Bents – Beams	7	7200	4640	5970

\* Tests performed by Kurtulus and Lee in University of Texas Soil Dynamics Laboratory

#### 4.6 MEASURED SOIL PROPERTIES

A thorough soil characterization was conducted in December 2004 (Kurtulus, et al., 2005). Two boreholes were drilled for Standard Penetration Tests (D1 and D2) and two boreholes were drilled to collect Shelby-tube samples (S1 and S2). The locations of the boreholes relative to the shafts are shown in Figure 4.16.

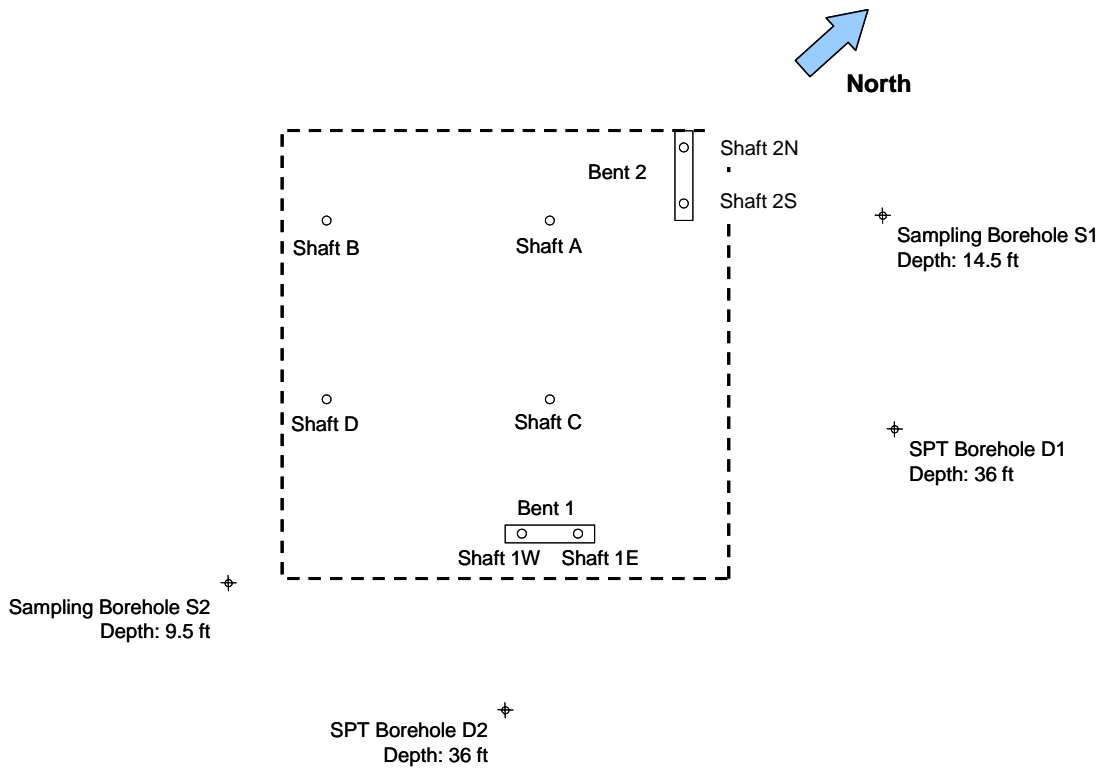


**Figure 4.16** Location of boreholes used to determine soil properties

The soil properties at the test site were similar to those at the preliminary site, but some differences were observed. The relative density and unit weight of the soil at the test site were higher than those at the preliminary site. The variations of unit weight with depth is reported in Table 4.2. An average unit weight of 112 pcf was considered to be appropriate.

The soil classification and fines content are given in Table 4.3. The fines content was also higher at the test site compared with the preliminary site. Based on this information, the soil was classified as nonplastic silt (ML), rather than silty sand (SM). The results from the standard penetration tests are given in Table 4.4 and Figure 4.17.

**Table 4.2 Summary of soil index properties (Kurtulus, et al., 2005)**

<b>Depth (ft)</b>	<b>Water Content (%)</b>	<b>Total Unit Weight (pcf)</b>	<b>Dry Unit Weight (pcf)</b>	<b>Void Ratio</b>	<b>Degree of Saturation (%)</b>
5.6	8	NA	NA	NA	NA
6.0	16	131.1	113.0	0.5	89
6.5	NA	112.3	NA	NA	NA
8.4	22	118.3	97.1	0.7	81
8.8	25	110.7	88.6	0.9	75
9.2	24	122.7	99.1	0.7	93
10.6	18	107.3	90.9	0.8	57
11.1	8	96.1	89.1	0.9	24
11.6	10	99.7	90.7	0.8	31

**Table 4.3 Soil classification and fines content (Kurtulus, et al., 2005)**

<b>Borehole</b>	<b>Depth Range (ft)</b>	<b>Soil Classification</b>	<b>Fines Content (%)</b>
D1	0 - 1.5	SM	28
	2.5 - 4.0	ML	58
	5.0 - 6.5	ML	65
	7.5 - 9.0	ML	82
	10.0 - 11.5	ML	83
	12.5 - 14.0	SM	25
D2	0 - 1.5	SM	14
	2.5 - 5.0	ML	51
	5.0 - 6.5	ML	61
	7.5 - 9.0	ML	84
	10.0 - 11.5	ML	80
	12.5 - 14.0	SM	23



*Table 4.4 Results from standard penetration tests (Kurtulus, et al., 2005)*

<b>Borehole</b>	<b>Depth (ft)</b>	<b>N<sub>SPT</sub> (bpf)</b>	<b>N<sub>60</sub> (bpf)</b>	<b>N<sub>1,60</sub> (bpf)</b>
D1	1.0	13	15	29
	3.5	8	9	18
	6.0	8	9	16
	8.5	14	16	24
	11.0	12	15	20
	13.5	19	24	29
	16.0	19	27	30
	18.5	6	9	9
	21.0	2	3	3
	23.5	22	31	28
	26.0	11	16	13
	31.0	13	19	15
	36.0	100	shale	shale
D2	1.0	12	13	27
	3.5	6	7	13
	6.0	8	9	16
	8.5	5	6	8
	11.0	13	16	17
	13.5	13	17	20
	16.0	9	13	14
	18.5	8	11	12
	21.0	10	14	14
	23.5	14	20	18
	26.0	6	9	7
	31.0	18	27	21
	36.0	100	shale	shale

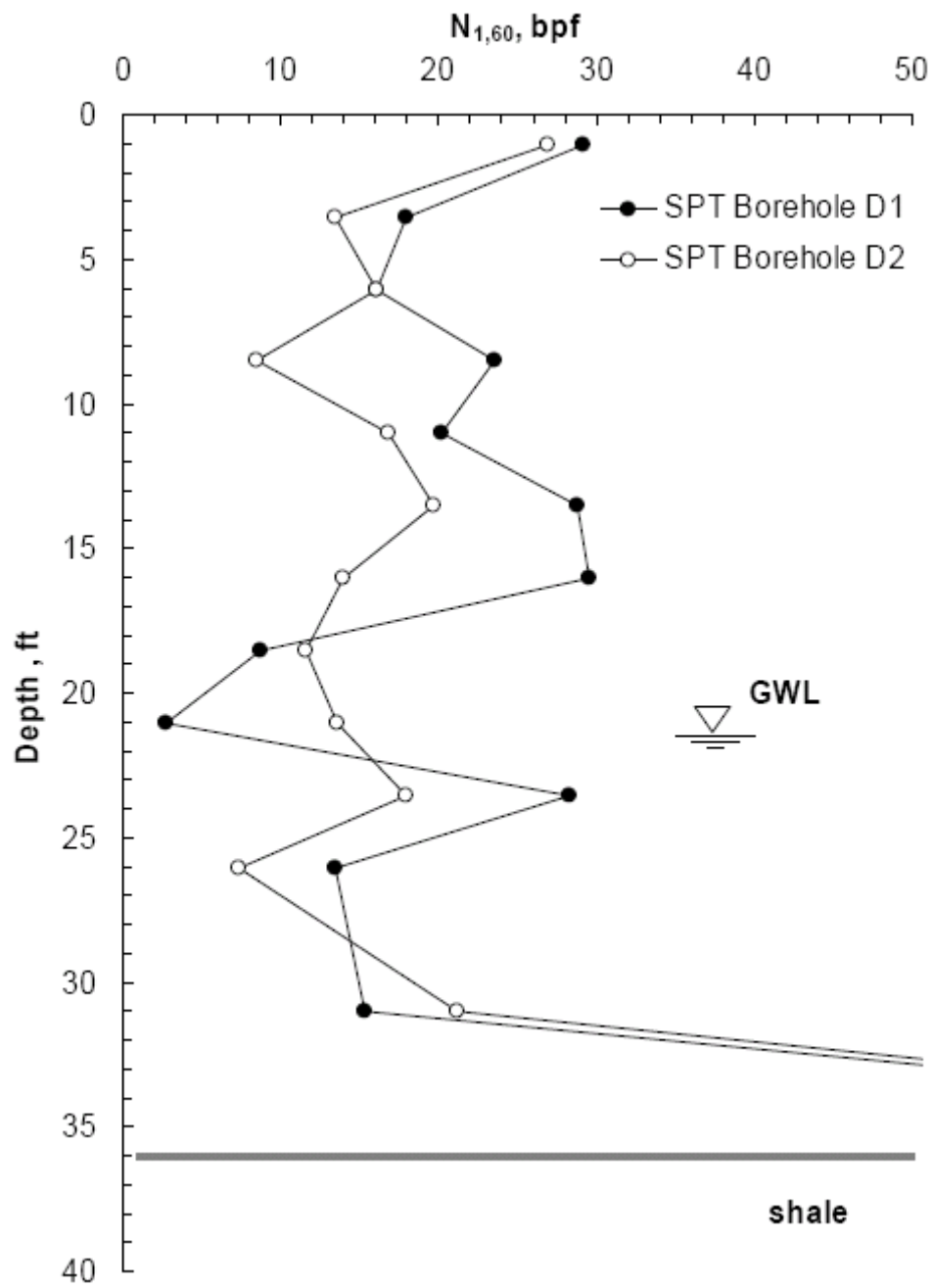


Figure 4.17 Corrected blow count profile (Kurtulus, et al., 2005)

#### **4.7 WEATHER PATTERNS**

The weather patterns in Austin varied considerably during the construction and testing of the field specimens. The fall of 2004 and winter of 2005 were cool and wet, while the late spring and early summer of 2005 were hot and dry. Although the properties of the concrete and steel do not depend on these fluctuations, the strength and stiffness of the top few feet of the soil may vary appreciably.

Weather data for a one-year period beginning 1 August 2004 recorded at the Austin-Bergstrom International Airport (NOAA, 2005) are summarized in Table 4.5 and Figure 4.18. The airport is located less than five miles from the field site.

The soil tests were performed in December 2004, after more than 16 in. of rain fell in October and November 2004. The first set of dynamic tests was conducted in June 2005 during a 4-week period with above average temperatures and no rainfall. The implications of these variations on the properties of the soil are beyond the scope of this investigation; however, the weather patterns are reported for completeness.

**Table 4.5 Summary of weather data in Austin, TX\***

Month	Temperature, °F				Total Monthly Rainfall, in.	Max. Rainfall in 24-hr Period, in.
	High	Average Daily High	Average Daily Low	Low		
Aug 2004	100	93.8	70.0	59	1.25	0.90
Sep 2004	96	90.6	66.1	57	1.17	1.00
Oct 2004	92	85.1	64.9	50	6.76	3.43
Nov 2004	83	69.7	48.2	31	9.91	4.36
Dec 2004	61	64.5	35.6	19	0.20	0.15
Jan 2005	80	64.2	43.8	25	2.44	1.45
Feb 2005	82	64.2	46.6	32	3.22	0.87
Mar 2005	88	72.5	45.7	30	3.46	1.03
Apr 2005	91	80.4	53.0	38	0.91	0.76
May 2005	97	85.8	63.5	42	3.10	1.37
Jun 2005	100	94.8	70.8	63	0.55	0.55
Jul 2005	104	96.8	72.4	67	1.78	0.47

\* Data recorded at the Austin-Begrstrom International Airport (NOAA, 2005)

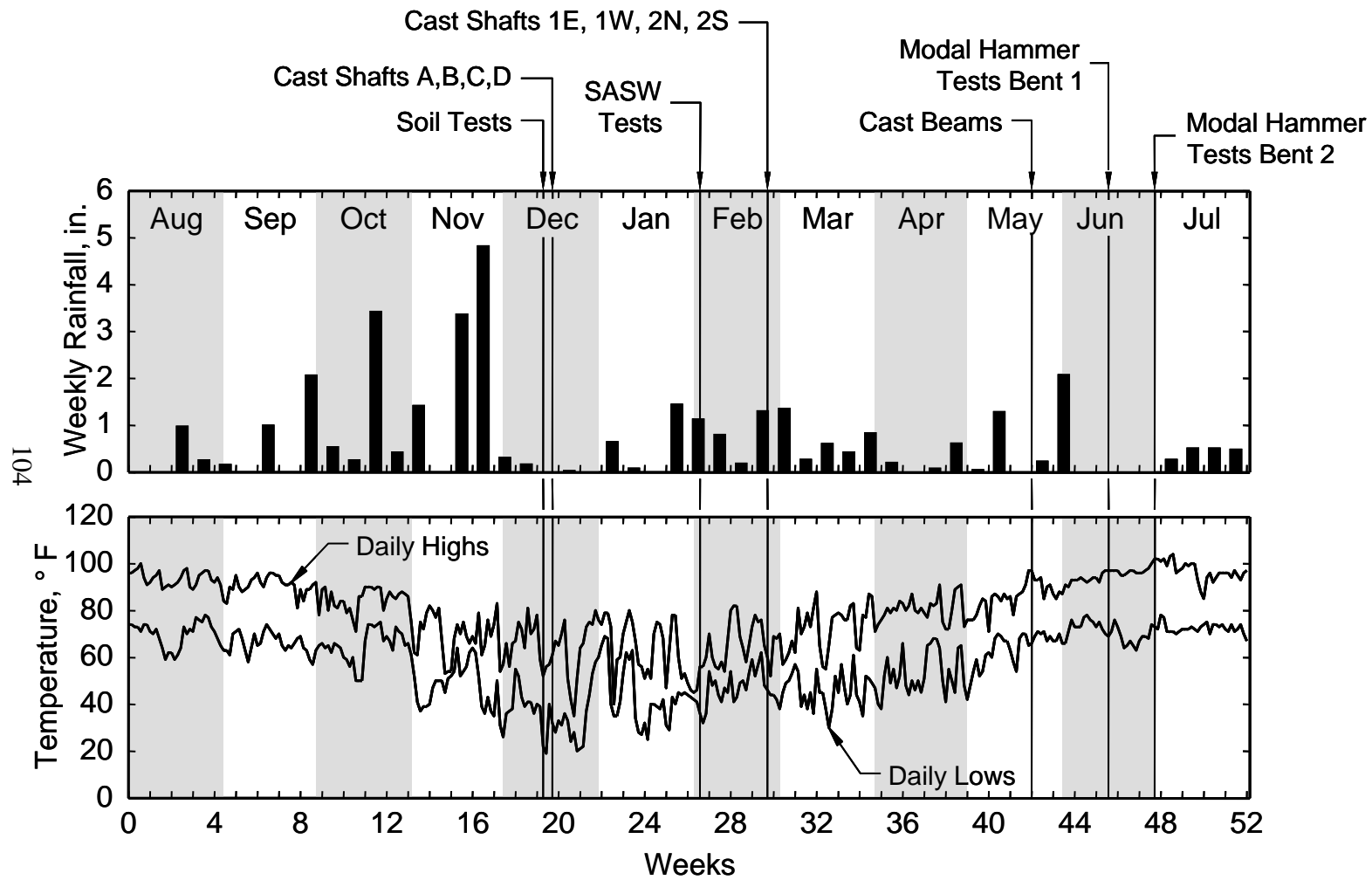


Figure 4.18 Weather data recorded at Austin Bergstrom International Airport (NOAA, 2005)

## 4.8 SUMMARY

Two bents and four isolated shafts were constructed at a field site in southeast Austin. Some significant deviations from the original design occurred during the construction phase of this project which are likely to affect the behavior of the specimens. These changes include:

- (a) The diameters of the holes for the shafts were larger than anticipated.
- (b) Partial caving of the soil within four feet of the ground surface was observed prior to placement of the concrete.
- (c) The compressive strength and modulus of elasticity of the concrete were higher than anticipated during design.
- (d) The soil was denser and had a higher fines content than assumed during design.
- (e) The soil properties were measured after a prolonged cool, wet period, while the first set of dynamic tests were conducted during a four-week hot, dry period.
- (f) The reinforcement cages may not have been aligned with the longitudinal axis of the shafts.
- (g) The longitudinal reinforcing bars slipped slightly within the cages during transportation to the site and positioning in the holes, which caused modest shifts in the locations of the strain gages.
- (h) The reinforcement cage for shaft 1W was twisted at the time that the concrete was placed.

Items (a) through (d) are likely to have the greatest effect on the specimen behavior because they involve significant changes in the stiffness of the shaft and the surrounding soil. The actual dimensions of the shafts will not be known until they are removed from the ground, however. Item (e) is likely to have an

influence on the strength and stiffness of the soil near the surface. Items (f) through (h) may influence the way that the test data are interpreted, but are not likely to change the behavior of the specimens.

The effects of the larger than expected shaft diameter, the increased soil stiffness, and the increase in concrete modulus on the specimen response is evaluated in Chapter 5 and Chapter 6.

## **CHAPTER 5**

### **Calculated Frequency Response of As-Built Specimens**

#### **5.1 OVERVIEW**

As discussed in Chapter 4, the cross-sectional dimensions of the as-built shafts were considerably larger than those assumed during design. In addition, the design calculations were based on the measured soil properties approximately 200 ft west of the final site. The concrete was also stronger than anticipated during design. All of these changes influenced the frequency response of the test specimens. A series of analyses are presented in this chapter with the goal of reproducing the measured frequency response of the bents.

Section 5.2 describes the soil parameters used to model the final site and Section 5.3 describes the cross-sectional and structural materials properties used to represent the as-built specimens. Modal hammer tests were used to determine the natural frequencies of the test specimens for low-amplitude excitations. Those tests are described briefly in Section 5.4. The calculated natural frequencies using the updated material properties are compared with the measured response in Section 5.5. In all cases, the calculated frequencies were less than the measured frequencies. The results of several parametric studies are presented in Section 5.6 in an attempt to bound the measured frequency response. The sensitivity of the calculated natural frequencies to the modulus of elasticity of the concrete, the shaft diameter, the subgrade modulus of the soil, and the variation of soil stiffness with depth is presented.



## 5.2 REVISED SOIL PARAMETERS

The results of the soil characterization studies at the test site are documented in Section 4.6. As discussed in Section 3.3.3, the model developed by Reese, et al. (1974) for sand above the water table was used to represent the soil at the site. Three parameters are used in this model and the values are reported in Table 5.1. The selection of these parameters is described below.

**Table 5.1** *Soil parameters used to analyze the as-built specimens*

Subgrade Modulus, $k$	225 lb/in. <sup>3</sup>
Friction Angle, $\phi$	42°
Unit Weight, $\gamma$	112 lb/ft <sup>3</sup>
Cohesion, $c$	0
Soil Classification	ML – Nonplastic Silt

As discussed in Section 4.7 the modal hammer tests were conducted during a month-long period of above-average temperature with no rainfall. Therefore, the value of the subgrade modulus was selected based on recommendations for desiccated sand (Isenhower, 2005). The friction angle,  $\phi$ , was estimated using the procedure described in Section 2.5, and the data are plotted in Figure 5.1. An average friction angle of 42° was assumed. As reported in Section 4.6, the unit weight was assumed to be 112 lb/ft<sup>3</sup>. The cohesion,  $c$ , was taken as zero, and the soil was classified as nonplastic silt.

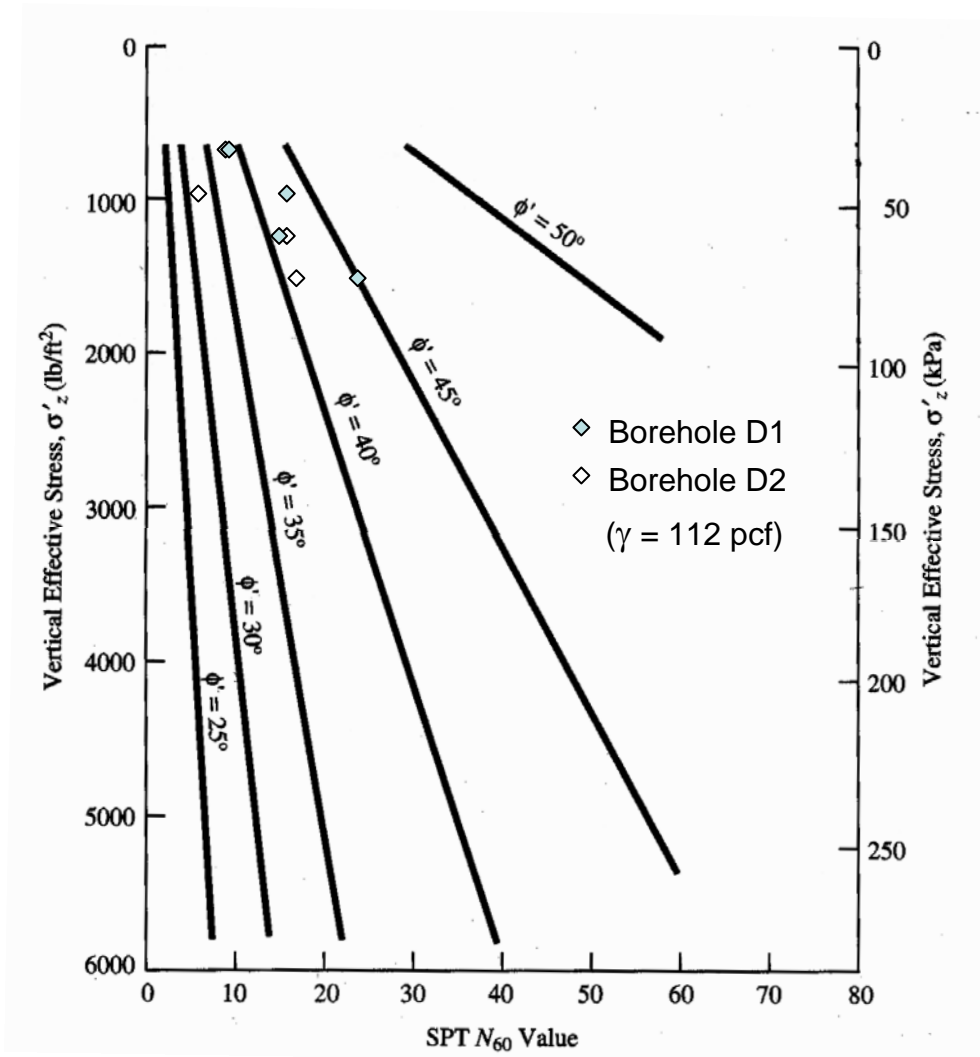
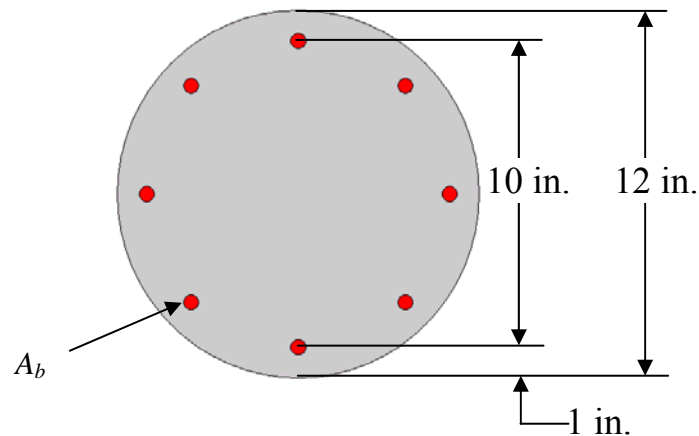


Figure 5.1 Effective friction angle from SPT  $N_{60}$  values (DeMello, 1971)

## 5.3 REVISED PROPERTIES OF SHAFTS AND COLUMNS

### 5.3.1 Arrangement of Longitudinal Reinforcement

As discussed in Section 4.2, the longitudinal reinforcement was bundled into eight pairs of #3 bars which were uniformly distributed around the perimeter of the cross section. This change was made to facilitate placement of the concrete. The idealized cross section used to calculate the moment-curvature response of the column is shown in Figure 5.2, where  $A_b$  is taken as 0.22 in.<sup>2</sup>



**Figure 5.2** Column cross section used to analyze the as-built specimens

*As discussed in Section 4.3, the diameters of the shafts were considerably larger than anticipated and the holes were irregularly shaped near the surface (Figure 4.5). For the analyses of the as-built specimens, the cross section of the shaft*

*was assumed to be circular with a diameter of 18 in.*

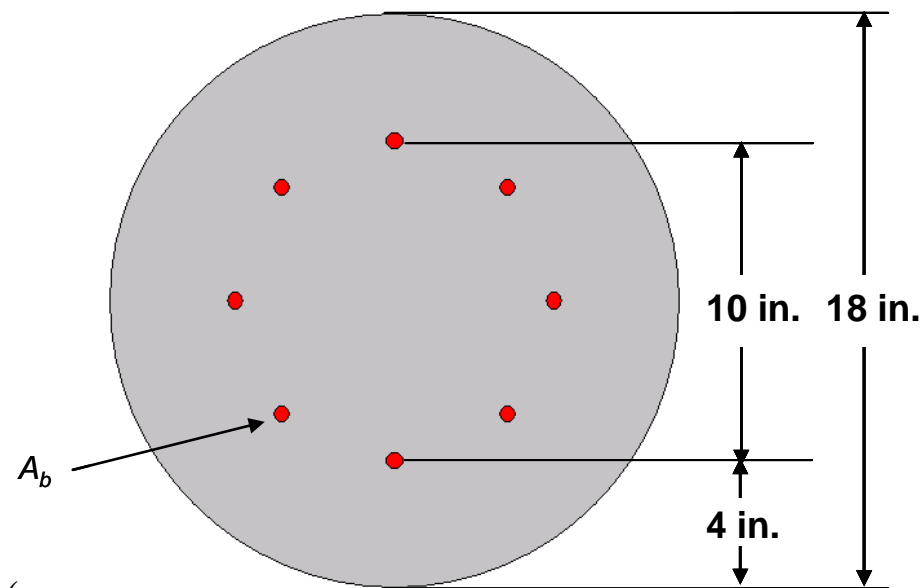


(  
Figure 5.3). The reinforcement cage was assumed to be centered along the longitudinal axis of the shaft.

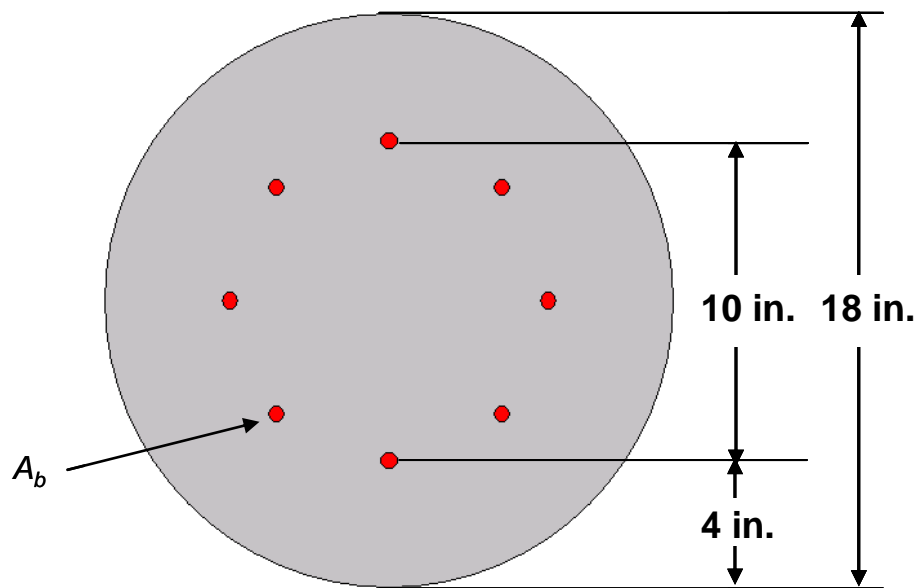


**Figure 5.3 Shaft cross section used to analyze the as-built specimens**

### **5.3.2 Structural Material Properties**

An average concrete compressive strength of 7200 psi was selected for the analyses (Table 4.1). The measured static elastic modulus of 4640 ksi was also assumed. The average measured yield stress of the longitudinal reinforcement was 60.8 ksi; therefore, the nominal value of 60 ksi was used in the calculations.

#### **5.4 MODAL HAMMER TESTS**

The test specimens were excited using a modal hammer to determine the initial frequency response. The specimens were struck with the modal hammer in both the longitudinal and transverse directions of the bridge (Figure 5.4). The impact caused essentially free-vibration response of the specimens.

Three-component accelerometers and geophones were attached to the beam and measured the response. Data were recorded in both the frequency and time domains. Evaluation of these records is beyond the scope of this thesis, but the measured natural frequencies of the first two modes are reported in Table 5.2 for both test specimens.



(a)



(b)

***Figure 5.4 Modal hammer tests on bent 2: (a) Excitation in transverse direction of bridge, (b) Excitation in longitudinal direction of bridge***

**Table 5.2 Measured natural frequencies of specimens during modal hammer tests (Agarwal, 2005)**

<b>Specimen</b>	<b>Date of Test</b>	<b>Mode *</b>	<b>Frequency (Hz)</b>
Bent 1	16 June 2005	1	8.5
		2	16.5
Bent 2	1 July 2005	1	16.6
		2	30.0

\* Mode 1 corresponds to longitudinal direction of bridge. Mode 2 corresponds to transverse direction of bridge.

## **5.5 CALCULATED RESPONSE OF AS-BUILT SPECIMENS**

The SAP model that was used to calculate the natural frequencies during design (Section 3.4) was revised using the dimensions and material properties corresponding to the as-built specimens. The soil spring constants with depth were calculated using a subgrade modulus of 225 lb/in.<sup>3</sup> (Table 5.3). The modulus of elasticity for the concrete was taken as 4640 ksi in these analyses.

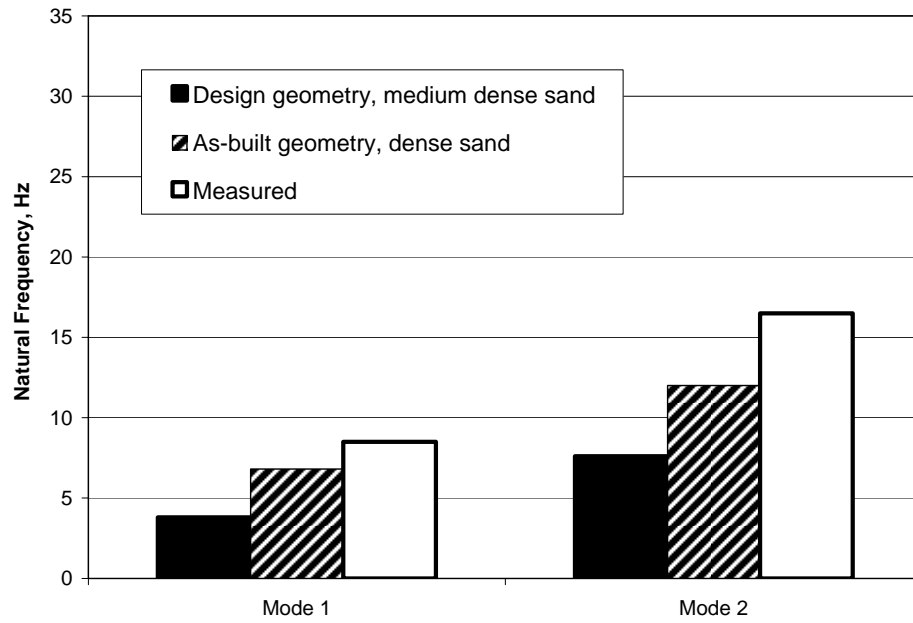


**Table 5.3 Soil spring constants used for modal analyses of as-built specimens**

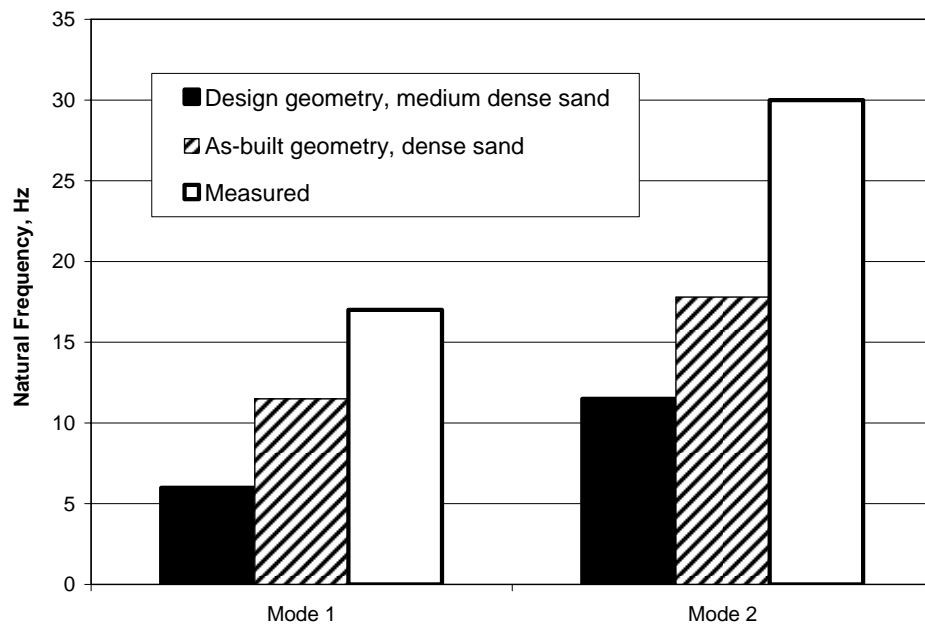
Depth below Grade (ft)	Spring Constant* (k/in.)
0.5	16.2
1.5	48.6
2.5	81.0
3.5	113.4
4.5	145.8
5.5	178.2
6.5	210.6
7.5	243.0
8.5	275.4
9.5	307.8
10.5	340.2
11.5	372.6

\* Subgrade modulus,  $k_s = 225 \text{ lb/in.}^3$

The calculated frequencies of the as-built specimens are reported in Table 5.4. The values are compared with the measured frequencies and the frequencies calculated during design for medium-density sand in Figure 5.5. As expected, the calculated frequencies for the as-built specimens were considerably higher than the frequencies calculated during design. All the changes to the model to represent the as-built conditions – stiffer soil springs, increased modulus of elasticity for concrete, and increased shaft diameter – increased the stiffness of the models. However, the measured natural frequencies of the two specimens were considerably higher than the calculated values, indicating that the soil and/or the structure were stiffer than represented in this model.



(a)



(b)

**Figure 5.5 Comparison of calculated and measured natural frequencies:  
(a) Bent 1, (b) Bent 2**

**Table 5.4** *Calculated frequencies of as-built specimens*

<b>Specimen</b>	<b>Natural Frequencies (Hz)</b>	
	Mode 1	Mode 2
Bent 1	6.8	12.0
Bent 2	11.5	17.0

## **5.6 SENSITIVITY ANALYSES**

### **5.6.1 Overview**

As discussed in Section 5.5, the initial attempts to model the frequency response of the as-built specimens were too flexible. Four parameters that influence the calculated stiffness of the bents were selected for further investigation:

- Modulus of elasticity of concrete,  $E_c$
- Subgrade modulus of soil,  $k$
- Diameter of shaft,  $D$
- Variation of soil stiffness with depth

Each of these parameters was varied to determine the sensitivity of the calculated frequencies to the value of the parameter. A second goal was to determine if the measured frequencies could be bounded using reasonable combinations of the four parameters.

Because low-amplitude vibrations were induced during the modal hammer tests and no damage had occurred in either the soil or the structure at the time of these tests, only the elastic response of the specimens was modeled in the sensitivity analyses. Therefore, all calculations were based on the gross cross-sectional properties of the members and the initial, linear portion of the  $p$ - $y$  curves for the soil.

Reasonable ranges for the input parameters are presented in Section 5.6.2. The sensitivity of the calculated frequencies for Bent 1 to variations in each of the parameters is discussed in Section 5.6.3. Multiple parameters are varied in the analyses presented in Section 5.6.4 to determine if the measured frequencies of both bents can be reproduced with the SAP models.

## **5.6.2 Range of Parameters Considered**

### ***5.6.2.1 Modulus of Elasticity of Concrete***

Three values of the modulus of elasticity of the concrete were considered: 3600 ksi, 4640 ksi, and 5850 ksi. The lowest value corresponds to the material properties assumed during design of the specimens (Table 2.5) and is the value typically assumed for concrete with a compressive strength of 4000 psi. The middle value corresponds to the average measured modulus under static loading and the highest value corresponds to the average measured value under low-amplitude dynamic loading (Table 4.1).

### ***5.6.2.2 Subgrade Modulus of Soil***

Three values of subgrade modulus were considered. Isenhower (2005) recommended using a value of 225 lb/in.<sup>3</sup> for desiccated sand above the water table (Table 2.3). Values of 175 lb/in.<sup>3</sup> and 275 lb/in.<sup>3</sup> were selected to provide a reasonable range for the sensitivity studies.. The corresponding values of the soil spring constants are given in Table 5.5.

**Table 5.5 Soil spring constants used in sensitivity studies to evaluate influence of subgrade modulus**

Depth below Grade (ft)	Spring Constant (k/in.)	
	$k = 175 \text{ lb/in.}^3$	$k = 275 \text{ lb/in.}^3$
0.5	12.6	19.8
1.5	37.8	59.4
2.5	63.0	99.0
3.5	88.2	138.6
4.5	113.4	178.2
5.5	138.6	217.8
6.5	163.8	257.4
7.5	189.0	297.0
8.5	214.2	336.6
9.5	239.4	376.2
10.5	264.6	415.8
11.5	289.8	455.4

### 5.6.2.3 Diameter of Shafts

As discussed in Section 4.3, the diameter of the shafts was approximately 18 in. at the ground surface and the shape varied with depth. Values of 16 in. and 20 in. were considered to be reasonable bounds to the diameter of the holes. No attempt was made to model a shaft with an irregular cross section.

### 5.6.2.4 Vertical Distribution of Soil Stiffness

The decision to vary the distribution of the soil stiffness is perhaps the most controversial, because it represents a significant deviation from common assumptions made during design. Typically, the stiffness of sand is assumed to be zero at the ground surface and to increase linearly with depth (Eq. 3.4). However, two observations indicate that this assumption may not be an appropriate representation of the conditions at the test site:

- The measured shear wave velocity profiles (Figure 5.6) indicate a nonzero soil stiffness at the ground surface.
- The modal hammer tests were conducted during a four-week period of above average temperatures and zero rainfall at the site (Figure 4.18). Increased soil stiffness near the ground surface could be attributed to desiccation of the soil.

Spectral-analysis-of-surface-waves (SASW) tests were conducted at the field site along two perpendicular arrays on 3 February 2005 (Kurtulus, et al., 2005). The two shear wave velocity profiles (Figure 5.6) are essentially the same, indicating essentially uniform soil conditions at the site.

Although no direct correlation is made between the measured shear wave velocities and the values of initial soil stiffness, the profile in Figure 5.6 was used to develop an idealized distribution of initial soil stiffness with depth. As discussed in Section 3.3.3, the initial stiffness of the  $p$ - $y$  curves is typically assumed to be:

$$K_i(x) = k \cdot x \quad (5.1)$$

where

$$K_i(x) = \text{initial stiffness of } p\text{-}y \text{ curve at depth } x, \text{ lb/in.}^2$$

$$k = \text{soil subgrade modulus, lb/in.}^3$$

Equation 5.1 is represented graphically in Figure 5.7(a).

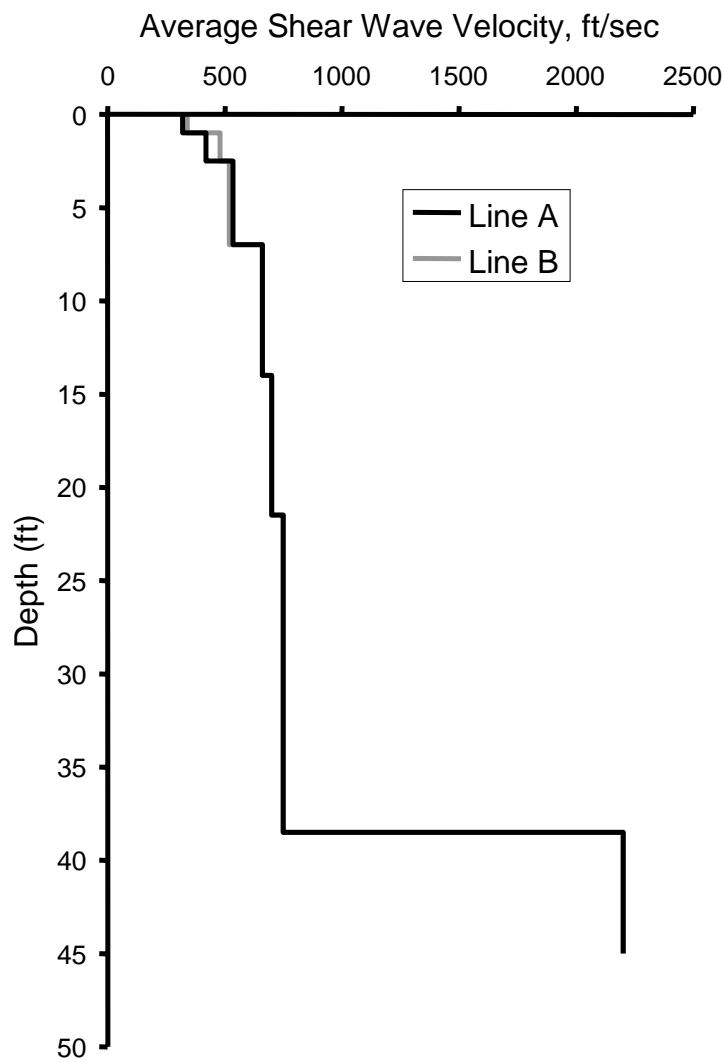


*Figure 5.6 Measured shear wave velocity profiles for test site (Kurtulus, et al., 2005)*

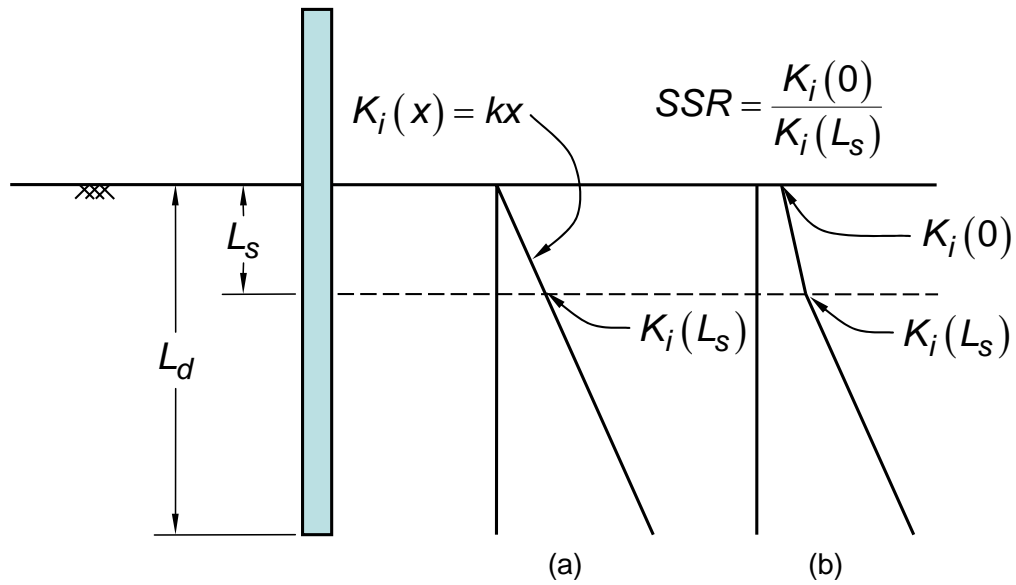


**Figure 5.7** Variation of initial soil stiffness with depth: (a) typical design assumption, (b) idealized distribution for field site

The assumed distribution of soil stiffness at the field site is shown in Figure 5.7(b). The soil stiffness is greater than zero at the surface and the variation with depth is modeled using two linear segments. Two parameters are required to define this distribution: the depth of the soil that is assumed to have an increased initial stiffness,  $L_s$ , and the relative stiffness of the soil at the surface. The soil stiffness ratio,  $SSR$ , is defined in Eq. 5.2:

$$SSR = \frac{K_i(0)}{K_i(L_s)} \quad (5.2)$$

where

$K_i(0)$  = assumed initial stiffness of  $p$ - $y$  curve at surface

$K_i(L_s)$  = initial stiffness of  $p$ - $y$  curve at  $L_s$

The value of  $K_i(L_s)$  is calculated using Eq. 5.1, and the initial stiffness of the soil is assumed to vary linearly between the ground surface and  $L_s$ .



Two values of  $L_s$  were considered in the sensitivity study: 3 ft and 6 ft. These values were assumed to bound the depths where desiccation of the soil was present during June 2005. Three values of  $SSR$  were considered: 0.0, 0.375, and 0.75. A value of 0.0 corresponds to the variation of soil stiffness typically used in design (Eq. 5.1 and Figure 5.9a). The other two values were selected arbitrarily.

Values of the spring constants used in the SAP analyses for various combinations of  $L_s$  and  $SSR$  are summarized in Table 5.6. The subgrade modulus,  $k$ , was taken as 225 lb/in.<sup>3</sup> in all cases.

The soil spring constants are the same for all analyses for depths below  $L_s$ . In addition, the soil spring constants do not depend on  $L_s$  when  $SSR$  is taken as zero.

**Table 5.6 Soil spring constants used in sensitivity studies to evaluate influence of vertical distribution of soil stiffness**

Depth below Grade (ft)	Spring Constant* (k/in.)				
	SSR=0	$L_s = 3$ ft		$L_s = 6$ ft	
		SSR=0.375	SSR=0.75	SSR=0.375	SSR=0.75
0.5	16.2	46.6	77.0	83.0	149.9
1.5	48.6	66.8	85.1	103.3	158.0
2.5	81.0	87.1	93.2	123.5	166.1
3.5	113.4	113.4	113.4	143.8	174.2
4.5	145.8	145.8	145.8	164.0	182.3
5.5	178.2	178.2	178.2	184.3	190.4
6.5	210.6	210.6	210.6	210.6	210.6
7.5	243.0	243.0	243.0	243.0	243.0
8.5	275.4	275.4	275.4	275.4	275.4
9.5	307.8	307.8	307.8	307.8	307.8
10.5	340.2	340.2	340.2	340.2	340.2
11.5	372.6	372.6	372.6	372.6	372.6

\*  $k = 225$  lb/in.<sup>3</sup>

### 5.6.3 Results of Sensitivity Studies for Bent 1

The results from four series of analyses of Bent 1 are described in this section. Each of the parameters presented in Section 5.6.2 are varied independently in a set of analyses and the results are compared with the measured natural frequencies. The results are summarized in Tables 5.7 through 5.10 and Figure 5.8 through Figure 5.11.

Of the four parameters considered, the modulus of elasticity of the concrete,  $E_c$ , is the only one that affects the stiffnesses of both the columns and the shafts. Because the lateral stiffness of the bents is expected to be directly related to the flexural stiffnesses of the columns and shafts, the natural frequencies of the bent would be expected to increase as a function of the square root of  $E_c$ . This trend may be observed in Figure 5.8

**Table 5.7 Sensitivity of calculated natural frequencies for Bent 1 to modulus of elasticity of concrete**

Modulus of Elasticity of Concrete (ksi)	Calculated Natural Frequencies* (Hz)	
	Mode 1	Mode 2
3600	6.1	11.0
4640	6.8	12.0
5850	7.4	12.9

\*  $k = 225 \text{ k/in.}^3$ ,  $D = 18 \text{ in.}$ ,  $SSR = 0$

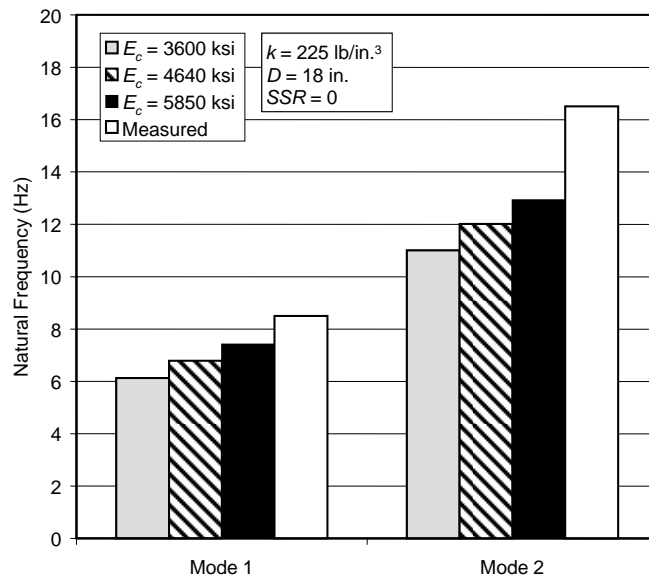


**Figure 5.8** Calculated variation in natural frequencies with concrete modulus

In contrast, the soil subgrade modulus,  $k$ , only affects the stiffness of the soil. In addition, if the soil stiffness ratio,  $SSR$ , is assumed to be zero, then varying the value of  $k$  has very little influence on the stiffness at the top of the shaft. As shown in Figure 5.9, the calculated frequencies increased with increasing  $k$ , but the range of the variations was significantly less than that for varying  $E_c$ .

**Table 5.8** Sensitivity of calculated natural frequencies for Bent 1 to subgrade modulus

Subgrade Modulus (lb/in. <sup>3</sup> )	Calculated Natural Frequencies* (Hz)	
	Mode 1	Mode 2
175	6.6	11.5
225	6.8	12.0
275	6.9	12.4

\*  $E_c = 4640$  ksi,  $D = 18$  in.,  $SSR = 0$

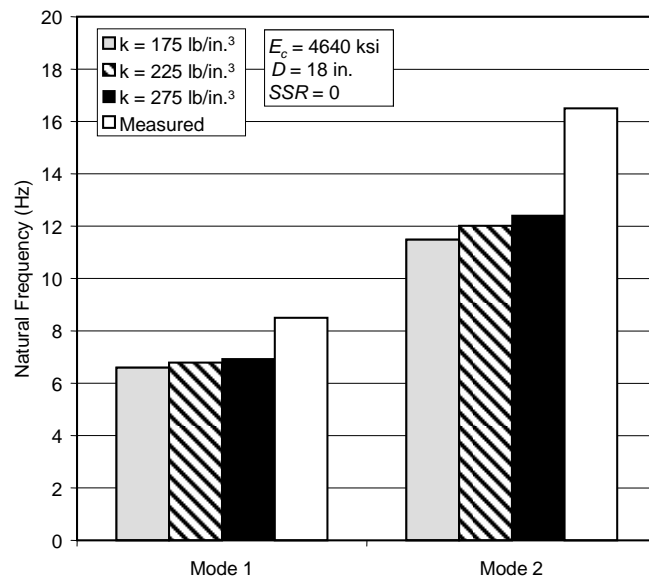


**Figure 5.9** Calculated variation in natural frequency with subgrade modulus

Varying the diameter of the shaft,  $D$ , also influences only the stiffness of the foundation. However, unlike the subgrade modulus, increasing  $D$  increases the stiffness of the shaft along its entire length. Therefore, the stiffness of the foundation is increased near the surface, where the impact on the frequency response of the bent is higher (Figure 5.10). The natural frequencies of the bent are more sensitive to changes in  $D$  than  $k$ , but less sensitive to changes in  $D$  than  $E_c$ .

**Table 5.9** Sensitivity of calculated natural frequencies for Bent 1 to diameter of shaft

Diameter of Shaft (in.)	Calculated Natural Frequencies* (Hz)	
	Mode 1	Mode 2
16	6.2	11.2
18	6.8	12.0
20	7.2	12.7

\*  $E_c = 4640$  ksi,  $k = 225$  k/in.<sup>3</sup>,  $SSR = 0$

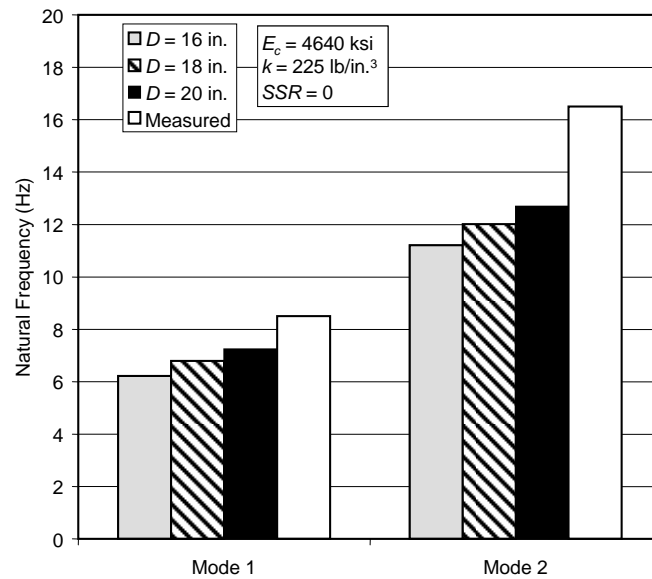


**Figure 5.10** Calculated variation in natural frequency with diameter of shaft

Unlike the subgrade modulus, the parameters  $L_s$  and  $SSR$  have a significant influence on the stiffness of the soil near the surface. As a result, the calculated natural frequencies are more sensitive to the choice of  $L_s$  and  $SSR$  (Figure 5.11) than to  $k$ . Although all the calculated natural frequencies in the four series of sensitivity analyses were less than the measured values, the frequencies corresponding to increased soil stiffness near the surface were closest to the measured values.

**Table 5.10** Sensitivity of calculated natural frequencies for Bent 1 to vertical distribution of soil stiffness

$L_s$ (ft)	$SSR$	Calculated Natural Frequencies* (Hz)	
		Mode 1	Mode 2
—	0.0	6.8	12.0
3	0.375	7.1	12.8
	0.75	7.3	13.4
6	0.375	7.4	13.7
	0.75	7.7	14.6

\*  $E_c = 4640$  ksi,  $k = 225$  k/in.<sup>3</sup>,  $D = 18$  in.

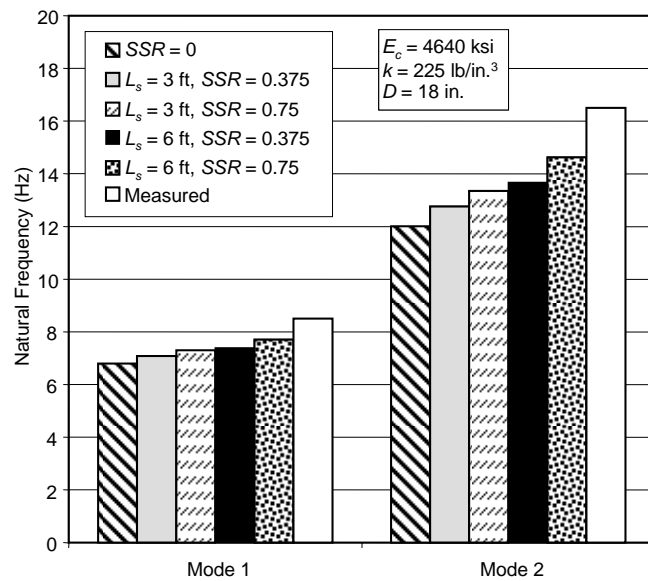


**Figure 5.11** Calculated variation in natural frequency with vertical distribution of soil stiffness

#### 5.6.4 Bounding the Measured Frequency Response of Bents

As discussed in the previous section, it was not possible to match the measured frequency response of Bent 1 by changing a single parameter. In all cases, the calculated frequencies were less than the measured values. However, by selecting appropriate combinations of parameters, it was possible to calculate frequencies that were slightly higher than the measured values in most cases.

The combination of increasing the modulus of elasticity of the concrete, increasing the diameter of the shaft, and assuming that the soil in the top 6 ft was stiffer than anticipated due to desiccation, was sufficient to bound the measured frequencies for the first and second modes for Bent 1 (Figure 5.12 and Table 5.11). This combination of parameters was considered to be reasonable given the low amplitude of the excitations induced during the modal hammer tests.

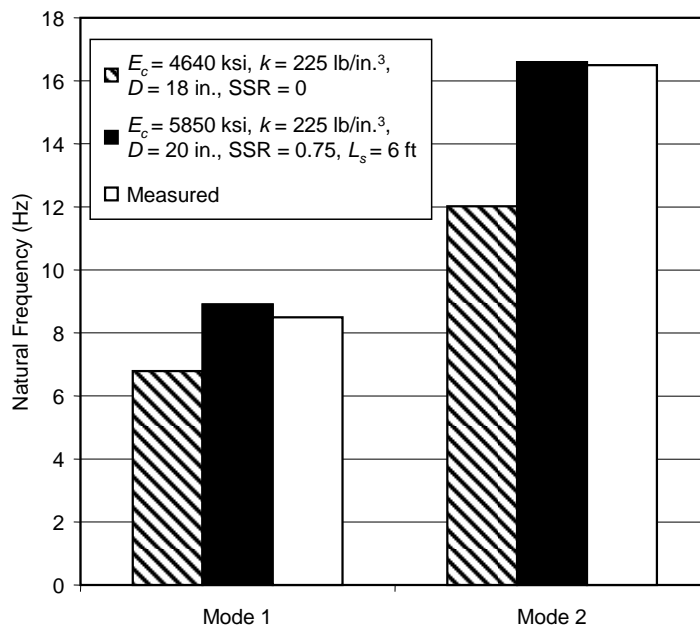


**Figure 5.12** Combinations of parameters used to bound the measured natural frequencies for modes 1 and 2 for Bent 1

**Table 5.11** Combinations of parameters used to bound the measured natural frequencies for modes 1 and 2 for Bent 1 and mode 1 for Bent 2

Bent	$E_c$ (ksi)	$D$ (in.)	$L_s$ (ft)	$SSR$	Calculated Natural Frequencies* (Hz)	
					Mode 1	Mode 2
1	4640	18	—	0.0	6.8	12.0
	5850	20	6	0.75	8.9	16.6
2	4640	18	—	0	11.5	17.8
	5850	20	6	0.75	16.6	26.2

\*  $k = 225$  k/in.<sup>3</sup>

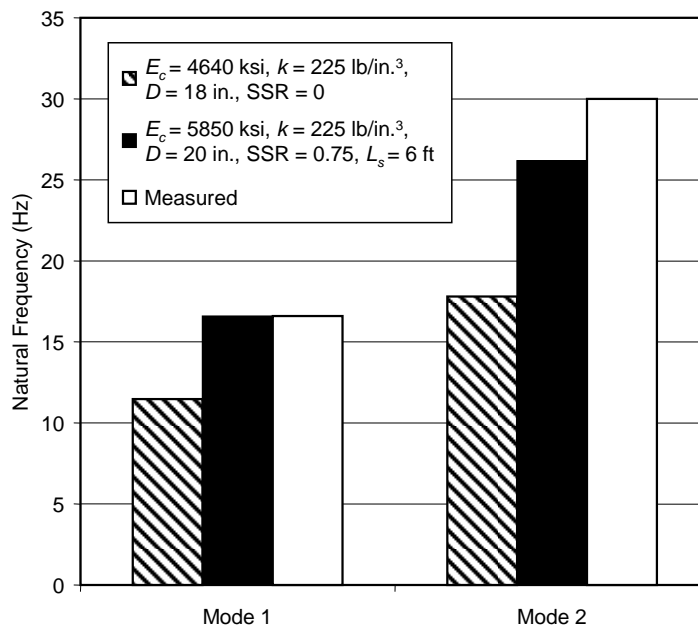


**Figure 5.13** *Combinations of parameters used to bound the measured natural frequency for mode 1 for Bent 2*

For Bent 2, however, the same combination of parameters was not sufficient to bound the measured frequency for the second mode (Figure 5.13 and Table 5.11). The measured frequency for the first mode was well-represented using these parameters, however.

In subsequent dynamic tests using T-Rex, the measured natural frequencies of both bents decreased significantly (Table 5.12). Although a thorough discussion of these data is beyond the scope of this thesis, the results indicate that the measured natural frequencies are very sensitive to the level of excitation. No rainfall was recorded at the test site between the dates of the modal hammer tests and the dynamic tests using T-Rex, and no evidence of damage was observed in the concrete or in the soil. Therefore, these differences can not be attributed to changes in the material properties.



**Table 5.12 Measured natural frequencies of specimens during ground excitation tests with T-Rex (Agarwal, 2005)**

<b>Specimen</b>	<b>Date of Test</b>	<b>Mode</b>	<b>Frequency (Hz)</b>
Bent 1	28 June 2005	1	6.5
		2	11.5
Bent 2	7 July 2005	1	14.6
		2	23.0

The only significant change was the amplitude of the vibrations in the test specimens. When excited at the fundamental natural frequency, the amplitudes of the peak accelerations and velocities measured at the bent cap were at least an order of magnitude higher during the ground excitation tests than the modal hammer tests. The natural frequencies plotted in Figure 5.12 and Figure 5.13, therefore, provide reasonable bounds to the measured frequency response of the test specimens.

## **5.7 SUMMARY**

In this chapter, two-dimensional models of the test specimens were updated to account for the as-built geometry of the specimens, the measured properties of the soil at the site, and the measured properties of the concrete. All of these changes increased the calculated stiffness of the specimens compared with the assumptions made during design (Chapter 3). The dynamic properties of the specimens were evaluated through low-amplitude impact testing with a modal hammer. Despite the increased stiffness of the updated models, the calculated frequencies were still much lower than those measured in the field.

In an attempt to better understand the reasons for the differences between measured and calculated frequencies, a parametric study was performed to determine the sensitivity of the calculated response to four parameters that affect

the stiffness of the specimens: shaft diameter, elastic modulus of concrete, subgrade modulus, and shape of the soil stiffness profile. The calculated frequency response was most sensitive to parameters that affected the stiffness of the soil-foundation system near the ground surface.

For that reason, the subgrade modulus was shown to be the smallest influence on the calculated frequencies. Because the soil stiffness is taken as zero at the ground surface for design regardless of the density of the soil, a large change in subgrade modulus causes a negligible change in soil stiffness near the surface. In contrast, the behavior of the system was most sensitive to changes in the shape of the soil stiffness profile, because, by definition, the stiffness of the soil near the surface was increased dramatically. Increases in modulus of the concrete and shaft diameter also led to increased frequencies.

In an attempt to bound the measured frequencies, the stiffness parameters were then combined, with moderately successful results. Three of the four natural frequencies determined from the modal hammer tests were bounded by the calculated frequencies when the combination of the increasing the modulus of elasticity of the concrete, increasing the diameter of the shaft, and assuming that the soil in the top 6 ft was stiffer than anticipated were considered in the analyses.

## **CHAPTER 6**

### **Lateral Capacity of As-Built Specimens**

#### **6.1 OVERVIEW**

The analyses presented in Chapter 5 focused on the low-amplitude, dynamic response of the test specimens. In contrast, the analyses presented in this chapter address the response of the specimens during static, pull-over tests. Large strains are expected in the soil, foundation, and columns during these tests. Unlike the dynamic test, the pull-over tests have not yet been conducted, and therefore, the actual response of the specimens is not known. The analyses described in this chapter represent predictions which are based on the results of the analyses presented in Chapter 5. LPile was used for all the analyses presented in this chapter.

A single set of parameters was selected to represent the geometry of the structural members, the concrete material properties, and the strength and stiffness of the soil. These parameters are described in Section 6.2. The updated moment-curvature relationships for the columns and shafts are presented in Section 6.3, and the calculated force-displacement relationships are discussed in Section 6.4. Although it was originally envisioned that the pull-over tests would be conducted in the transverse direction of the bridge, results are presented for lateral forced in both the longitudinal and transverse directions. Testing in the longitudinal direction may be necessary due to limits on the lateral forces that can be developed in the field.

## **6.2 SOIL AND SPECIMEN PROPERTIES**

The LPile models used to design the test specimens (Section 3.3) were updated to reflect the as-built dimensions of the shafts, the measured properties of the concrete, and the measured soil properties at the field site. Unlike the analyses presented in Chapter 5, the analyses discussed in this chapter are intended to capture the large-strain response of the specimens and the surrounding soil. In addition, the input parameters were selected to provide an upper bound to the lateral strength of the specimens so that the loading apparatus for the pull-over tests could be designed.

The results of the pull-over analyses are sensitive to three factors: (a) the flexural capacity of the shaft, (b) the flexural capacity of the column, and (c) the locations of the plastic hinges. The flexural capacities of the columns and shafts depend only on the cross-sectional dimensions and the concrete material properties. However, the locations of the flexural hinges depend on the strength and stiffness of the soil and the clear height of the column. The selection of the input parameters are described briefly in the sections below and the final values are summarized in Table 6.1.

### **6.2.1 Shaft Diameter**

As discussed in Section 4.3, the cross section of the shafts varied with depth and the actual dimensions are not known. The shafts were idealized as having a circular cross section in Section 5.6, and the average diameter is believed to be between 18 and 20 in. A diameter of 20 in. was selected for the pull-over analyses to provide an upper bound to the calculated flexural capacity of the shafts.

**Table 6.1 Soil and Specimen properties used for as-built lateral analysis**

Shaft Diameter, $D$	20 in.
Concrete Compressive Strength, $f'_c$	7200 psi
Subgrade Modulus, $k$	225 pci
Soil Stiffness Ratio, $SSR$	0

### **6.2.2 Concrete Material Properties**

As discussed in Section 4.5, the average compressive strength of the concrete in the columns and shafts was 7200 psi. This value was used in the LPile analyses, and the modulus of elasticity of the concrete was estimated from the compressive strength using Eq. 3.2. The value of  $E_c$  used in the LPile analyses was 4840 ksi, which is approximately equal to the measured value of 4640 ksi determined from static tests.

### **6.2.3 Soil Properties**

The soil at the field site was represented using the model developed by Reese, et al. (1974) for sand. The soil affects the magnitude of the applied lateral force required to form a mechanism in the bents because the location of the plastic hinges depends on the assumed soil properties. If the soil is assumed to be stiff and strong, the soil reaction is concentrated over a relatively short length of the shaft and the maximum moment in the shaft will be located near the ground surface. As the stiffness and strength of the soil decreases, the depth of the maximum moment increases. The depth of the maximum moment is important because the applied force required to form a mechanism in the bent increases as the distance between the maximum moment in the shaft and the applied force decreases. Therefore, the soil was assumed to be stiff (subgrade modulus of

225 pci) such that the maximum moment in the shaft would be located near the ground surface.

Although it was necessary to change the shape of the soil stiffness profile in Chapter 5 to bound the frequency response of the specimens, such a change was not considered to be appropriate for the pull-over analyses. The strains induced during the modal hammer tests were extremely small, and the soil was still in the linear range of response. Changing the shape of the assumed soil stiffness profile, therefore, only involved scaling the initial portion of the  $p$ - $y$  curves. If, however, the lateral deflections of the soil exceed the proportional limit, many more assumptions must be made regarding the shape of the  $p$ - $y$  curves. These assumptions are beyond the scope of this investigation. Therefore, the initial stiffness of the soil is assumed to vary linearly with depth ( $SSR=0$ ). Representative  $p$ - $y$  curves are shown in Figure 6.1.

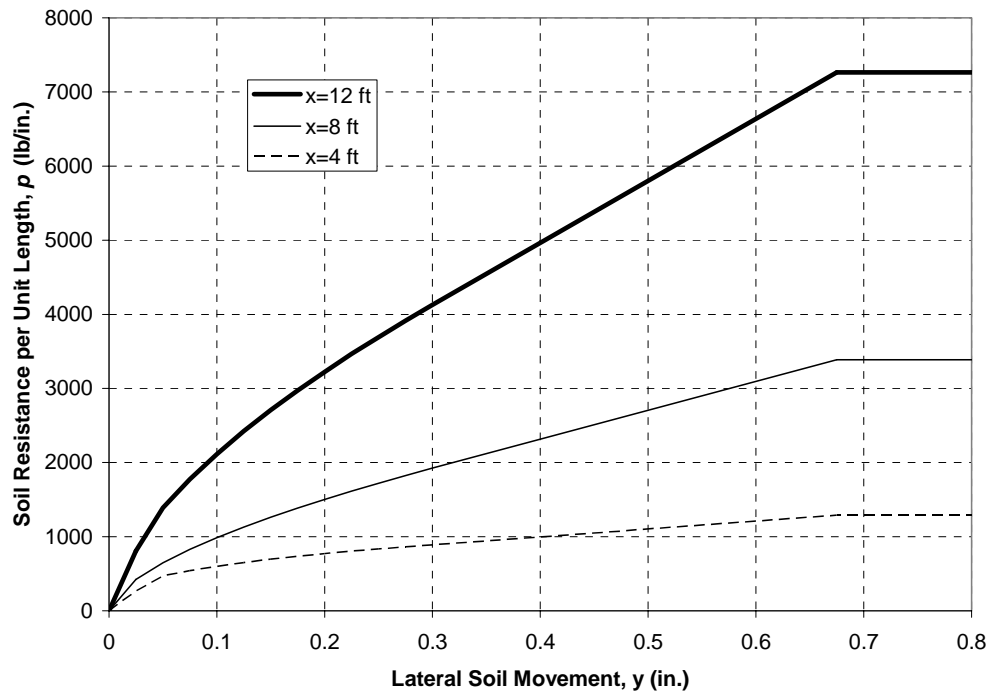


**Figure 6.1** Representative *p-y* curves for pull-over analyses

### 6.3 MOMENT-CURVATURE RELATIONSHIPS

The calculated moment-curvature relationships using the assumed as-built diameter of the shafts and the measured concrete compressive strength are plotted in Figure 6.2. The relationship calculated using the design assumptions (Figure 3.3) are also shown for comparison.

Increasing the compressive strength of the concrete from 4000 psi to 7200 psi led to a 30% increase in the cracking moment for the column, but only a 6% increase in the nominal flexural capacity. Increasing both the compressive strength of the concrete and the diameter of the cross section from 12 in. to 20 in. led to a 330% increase in the cracking moment and a 100% increase in the nominal flexural capacity. The corresponding variations between bending stiffness and moment are shown in Figure 6.3.

Moments corresponding to initial cracking of the concrete,  $M_{cr}$ ; first yielding of the reinforcement,  $M_y$ ; and the nominal flexural capacity,  $M_n$ , are reported in Table 6.2 for the idealized column and shaft cross sections. Strain hardening of the steel and confinement of the concrete due to the presence of closely-spaced spiral reinforcement were not included in the analyses.

**Table 6.2** *Calculated limiting moments in columns and shafts*

Cross-Section	$M_{cr}$ (kip-in.)	$M_y$ (kip-in.)	$M_n$ (kip-in.)
Column ( $D = 12$ in.)	116	400	500
Shaft ( $D = 20$ in.)	500	750	1000

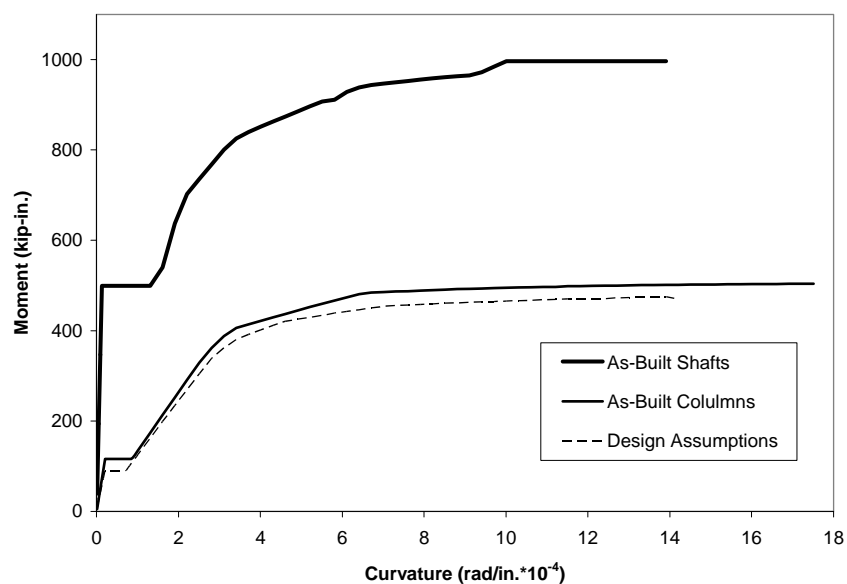


**Figure 6.2** *Calculated moment-curvature response of columns and shafts*



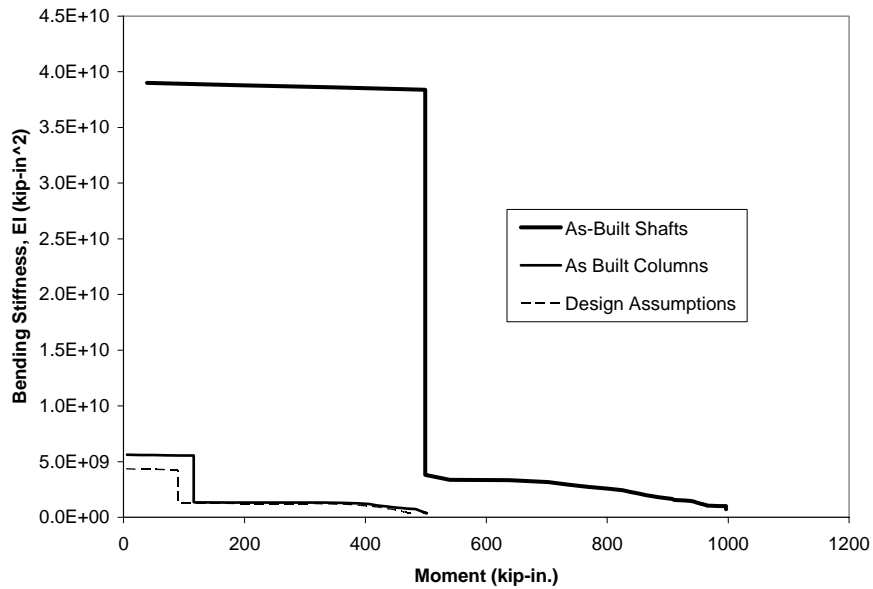


**Figure 6.3** *Calculated relationship between flexural stiffness and moment for columns and shafts*

## **6.4 LATERAL RESPONSE OF THE SPECIMENS**

### **6.4.1 Overview**

The objective of the pull-over analyses was to determine the lateral capacity of the test specimens and the corresponding modes of failure. The results of the analyses are presented in two parts. Section 6.4.2 summarizes the calculated distributions of the lateral deflections and moments along the length of the columns and shafts. The force-displacement relationships are discussed in Section 6.4.3. Results are presented for both the longitudinal and transverse directions of the bridge. The tops of the columns were assumed to be free to rotate in the longitudinal direction, but were fixed against rotation in the transverse direction.

The lateral load was increased monotonically from zero to the capacity of the bent in all analyses. It should be noted LPile does not account for moment redistribution within the structure. The analyses fail to converge when the nominal flexural capacity is reached at any location along the column or shaft. Therefore, the test specimens are expected to be able to resist larger displacements in the field without an appreciable drop in lateral strength, but more detailed analyses are required to reproduce that behavior.

Because the diameter of the shaft is larger than the diameter of the column, two possible failure mechanisms exist for the bents, as illustrated in Figure 6.4 for loads applied in the transverse direction of the bridge. Plastic hinges may form in the columns at the beam-column interface and at the ground level (Figure 6.4a) or in the columns at the beam-column interface and in the shaft below grade (Figure 6.4b). The shape of the moment diagram and the flexural capacities of the column and shaft determine the governing mechanism.

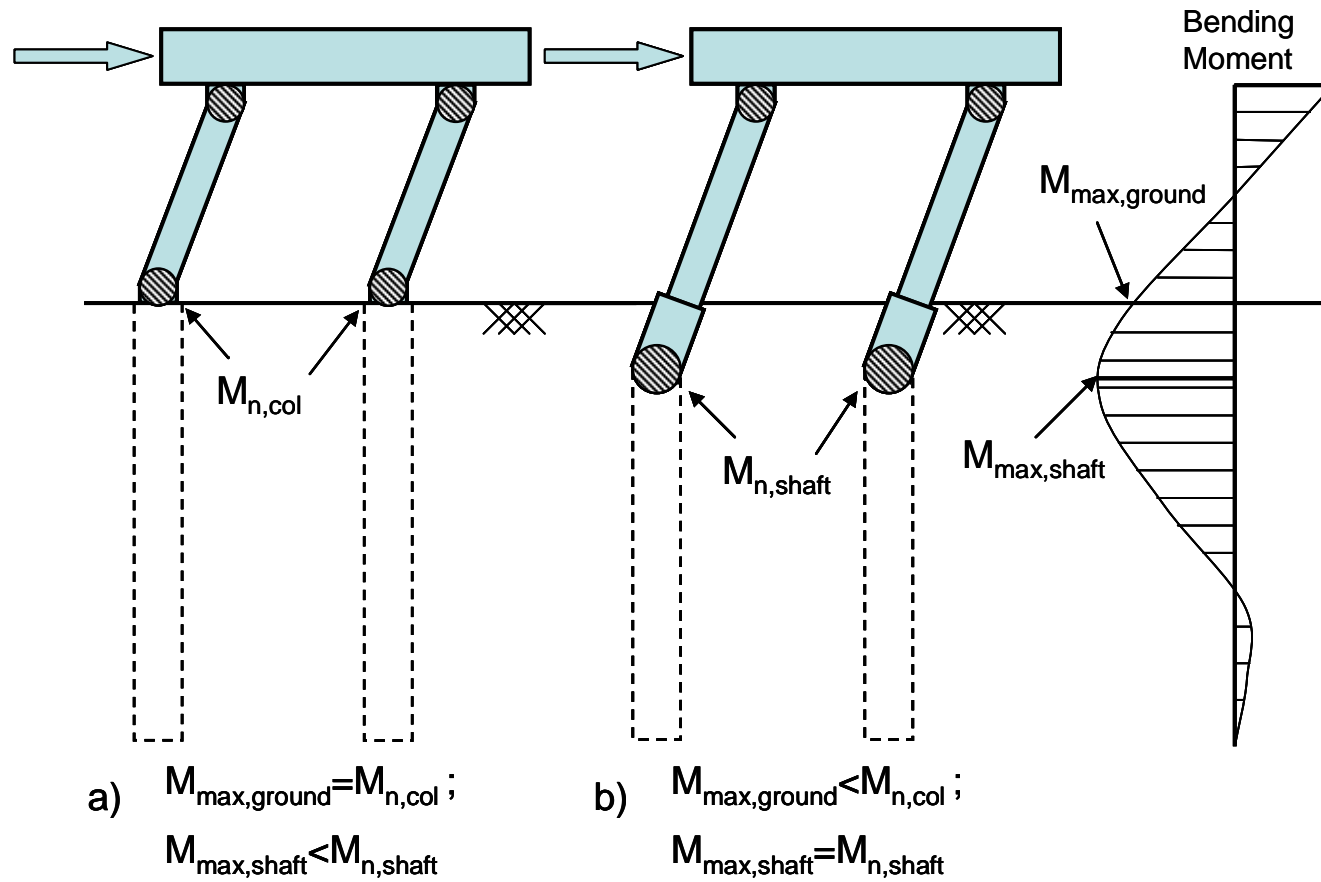


*Figure 6.4 Possible mechanisms for specimen pullover tests: (a) Hinges develop in column at ground surface, (b) Hinges develop in shaft below grade*

### 6.4.2 Calculated Deflected Shapes and Moment Diagrams

The response of the shafts was evaluated in both directions for two levels of applied load. In the first set of analyses, the maximum moment in the shaft was taken equal to the cracking moment. The bents exhibit essentially linear response in this set of analyses. The displacement profiles are presented in Figure 6.5 and the moment diagrams are given in Figure 6.6.

The calculated response of the two bents is similar at this level of response. Key parameters are summarized in Table 6.3. Moments in the column at the ground surface exceeded the cracking moment in all cases, but were less than the yield moment. When loading was applied in the transverse direction, cracking was also expected at the top of the column. Lateral displacements of the shaft at the ground surface were expected to approach 0.1 in. The location of the maximum moment in the shaft varied from 2.9 to 3.6 ft below grade in Bent 1 and from 3.6 to 4.2 ft below grade in Bent 2.

**Table 6.3** *Calculated response of individual shafts corresponding to cracking of shaft*

Bent	Rotational Restraint at Top of Column	Applied Lateral Force <sup>†</sup> (kip)	Lateral Displacement		Depth to Maximum Moment (ft)
			Ground Surface (in.)	Top of Column (in.)	
1	Fixed	8.5	0.08	0.33	3.58
	Free	5.5	0.08	0.72	2.92
2	Fixed	11.4	0.09	0.14	4.17
	Free	8.0	0.07	0.21	3.58

<sup>†</sup> Lateral force level corresponds to a single column/shaft.

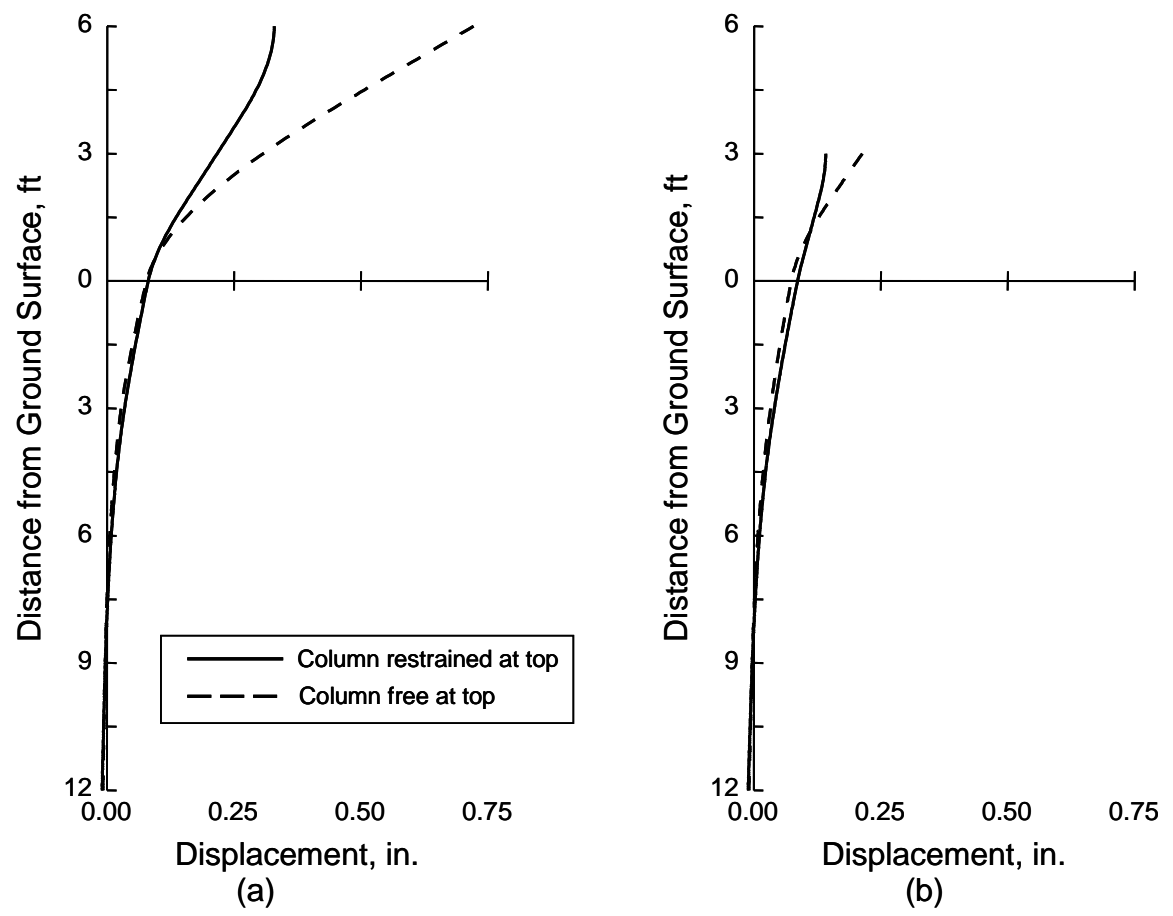


Figure 6.5 Calculated deflections corresponding to cracking of shafts: (a) Bent 1, (b) Bent 2

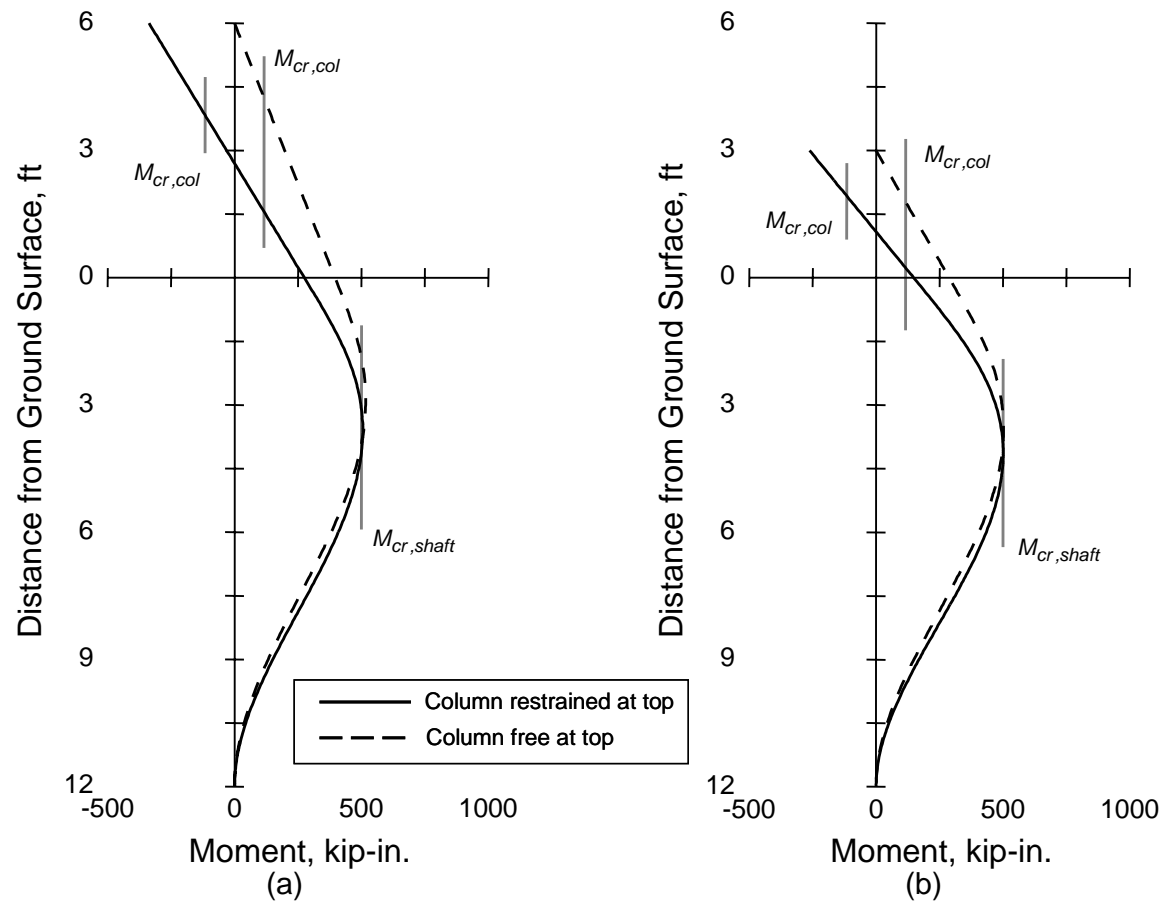


Figure 6.6 Moment distributions corresponding to cracking of shafts: (a) Bent 1, (b) Bent 2

In the second set of analyses, the capacity of the individual shafts was determined. As shown in Figure 6.4, the capacity of a shaft could be limited by the flexural capacity of the column at the ground surface or by the flexural capacity of the shaft below grade. The displacement profiles corresponding to capacity are shown in Figure 6.7 and the moment diagrams are given in Figure 6.8. Unlike the previous set of analyses, the results are sensitive to the clear height of the columns and the direction of loading (Table 6.4).

When the lateral force is applied in the transverse direction of the bridge, the capacity of Bent 1 is limited by the formation of plastic hinges at the top and bottom of the columns. The maximum moment in the shaft exceeds the yield moment, but is approximately 15% less than the nominal flexural capacity. In contrast, the capacity of Bent 2 is limited by the flexural capacity of the shafts. Yielding is not expected at the base of the columns in Bent 2 for loading in the transverse direction.

**Table 6.4** *Calculated response of individual shafts corresponding to capacity of bent*

Bent	Rotational Restraint at Top of Column	Applied Lateral Force <sup>†</sup> (kip)	Lateral Displacement		Depth to Maximum Moment (ft)	Location of Limiting Moment
			Ground Surface (in.)	Top of Column (in.)		
1	Fixed	14.1	0.80	2.9	3.17	Column
	Free	6.9	0.33	2.0	2.58	Column
2	Fixed	23.2	1.73	3.1	3.67	Shaft
	Free	13.9	0.77	1.8	3.17	Column

<sup>†</sup> Lateral force level corresponds to a single column/shaft.

When the lateral load is applied in the longitudinal direction of the bridge, the capacity of both bents is limited by the formation of a plastic hinge at the base of the column. The maximum moment in the shaft is not expected to exceed the yield moment in Bent 1, while yielding of the shaft is expected in Bent 2.

The applied force levels are considerably higher in the transverse direction compared with the longitudinal direction. This is because two plastic hinges must form in each column/shaft to form a mechanism when the top of the column is restrained against rotation, while only one hinge must form in each column/shaft when the top of the column is free to rotate.

The magnitudes of the calculated displacements vary considerably depending on the direction of loading. Because the applied force levels are considerably higher in the transverse direction, the calculated displacements at the ground surface in the longitudinal direction are less than half those in the transverse direction. The displacements at the top of the column are between 50 and 70% larger when the load is applied in the transverse direction.

The location of the maximum moment in the shaft varied from 2.6 to 3.2 ft below grade in Bent 1 and 3.2 to 3.7 ft below grade in Bent 2.



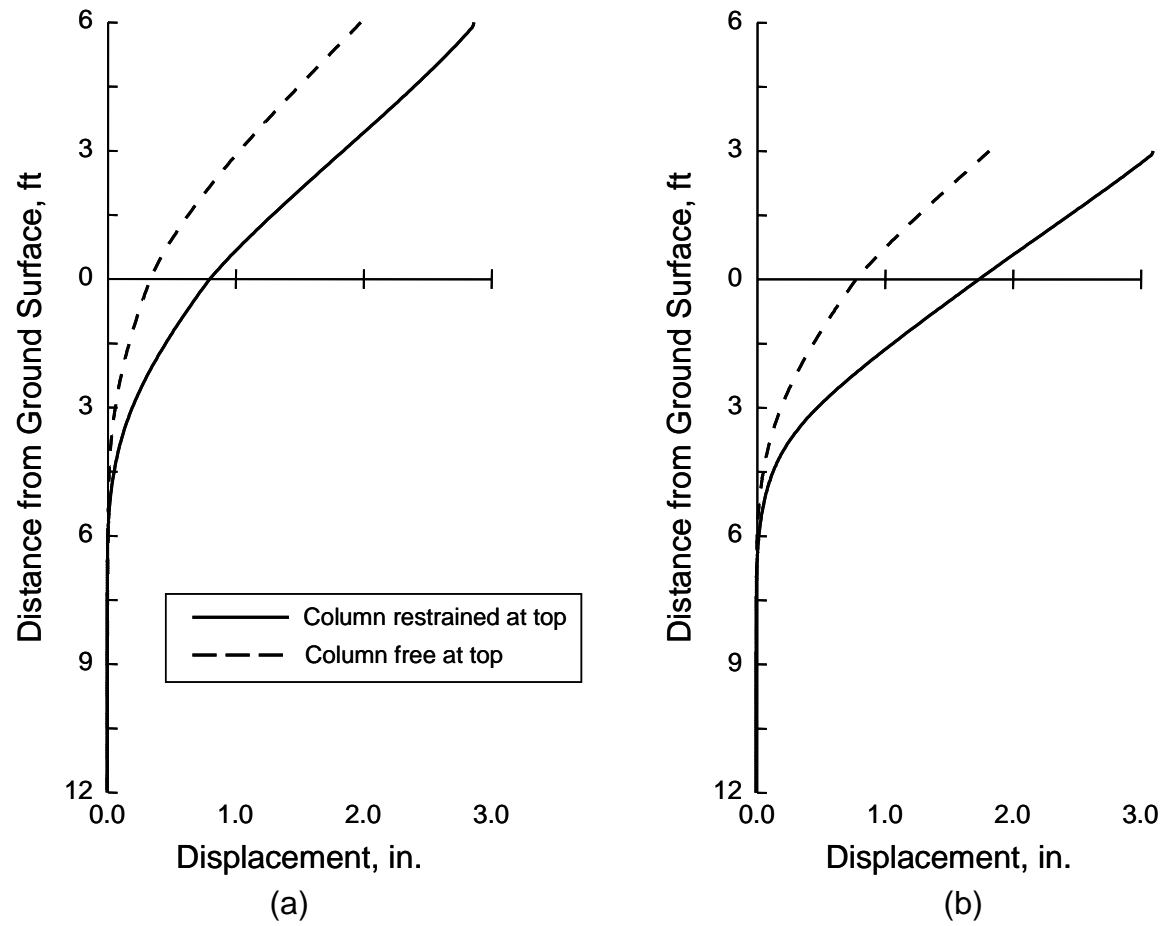


Figure 6.7 Calculated deflections corresponding to capacity of bent: (a) Bent 1, (b) Bent 2

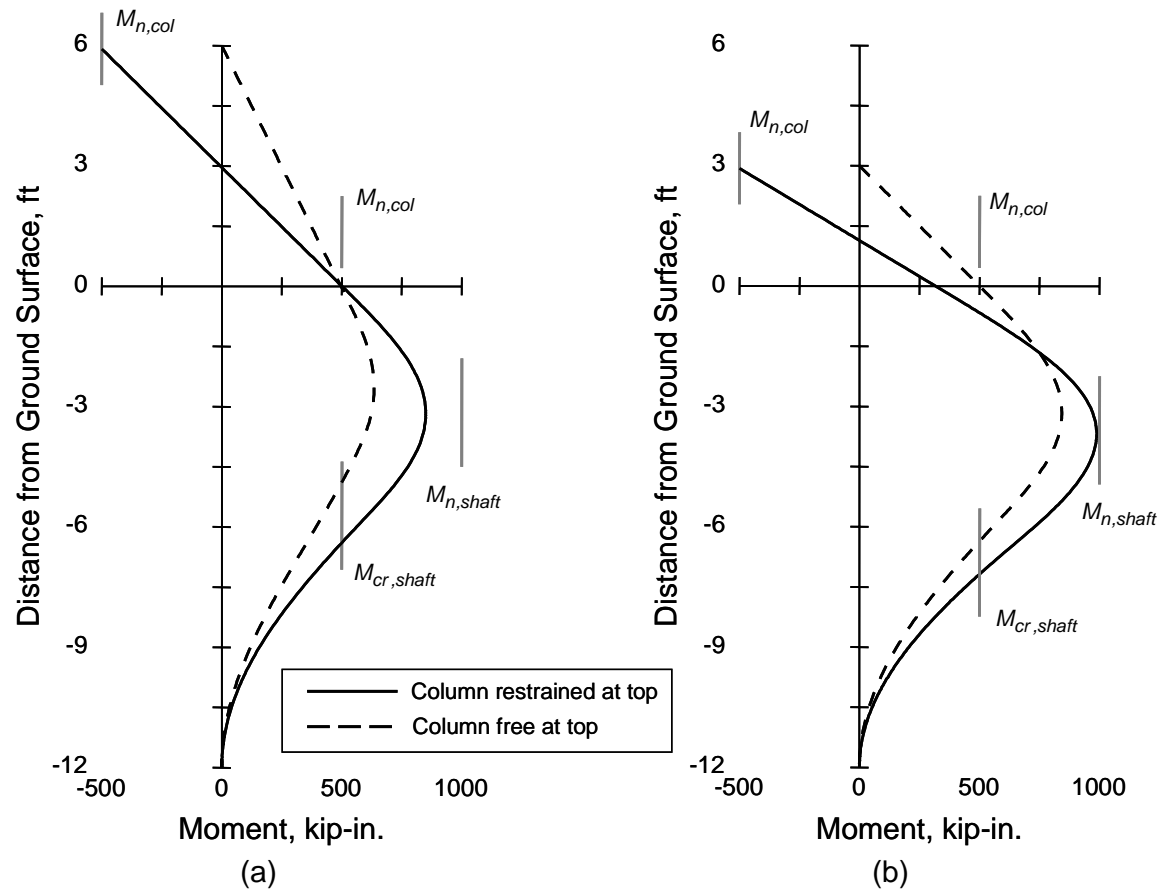


Figure 6.8 Moment distributions corresponding to capacity of bent: (a) Bent 1, (b) Bent 2

### 6.4.3 Calculated Load-Deflection Response

The calculated load-deflection curves for the two specimens are shown in

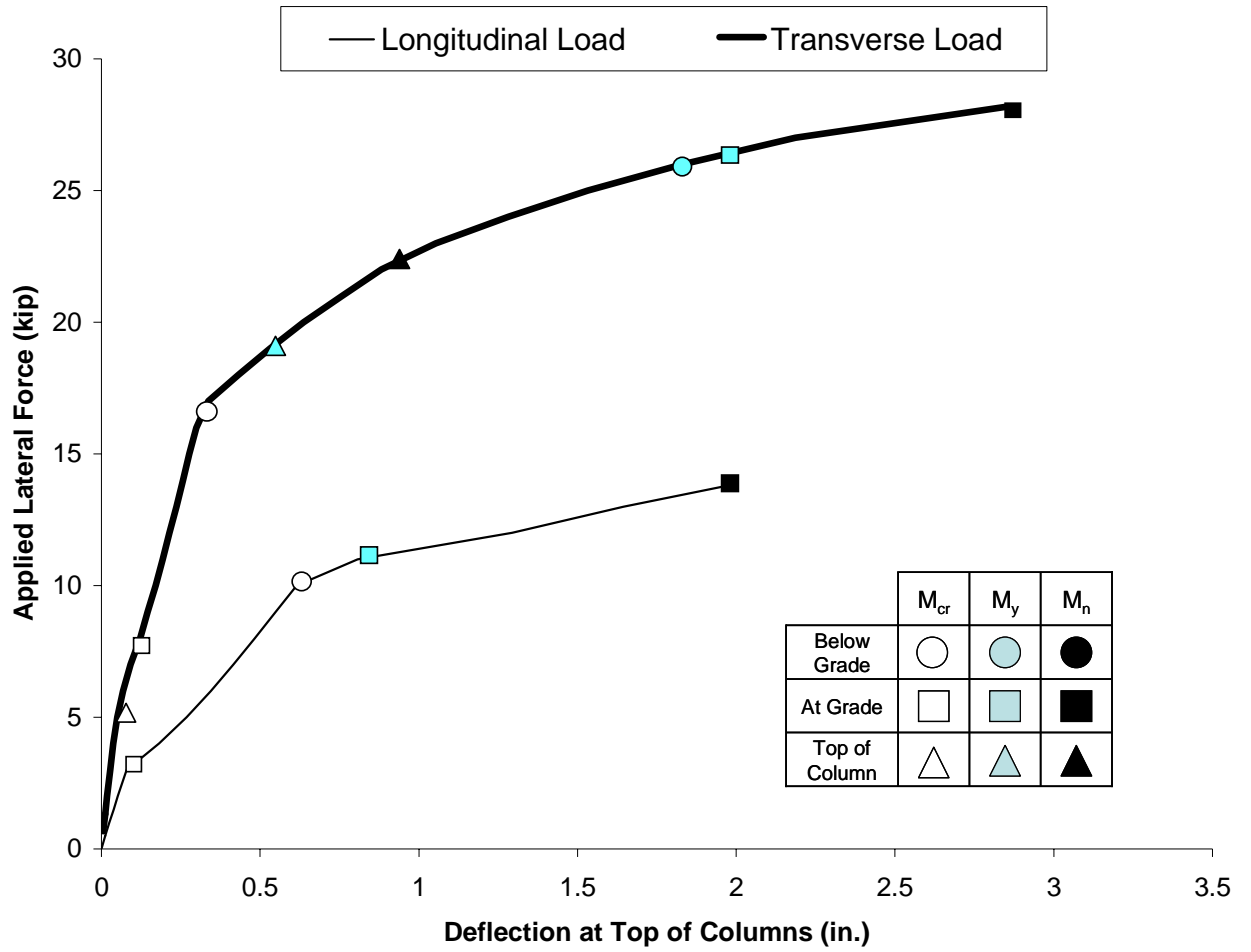


Figure 6.9 and

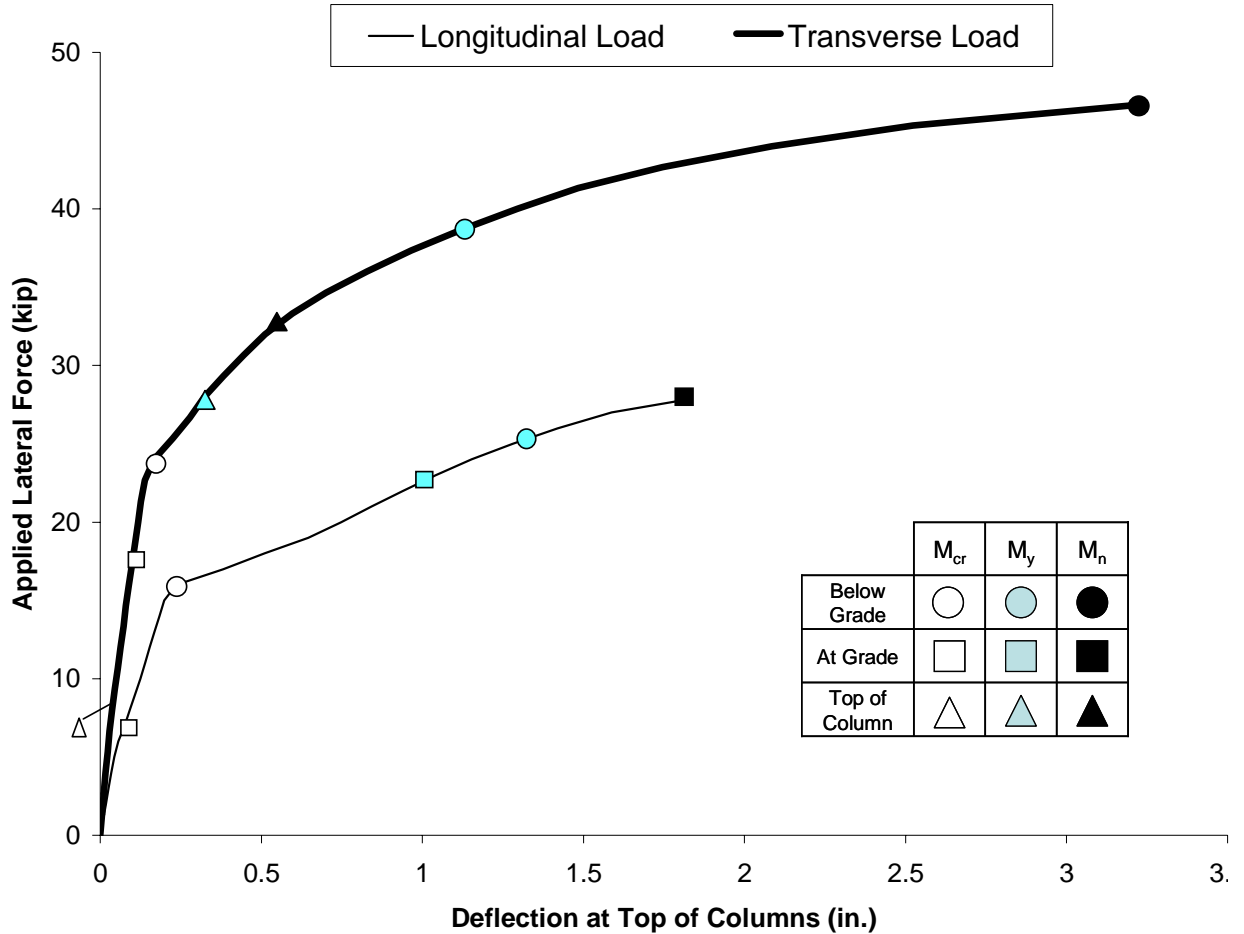


Figure 6.10. Symbols are used to identify significant changes in the stiffness of the columns and shafts. The same general information can be obtained from Figure 6.8; however, it is much easier to determine the sequence of events leading to failure from the load-deflection plots.

The force levels corresponding to the lateral capacity of the bents are summarized in Table 6.5. Because each bent comprises two columns, the lateral forces reported in Table 6.5 are two times the values reported in Table 6.4.

**Table 6.5 Lateral Capacity of Bents**

Bent	Direction of Loading	Rotational Restraint at Top of Column	Required Lateral Force (kip)
1	Transverse	Fixed	28.2
	Longitudinal	Free	13.8
2	Transverse	Fixed	46.4
	Longitudinal	Free	27.8

As discussed in Section 6.4.2, flexural hinges are only expected to form in the shafts when Bent 2 is loaded in the transverse direction of the bridge. In all other cases, the limiting mechanism is expected to develop when plastic hinges form at the base of the columns. Significant inelastic response in the structure, foundation, and soil are expected in all tests, however.

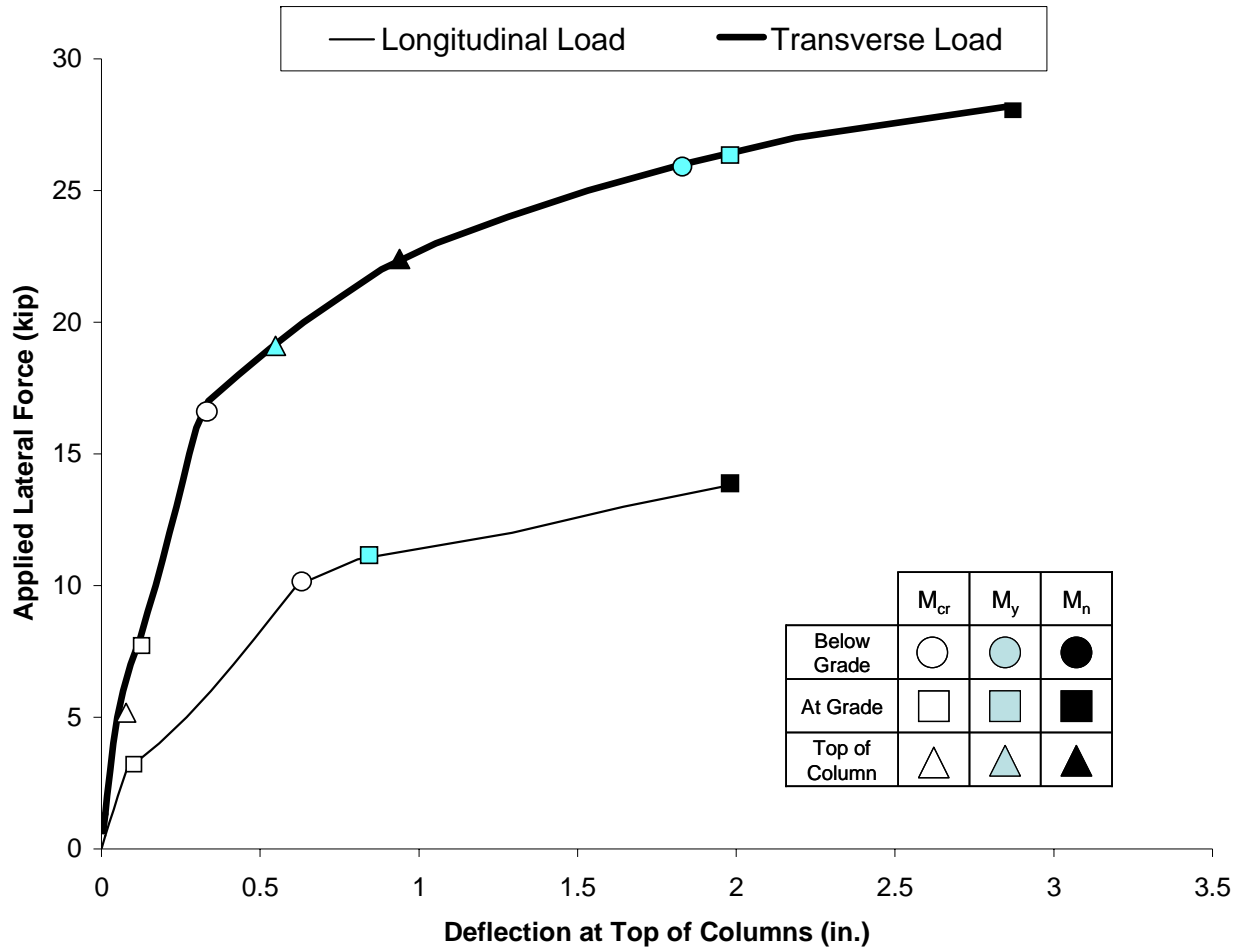


Figure 6.9 Calculated load-deflection curves for Bent 1

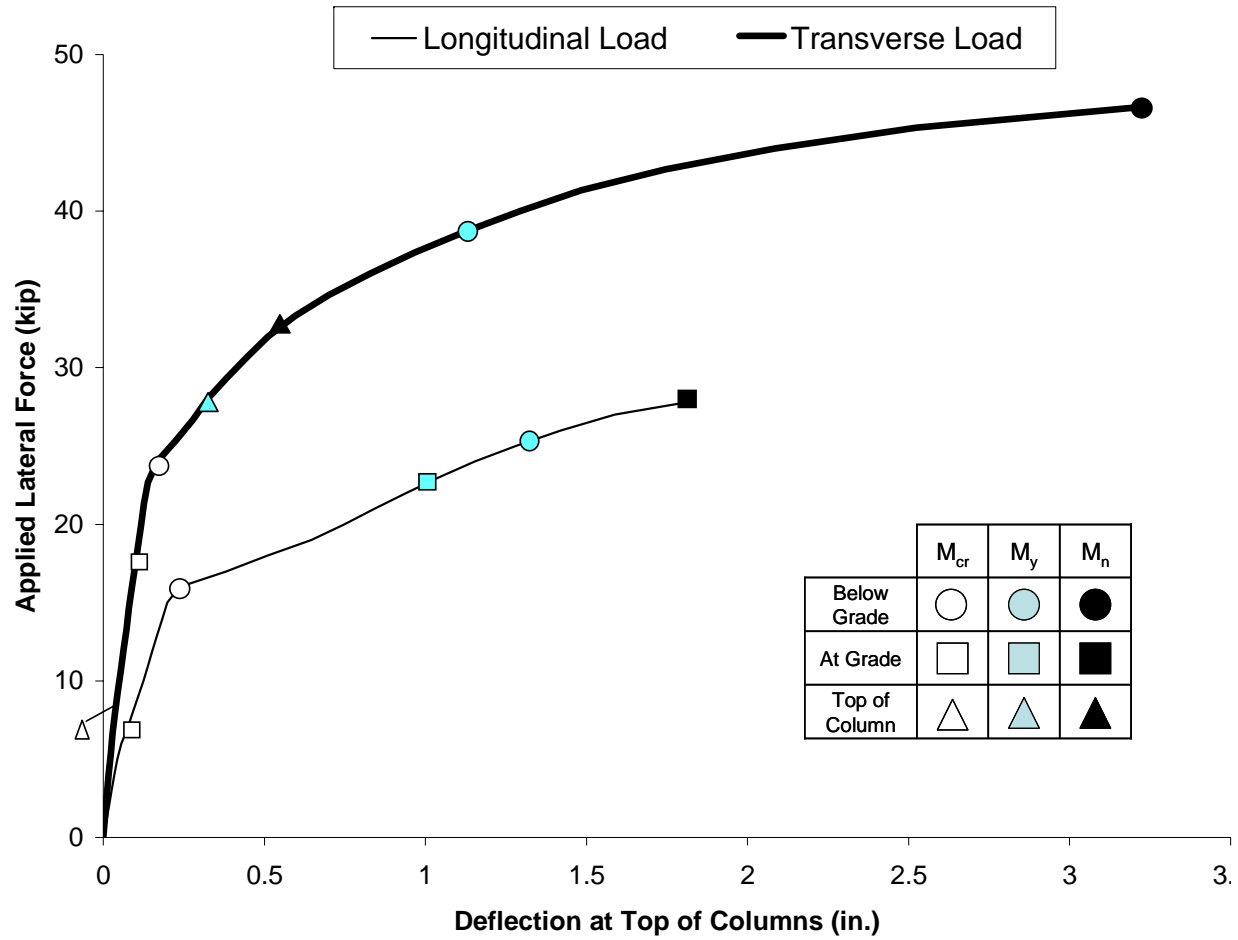


Figure 6.10 Calculated load-deflection curves for Bent 2

It was originally envisioned that cables would be attached to the winch on T-Rex to apply the lateral force to the test specimens in the transverse direction of the bridge. The capacity of the winch is 30 kip; therefore, this force level is not expected to be sufficient to form a mechanism in Bent 2 for loading in this direction. Other options for applying load will be investigated, or Bent 2 will be tested in the longitudinal direction of the bridge.

## **6.5 SUMMARY**

A series of nonlinear analyses were performed to determine the lateral capacity of the test specimens. The results of these analyses will be used to plan the instrumentation and loading apparatus for the pull-over tests.

The lateral capacity of Bent 1 is expected to be limited by the formation of plastic hinges at the base of the columns in both directions. However, yielding of the shafts is expected only for loading in the transverse direction of the bridge. When loaded in the transverse direction, the lateral capacity of Bent 2 is expected to be limited by the formation of plastic hinges in the shaft. When loaded in the longitudinal direction, the lateral capacity of the bent is expected to be limited by formation of plastic hinges at the base of the columns.



## **CHAPTER 7**

### **Conclusion**

#### **7.1 OVERVIEW**

This thesis has presented the design and construction of two field test specimens which represent one component of a collaborative investigation of soil-foundation-structure interaction. Each specimen comprised a two-column bent supported by drilled shaft foundations. The bents represent supporting elements from the prototype bridge (Figure 1.1) and were similar in geometry to those tested on the shaking tables at the University of Nevada, Reno (Figure 1.3).

Two of the mobile shakers from the NEES Equipment Site at the University of Texas at Austin will be used to test the bents. The proposed testing protocols for the field specimens involved dynamic excitation of the surrounding ground surface using T-Rex and direct excitation of the specimens using the hydraulic shaker from Thumper. Static, pull-over tests are also planned.

The purpose of the tests is to provide information on the response of the complete soil-foundation-structure system for different levels of response. The first set of dynamic tests were conducted in June and July 2005. Analysis of these data are beyond the scope of this thesis.

#### **7.2 CONCLUSIONS**

The objectives of this thesis were to (1) understand the dynamic response of the complete soil-foundation-structure system, (2) evaluate if simple design approaches should be used to represent the flexibility of drilled shaft foundations, and (3) monitor the movement of the location of maximum moment in the shaft as the intensity of the applied loading increases.

The evaluation of item (1) is ongoing and much of experimental data will be analyzed by subsequent researchers at the University of Texas. Modal hammer test data; however, were reported in Chapter 5 and attempts were made to bound the measured frequency response by varying the parameters needed to model the specimens. The results of the analyses were found to be very sensitive to the soil stiffness near the ground surface. In order to bound the measured frequency response, the vertical distribution of the initial soil stiffness was modified such that appreciable resistance was provided near the ground surface. This approach may be valid only for excitation at extremely small strain levels. Further investigation by the University of Texas will track changes in the frequency of the specimens as strain levels increase.

A key part of the ongoing field study will be the static pull-over tests of the specimens. The analyses in Chapter 6 were used to estimate the lateral capacity of the specimens. Because the diameter of the shafts exceeds the diameter of the columns, hinging of the columns at the ground surface is expected to limit the lateral capacity of Bent 1 in both directions of loading. Hinges are expected to develop in the shafts if Bent 2 is loaded in the transverse direction of the bridge, but the force levels required are likely to exceed the capacity of the available equipment in the field. Regardless of the direction of loading, significant inelastic response is expected in the soil and foundations during the pull-over tests.

The simple design approach of fixing the base of the columns at the depth of maximum moment below the ground surface was evaluated in Chapter 3. In general, this method was found to underestimate the flexibility of the drilled shaft foundations. The model is also limited in that the response of the system is dependent upon the boundary conditions at the top of the column. Because these

boundary conditions are likely to change with the direction of loading, the design approach must be used with care in three-dimensional modeling.

Variations in the depth to maximum moment in the shafts were investigated using the LPILE design software. These analyses have yet to be verified by experimental results, but the preliminary studies indicate that the depth to maximum moment decreases with increasing soil stiffness and increasing flexibility of the structure.

# **APPENDIX A**

## **Material Properties**

### **A.1 PROPERTIES OF CONCRETE**

Concrete cylinders were cast from the same batches of concrete used for the test specimens. The cylinders were stored in an environmental chamber at a temperature of 73 °F with 100% humidity until they were tested. The measured compressive strengths of cylinders from the three batches of concrete are reported in Table A.1. Load-displacement data were recorded for three cylinders from the third batch of concrete (Table A.2). The corresponding stress-strain data used to determine the modulus of elasticity of the concrete are presented in Table A.3. A representative stress-strain plot is shown in Figure A.1. Tests were conducted in accordance with ASTM C 39 and ASTM C 469.

As discussed in Section 4.5, nondestructive testing was also performed on concrete cylinders by Kurtulus and Lee at the University of Texas Soil Dynamics Laboratory. Data from these tests are presented in Table A.4.

**Table A.1 Measured compressive strength of concrete**

Primary Element Constructed	Single Shaft Specimens	Bents – Shafts and Columns	Bents – Beams
Date of Placement	Dec 17, 2004	Feb 25, 2005	May 17, 2005
Date of Test	Jan 14, 2005	March 25, 2005	July 5, 2005
Age at Test (days)	28	28	49
Size of Cylinder	4 x 8 in.	6 x 12 in.	6 x 12 in.
Compressive Strength of Each Cylinder (psi) (ASTM C39)	5033	7202	7723
	5089	6897	7773
	4556	7331	7547
	5087	6942	7151
	4713	7325	7521
	4739	7250	7525
	4456	6978	7450
	4869	6659	4372
		8071	7779
		7255	
Average Compressive Strength, $f'_c$ (psi)	4820	7190	7200

**Table A.2 Measured load and displacement data for three concrete cylinders\*<sup>†</sup>**

Cylinder 1		Cylinder 2		Cylinder 3	
Gage Length	6.68 in.	Gage Length	6.70 in.	Gage Length	6.72 in.
Load (kip)	Displ. (in.)	Load (kip)	Displ. (in.)	Load (kip)	Displ. (in.)
10.8	0.0010	10.8	0.0011	11.5	0.0012
21.7	0.0020	21.6	0.0023	21.7	0.0023
32.8	0.0031	32.9	0.0035	32.7	0.0034
43.4	0.0041	43.7	0.0047	43.9	0.0047
54.5	0.0051	54.8	0.0058	54.3	0.0058
65.4	0.0062	65.4	0.0071	65.5	0.0070
76.5	0.0073	76.3	0.0082	76.4	0.0082
87.4	0.0083	87.5	0.0095	87.2	0.0094
98.1	0.0094	98.1	0.0108	98.1	0.0106
109.0	0.0106	109.3	0.0123	109.0	0.0119

\* Concrete was placed on May 17, 2005 and cylinders were tested on July 5, 2005.

<sup>†</sup> All three cylinders had dimensions of 6 x 12 in.

**Table A.3 Values of stress and strain used to determine modulus of elasticity of concrete**

Cylinder 1		Cylinder 2		Cylinder 3	
Stress (ksi)	Strain	Stress (ksi)	Strain	Stress (ksi)	Strain
0.38	0.00007	0.38	0.00008	11.5	0.00009
0.77	0.00015	0.77	0.00017	21.7	0.00017
1.16	0.00023	1.16	0.00026	32.7	0.00025
1.54	0.00030	1.55	0.00035	43.9	0.00035
1.93	0.00038	1.94	0.00043	54.3	0.00043
2.31	0.00046	2.31	0.00052	65.5	0.00052
2.70	0.00054	2.70	0.00061	76.4	0.00061
3.09	0.00062	3.09	0.00071	87.2	0.00070
3.47	0.00070	3.47	0.00080	98.1	0.00079
3.86	0.00079	3.87	0.00091	3.86	0.00089
$E_c = 5090$ ksi		$E_c = 4450$ ksi		$E_c = 4460$ ksi	

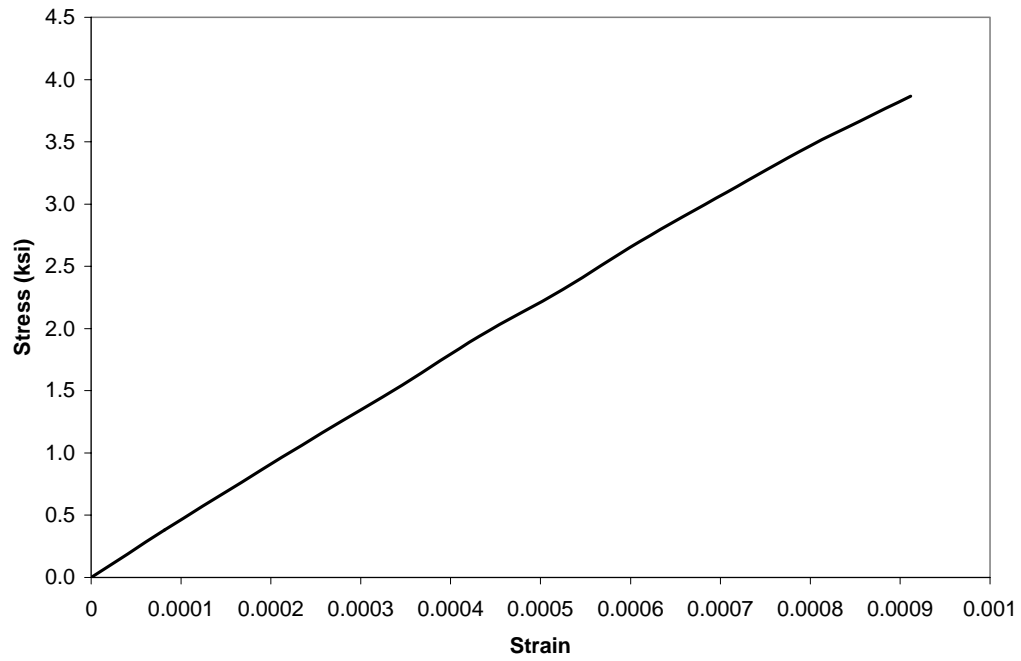


*Figure A.1 Representative stress-strain curve for concrete cylinder*



*Table A.4 Measured dynamic modulus of concrete cylinders\**

Cylinder No.	Date of Placement	Date of Test	Age (days)	Length (in.)	Diameter (in.)	Modulus of Elasticity (ksi)
1	Dec 17, 2004	Jan 16, 2005	31	8.03	4.03	4530
2	Dec 17, 2004	Jan 16, 2005	31	8.04	4.03	4490
3	Dec 17, 2004	Jan 16, 2005	31	8.04	4.04	4410
4	Feb 25, 2004	Apr 13, 2005	48	11.77	5.99	5790
5	Feb 25, 2004	Apr 13, 2005	48	11.80	5.99	5930
6	May 17, 2004	July 19, 2005	63	11.97	6.00	5870
7	May 17, 2004	July 19, 2005	63	11.97	6.01	6020
8	May 17, 2004	July 19, 2005	63	12.00	6.01	6010

\* Tests performed by Kurtulus and Lee in University of Texas Soil Dynamics Laboratory

## A.2 PROPERTIES OF REINFORCING STEEL

Five tension test were performed on X-in. samples from the longitudinal reinforcing bars used to fabricate the cages for the shafts and columns. Reinforcement from the same heat was used in all specimens. The tension tests were conducted at the Ferguson Structural Engineering Laboratory using a 60-kip load frame. A gage length of 8 in. was used for all tension tests. A representative plot of the stress-strain response is shown in Figure A.2. The measured material properties are summarized in Table A.5.

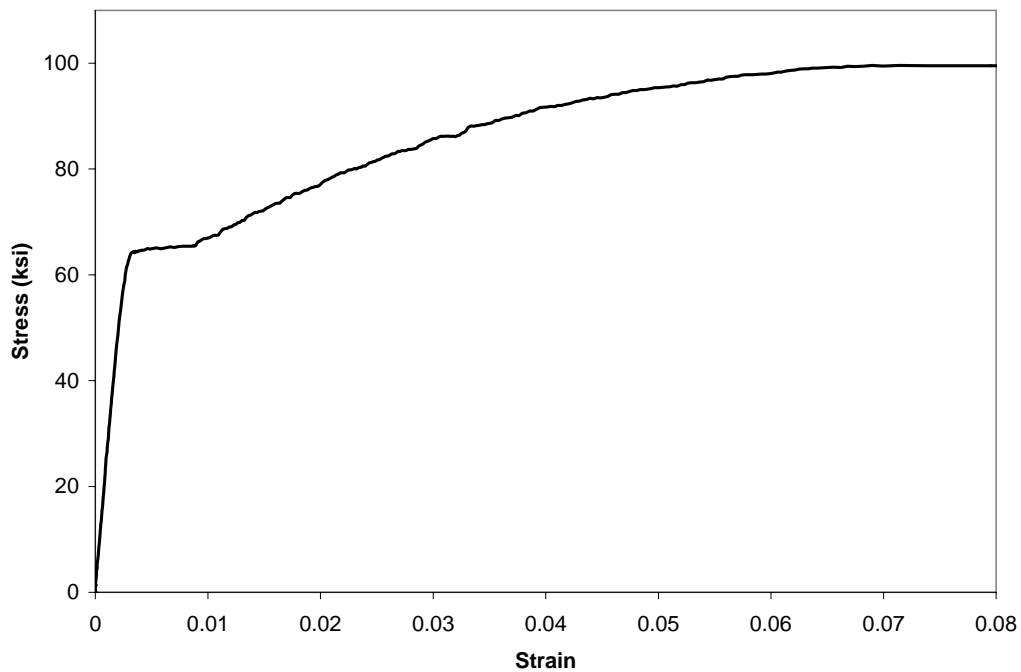


*Figure A.2 Representative stress-strain curve for steel reinforcement*

*Table A.5 Measured properties of longitudinal reinforcement*

Test Number	Yield Stress (ksi)	Tensile Stress (ksi)
1	60	103
2	58	97
3	64	105
4	59	103
5	63	102
Average	60.8	102

## **APPENDIX B**

### **Procedures Used to Install Strain Gages**

#### **B.1 OVERVIEW**

This appendix describes the procedures used to attach strain gages to the longitudinal reinforcing bars. A description of the strain gages is first provided in Section B.2. Procedures used to prepare the surface of the bars are described in Section B.3. The procedure used to attach the strain gages is presented in Section B.4, and Section B.5 provides a brief discussion of the techniques used to verify that the strain gages had been attached properly. The appendix concludes with a discussion of the procedures used to protect and waterproof the individual gages in Section B.6.

#### **B.2 STRAIN GAGE DESCRIPTION**

The strain gages used on the project were purchased from Texas Measurements, Inc., a subsidiary of Tokyo Sokki Kenkyujo, Co., Ltd. Specifications for the strain gages are given in Table B.1.

*Table B.1 Strain gage specifications*

Brand	TML
Gage Types	FLA-3-11-3LT FLA-3-11-5LT
Gage Length	3 mm
Gage Factor	2.13 $\pm$ 1%
Gage Resistance	120 ohms
Lead type	3-wire paralleled vinyl
Lead Lengths	3 m and 5 m

### **B.3 SURFACE PREPARATION**

The surface of a typical reinforcing bar was prepared by first grinding an area of the bar slightly larger than the nominal dimensions of the strain gage with an electric grinder to remove the rough, oxidized surface of the steel. Care was taken to maintain the cross-sectional shape of the bar and minimize the reduction of the cross-sectional area. The surface was then sanded with wet, 220-grit sand paper and a mild phosphoric acid solution. Following sanding, the surface was washed with the same acidic solution. The acidic solution was then wiped from the surface of the bars using clean gauze pads. The ground area was wiped in one direction only, to reduce the risk of contamination with dirt or oil. Care was taken not to scrub the surface of the bar. The surface of the bar then was neutralized with a mild ammonia-based solution. Excess solution was removed by patting the surface with clean gauze pads. The surface was then allowed to air dry for up to one minute.

#### **B.4 STRAIN GAGE APPLICATION**

To handle the gage prior and during application, a strip of cellophane tape was temporarily adhered to the back of the gage. A drop of cyanoacrylate glue was then applied to the surface of the steel within the prepared area. The gage was then placed on top of the glue. The cellophane tape directly over the gage was then rubbed using strips of Teflon to remove air bubbles and ensure bonding of the gage to the steel. After the glue was allowed to cure for several minutes, the cellophane tape was carefully removed and the lead wires were pulled up such that they were no longer in contact with the surface of the bar. If part of the gage remained unbonded to the bar, the gage was removed, the surface was ground again, and all steps were repeated.

#### **B.5 DIAGNOSTICS**

In preparation for diagnostics, the lead wires for the gage were isolated from the surface of the bar using electrical tape. The gage was then connected to a quarter-bridge diagnostic tool. Once connected, the readings from the strain gage were zeroed. Slight deflections were then imposed on the bar and readings observed. If the readings were illogical or if the strain readings could not be zeroed, the gage resistance was checked using an ohmmeter. If the ohmmeter showed increased resistance, then the leads were checked to make sure they were adequately isolated from the bar. The gage was then rechecked using the diagnostic tool. If these issues could not be resolved, the gage was removed from the surface of the bar and the entire process was repeated.

#### **B.6 PROTECTION AND WATERPROOFING**

Following a successful diagnostic test, the strain gage was then protected and waterproofed. First, the gage was covered with a solvent-thinned acrylic coating, which acted as a moisture barrier. A thin strip of neoprene was then

placed on the gage to protect against accidental impact. The coating was allowed to cure for about one minute, after which the gage and the neoprene were wrapped with foil tape. Care was taken to seal the edges of the tape around the bar both above and below the gage.

To protect the strain gage from de-bonding due to incidental snagging of the lead wires, approximately a six-in. length of lead wires was looped and connected to the bar with plastic zip connectors to prevent additional loads from being applied to the gage. The leads were then bundled into plastic tubing as described in Chapter 4.

## **APPENDIX C**

### **Identification Labels for Strain Gages**

#### **C.1 OVERVIEW**

The following information is being provided for the benefit of subsequent researchers at the University of Texas who will need to connect the lead wires from the strain gages to a data acquisition system. Customized connectors, cables, and terminal blocks were fabricated for these experiments and will be discussed in this appendix. The strain gages are identified based on shaft, bar, and station designations presented in Chapter 3.

Lead wires from the strain gages were terminated at the site into 25-pin connectors. These connectors were selected to allow the instruments to be connected quickly and efficiently to the data acquisition system in the field during tests. Connectors for Bent 1 were called A6 through L6, connectors for Bent 2 were called A3 through L3, and connectors for Shafts C and D were called A through F.

Before the strain gages were terminated into connectors, each gage was checked with an ohmmeter to determine it was still intact and likely to function normally. If the ohmmeter readings indicated a resistance close to the nominal resistance of 120 ohms, then the strain gage was terminated into a connector. Only one strain gage was found which did not appear to be functioning normally. This faulty gage, located on shaft 2S, bar N, gage station 84, was not terminated into a connector.

Because each strain gage has three lead wires, a maximum of eight strain gages can be linked to the data acquisition system through each connector. Each



of the eight strain gages was assigned a channel number between 0 and 7. Channel 0 corresponds to pins 1 through 3 in the connector, Channel 1 corresponds to pins 4 through 6, and so forth.

Custom, 25-wire cables were fabricated and connected to terminal blocks to link the strain gages to the data acquisition system. The cables and terminal blocks were numbered 1 through 12, and cable 1 was always attached to terminal block 1.

A maximum of twelve terminal blocks can be connected to the data acquisition system at any time. Ideally, the twelve terminal blocks were attached to the data acquisition system in the same order for each test providing 96 channels of strain data, which are numbered 0 through 95. In reality, only ten terminal blocks, providing 80 channels of strain data, were connected to the data acquisition system during the dynamic field tests. Of the two remaining slots, one terminal block was connected to accelerometers and one was connected to geophones. Detailed descriptions of the instruments used to monitor the response of the specimens during each dynamic test are beyond the scope of this thesis.

The identification labels for each strain gage, including the connector, connector channel, terminal block, and data acquisition channel are reported in

Table C.1 for Bent 1, Table C.2 for Bent 2, Table C.3 for Shafts C and D. The identification labels are identical for Shafts C and D. The data acquisition system channel number assigned to each strain gage corresponds to the ideal configuration of the terminal blocks and does not necessarily represent the configuration that was used during the dynamic tests.

**Table C.1 Identification labels for strain gages in Bent 1**

Shaft	Bar	Station	Connector Label	Connector Channel ID	Terminal Block and Cable ID	DAQ Channel ID
1E	N	-72	F6	0	6	40
1E	N	-66	F6	1	6	41
1E	N	0	G6	0	7	48
1E	N	12	G6	1	7	49
1E	N	24	G6	2	7	50
1E	N	36	G6	3	7	51
1E	N	48	G6	4	7	52
1E	N	60	G6	5	7	53
1E	N	72	G6	6	7	54
1E	N	84	G6	7	7	55
1E	N	96	H6	5	8	61
1E	N	108	H6	6	8	62
1E	N	120	H6	7	8	63
1E	S	-72	F6	4	6	44
1E	S	-66	F6	5	6	45
1E	S	0	J6	0	10	72
1E	S	12	J6	1	10	73
1E	S	24	J6	2	10	74
1E	S	36	J6	3	10	75
1E	S	48	J6	4	10	76
1E	S	60	J6	5	10	77
1E	S	72	J6	6	10	78
1E	S	84	J6	7	10	79
1E	S	96	K6	5	11	85
1E	S	108	K6	6	11	86
1E	S	120	K6	7	11	87
1E	E	-72	F6	6	6	46
1E	E	-66	F6	7	6	47
1E	E	12	L6	0	12	88
1E	E	24	L6	1	12	89
1E	E	36	L6	2	12	90
1E	E	48	L6	3	12	91
1E	E	60	L6	4	12	92
1E	E	72	L6	5	12	93
1E	E	84	L6	6	12	94
1E	E	96	L6	7	12	95

Shaft	Bar	Station	Connector Label	Connector Channel ID	Terminal Block and Cable ID	DAQ Channel ID
1E	W	-72	F6	2	6	42
1E	W	-66	F6	3	6	43
1E	W	12	I6	0	9	64
1E	W	24	I6	1	9	65
1E	W	36	I6	2	9	66
1E	W	48	I6	3	9	67
1E	W	60	I6	4	9	68
1E	W	72	I6	5	9	69
1E	W	84	I6	6	9	70
1E	W	96	I6	7	9	71
1E	NW	24	H6	0	8	56
1E	NW	36	H6	1	8	57
1E	NW	48	H6	2	8	58
1E	NW	60	H6	3	8	59
1E	NW	72	H6	4	8	60
1E	SW	24	K6	0	11	80
1E	SW	36	K6	1	11	81
1E	SW	48	K6	2	11	82
1E	SW	60	K6	3	11	83
1E	SW	72	K6	4	11	84
1W	N	-72	A6	0	1	0
1W	N	-66	A6	1	1	1
1W	N	0	B6	0	2	8
1W	N	12	B6	1	2	9
1W	N	24	B6	2	2	10
1W	N	36	B6	3	2	11
1W	N	48	B6	4	2	12
1W	N	60	B6	5	2	13
1W	N	72	B6	6	2	14
1W	N	84	B6	7	2	15
1W	N	96	C6	5	3	21
1W	N	108	C6	6	3	22
1W	N	120	C6	7	3	23
1W	S	-72	A6	2	1	2
1W	S	-66	A6	3	1	3
1W	S	0	D6	0	4	24
1W	S	12	D6	1	4	25
1W	S	24	D6	2	4	26

Shaft	Bar	Station	Connector Label	Connector Channel ID	Terminal Block and Cable ID	DAQ Channel ID
1W	S	36	D6	3	4	27
1W	S	48	D6	4	4	28
1W	S	60	D6	5	4	29
1W	S	72	D6	6	4	30
1W	S	84	D6	7	4	31
1W	S	96	E6	5	5	37
1W	S	108	E6	6	5	38
1W	S	120	E6	7	5	39
1W	E	24	E6	0	5	32
1W	E	36	E6	1	5	33
1W	E	48	E6	2	5	34
1W	E	60	E6	3	5	35
1W	E	72	E6	4	5	36
1W	W	24	C6	0	3	16
1W	W	36	C6	1	3	17
1W	W	48	C6	2	3	18
1W	W	60	C6	3	3	19
1W	W	72	C6	4	3	20
Blank	Blank	Blank	A6	4	1	4
Blank	Blank	Blank	A6	5	1	5
Blank	Blank	Blank	A6	6	1	6
Blank	Blank	Blank	A6	7	1	7

**Table C.2 Identification labels for strain gages in Bent 2**

Shaft	Bar	Station	Connector Label	Connector Channel ID	Terminal Block and Cable ID	DAQ Channel ID
2N	N	-36	A3	0	1	0
2N	N	-30	A3	1	1	1
2N	N	0	B3	0	2	8
2N	N	12	B3	1	2	9
2N	N	24	B3	2	2	10
2N	N	36	B3	3	2	11
2N	N	48	B3	4	2	12
2N	N	60	B3	5	2	13
2N	N	72	B3	6	2	14
2N	N	84	B3	7	2	15
2N	N	96	C3	5	3	21
2N	N	108	C3	6	3	22
2N	N	120	C3	7	3	23
2N	S	-36	A3	2	1	2
2N	S	-30	A3	3	1	3
2N	S	0	D3	0	4	24
2N	S	12	D3	1	4	25
2N	S	24	D3	2	4	26
2N	S	36	D3	3	4	27
2N	S	48	D3	4	4	28
2N	S	60	D3	5	4	29
2N	S	72	D3	6	4	30
2N	S	84	D3	7	4	31
2N	S	96	E3	5	5	37
2N	S	108	E3	6	5	38
2N	S	120	E3	7	5	39
2N	E	24	E3	0	5	32
2N	E	36	E3	1	5	33
2N	E	48	E3	2	5	34
2N	E	60	E3	3	5	35
2N	E	72	E3	4	5	36
2N	W	24	C3	0	3	16
2N	W	36	C3	1	3	17
2N	W	48	C3	2	3	18
2N	W	60	C3	3	3	19
2N	W	72	C3	4	3	20

Shaft	Bar	Station	Connector Label	Connector Channel ID	Terminal Block and Cable ID	DAQ Channel ID
2S	N	-36	F3	3	6	43
2S	N	-30	F3	4	6	44
2S	N	0	G3	0	7	48
2S	N	12	G3	1	7	49
2S	N	24	G3	2	7	50
2S	N	36	G3	3	7	51
2S	N	48	G3	4	7	52
2S	N	60	G3	5	7	53
2S	N	72	G3	6	7	54
2S	N	84	G3*	7*	7*	55*
2S	N	96	H3	5	8	61
2S	N	108	H3	6	8	62
2S	N	120	H3	7	8	63
2S	S	-36	F3	0	6	40
2S	S	-30	F3	5	6	45
2S	S	0	J3	0	10	72
2S	S	12	J3	1	10	73
2S	S	24	J3	2	10	74
2S	S	36	J3	3	10	75
2S	S	48	J3	4	10	76
2S	S	60	J3	5	10	77
2S	S	72	J3	6	10	78
2S	S	84	J3	7	10	79
2S	S	96	K3	5	11	85
2S	S	108	K3	6	11	86
2S	S	120	K3	7	11	87
2S	E	-36	F3	6	6	46
2S	E	-30	F3	7	6	47
2S	E	12	L3	0	12	88
2S	E	24	L3	1	12	89
2S	E	36	L3	2	12	90
2S	E	48	L3	3	12	91
2S	E	60	L3	4	12	92
2S	E	72	L3	5	12	93
2S	E	84	L3	6	12	94
2S	E	96	L3	7	12	95
2S	W	-36	F3	1	6	41
2S	W	-30	F3	2	6	42

Shaft	Bar	Station	Connector Label	Connector Channel ID	Terminal Block and Cable ID	DAQ Channel ID
2S	W	12	I3	0	9	64
2S	W	24	I3	1	9	65
2S	W	36	I3	2	9	66
2S	W	48	I3	3	9	67
2S	W	60	I3	4	9	68
2S	W	72	I3	5	9	69
2S	W	84	I3	6	9	70
2S	W	96	I3	7	9	71
2S	NW	24	H3	0	8	56
2S	NW	36	H3	1	8	57
2S	NW	48	H3	2	8	58
2S	NW	60	H3	3	8	59
2S	NW	72	H3	4	8	60
2S	SW	24	K3	0	11	80
2S	SW	36	K3	1	11	81
2S	SW	48	K3	2	11	82
2S	SW	60	K3	3	11	83
2S	SW	72	K3	4	11	84
Blank	Blank	Blank	A3	4	1	4
Blank	Blank	Blank	A3	5	1	5
Blank	Blank	Blank	A3	6	1	6
Blank	Blank	Blank	A3	7	1	7

\* Not connected due to bad Ohmmeter reading



**Table C.3 Identification labels for strain gages in Shafts C and D**

Bar	Station	Connector Label	Connector Channel ID	DAQ Terminal Block #	DAQ Channel ID
N	0	A	0	1	0
N	6	A	1	1	1
N	18	A	2	1	2
N	26	A	3	1	3
N	34	A	4	1	4
N	42	A	5	1	5
N	50	A	6	1	6
N	58	A	7	1	7
N	70	B	0	2	8
N	82	B	1	2	9
N	100	B	2	2	10
N	118	B	3	2	11
N	136	B	4	2	12
S	0	C	0	3	16
S	6	C	1	3	17
S	18	C	2	3	18
S	26	C	3	3	19
S	34	C	4	3	20
S	42	C	5	3	21
S	50	C	6	3	22
S	58	C	7	3	23
S	70	D	0	4	24
S	82	D	1	4	25
S	100	D	2	4	26
S	118	D	3	4	27
S	136	D	4	4	28
E	0	E	0	5	32
E	6	E	1	5	33
E	34	E	2	5	34
E	42	E	3	5	35
E	50	E	4	5	36
W	0	F	0	6	40
W	6	F	1	6	41
W	34	F	2	6	42
W	42	F	3	6	43
W	50	F	4	6	44

## **APPENDIX D**

### **Shaker Connection Details**

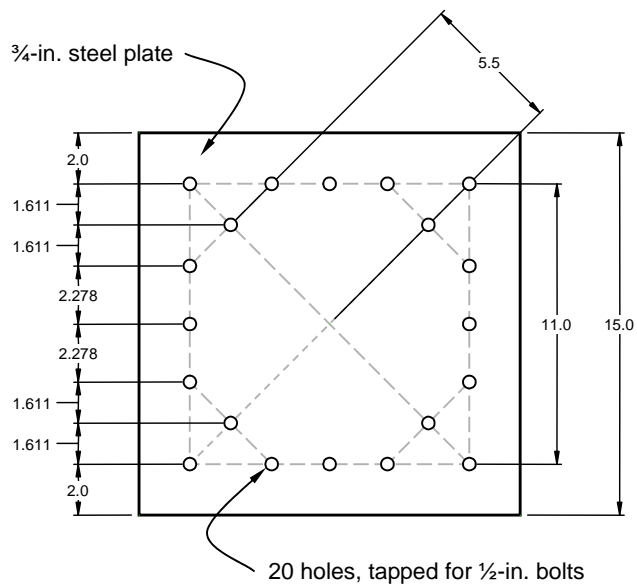
#### **D.1 OVERVIEW**

As discussed in Section 3.5.4, the beams were constructed with an embedded plate to permit the hydraulic shaker from Thumper to be attached directly to the bent. The connection plates were designed such that the shaker could be rotated in 45-degree increments easily in the field.

The dimensions of the embedded plate are given in Figure D.1. The shear studs that were embedded in the concrete are not shown. The plate was fabricated with 20 holes that were tapped to accommodate ½-in. diameter bolts.

The cradle that supported the shaker was attached to the adapter plate with six, ½-in. diameter bolts (Figure D.2). The size and orientation of the holes in the adapter plate were selected to match the dimensions of the cradle. Ten additional holes were drilled in the adapter plate.

The cradle and adapter plate could be rotated relative to the embedded plate to accommodate different alignments of the shaker. A single 1-in. diameter hole was drilled in each of the plates to accommodate a matching one-inch vertical dowel pin that was designed to align the plates at the desired point of rotation. This pin facilitated the relative rotation of the plates and helped to align bolt holes in the two plates during changes in shaker orientation. The axis of the shaker is aligned along the transverse axis of the bridge in Figure D.3, along the longitudinal axis of the bridge in Figure D.4, and 45 degrees from the transverse axis of the bridge in Figure D.5. Eight, ½-in. bolts were used to attach the adapter plate to the embedded plate in each configuration.



Dimensions in inches.

**Figure D.1 Dimensions of embedded plate**

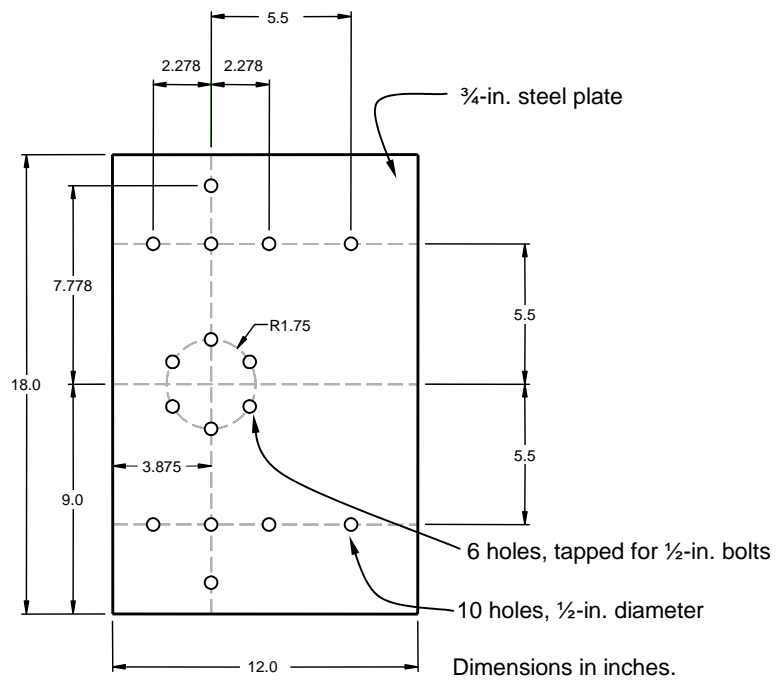
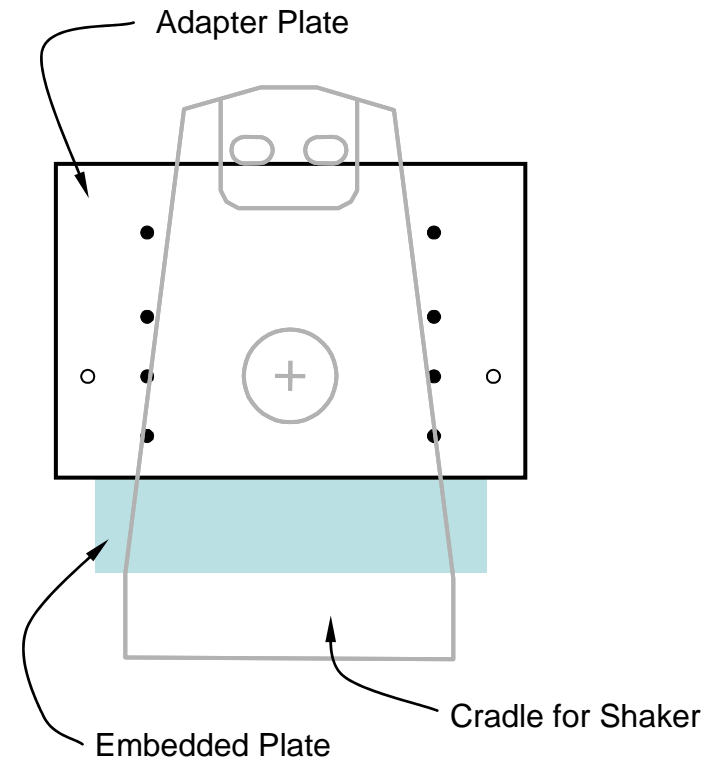
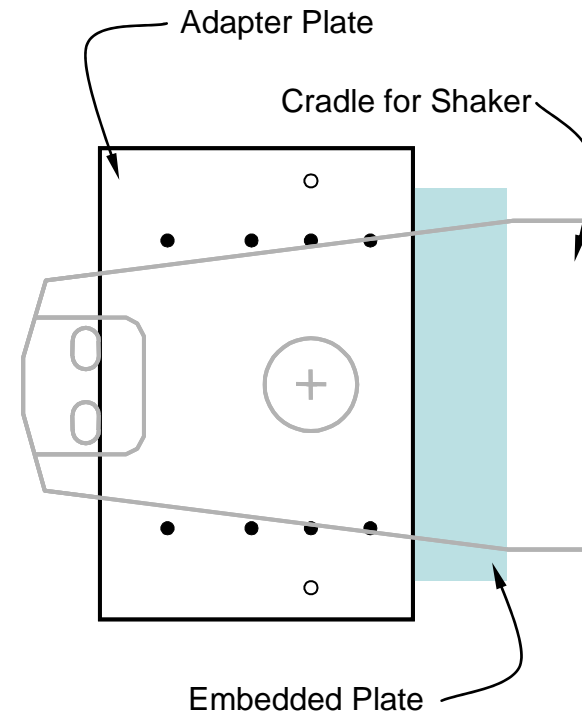


**Figure D.2 Dimensions of adapter plate**



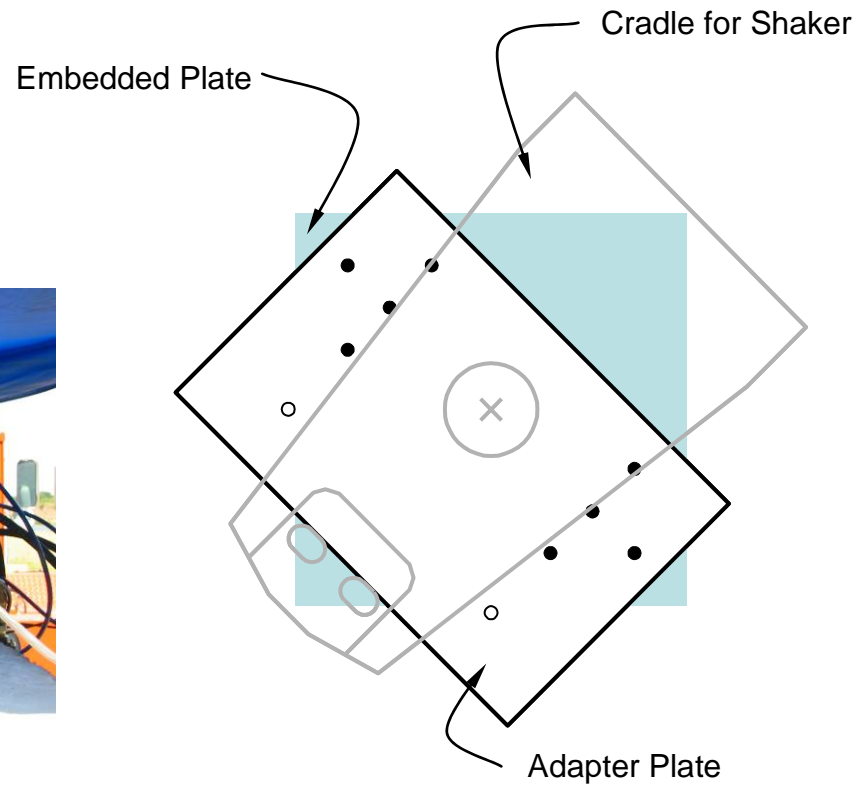
- Bolt connecting adapter plate to embedded plate
- Hole with no bolt

*Figure D.3 Shaker oriented along transverse axis of bridge*



- Bolt connecting adapter plate to embedded plate
- Hole with no bolt

*Figure D.4 Shaker oriented along longitudinal axis of bridge*



- Bolt connecting adapter plate to embedded plate
- Hole with no bolt

*Figure D.5 Shaker oriented 45° from transverse axis of bridge*

## **Appendix E**

### **Design of Threaded Rods**

#### **E.1 DESIGN CALCULATIONS**

The calculations used to design the threaded rods that will be used for the pull-over tests are documented in Table E.1. For purposes of design, lateral loads were assumed to be applied in the lateral direction of the bridge and flexural hinges were assumed to form in the columns of Bent 2 at the ground surface and at the beam-column interface. The resulting shear force in each column represents the maximum force that can be transmitted to the foundation. Therefore, the maximum lateral force that is expected to be applied to the bent is equal to two times the maximum shear in one column.

A 1.0-in. diameter threaded rod was selected to be embedded in the beams. The nominal shear strength provided by the rods, acting on the four shear planes, exceeded the maximum lateral force expected in the bent.. The shear capacity of the rods exceeded the maximum expected force by a factor of 2.8.

As discussed in Chapter 6, flexural hinges are expected to form in the shaft, rather than at the base of the column, when Bent 2 is subjected to lateral loading in the transverse direction of the bridge. Therefore, the maximum lateral force is not expected to exceed 46.4 kip, and the actual capacity to demand ratio will be larger.

**Table E.1** Calculations to check the shear capacity of threaded rods used for pull-over tests.

Description	Calculation	Result
Nominal flexural capacity of column	$M_n$	500 kip-in.
Shear induced by the development of flexural hinges at the top and bottom of the column	$V_c = \frac{2M_n}{L_c}$ $L_c = 36 \text{ in.}$	27.8 kip
Maximum shear in bent	$V_b = 2 \cdot V_c$	55.6 kip
Nominal shear capacity of 1-in. diameter Gr. B7 threaded rod	$R_n = A_b \cdot 0.4 \cdot F_u$ $A_b = 0.79 \text{ in.}^2$ $F_u = 125 \text{ ksi}$	39.3 kip
Shear capacity of rods across four shear planes	$V_r = 4 \cdot R_n$	157 kip
Capacity / Demand Ratio	$\frac{V_r}{V_b}$	2.8



## References

- ACI 318-05, (2005). *Building Code Requirements for Structural Concrete and Commentary*, American Concrete Institute, Farmington Hills, Michigan.
- Agarwal, Puneet, (2005). Personal communication.
- ASTM C 39, (2004). *Standard Test Method for Compressive Strength of Cylindrical Concrete Specimens*, American Society for Testing and Materials, West Conshohocken, Pennsylvania.
- ASTM C 469, (2002). *Standard Test Method for Static Modulus of Elasticity and Poisson's Ratio of Concrete in Compression*, American Society for Testing and Materials, West Conshohocken, PA.
- Chai, Y. H. (2002). "Flexural Strength and Ductility of Extended Pile-Shafts. I: Analytical Model." *Journal of Structural Engineering*. Vol. 128, No. 5, pp. 586-594.
- Computers and Structures, Inc., (2004) *SAP2000 Advanced 8.3.7*. Berkeley, California.
- DeMello, V. (1971). "The Standard Penetration Test—A State of the Art Report," *Fourth PanAmerican Conference on Soil Mechanics and Foundation Engineering*, Vol. 1, p. 1-86
- Ensoft, Inc., (2004). *LPile Plus Version 5.0*. Austin, TX

- Hognestad, E. (1951). "A Study of Combined Bending and Axial Load in Reinforced Concrete Members," Engineering Experiment Station, *Bulletin* 399, University of Illinois, Urbana, 128 pp.
- Isenhower, W. H. (2005). Personal communication.
- Kurtulus, A. and Stokoe, K. H. (2004). Personal communication.
- Kurtulus, A., Lee, J. J., and Stokoe, K. H. (2005). *Summary Report, Site Characterization of Capitol Aggregates Test Site*. 47 pp.
- Malhotra, V.M. and Sivasundaram, V. (1990). "Resonant Frequency Methods," Chapter 6, *Handbook of Nondestructive Testing*, V.M. Malhotra and N.J. Carino, ed., CRC Press, Boca Raton, Florida, pp. 147-168.
- Maps.google.com (2005).
- National Oceanographic and Atmospheric Administration (NOAA), (2005). National Weather Service, Austin and San Antonio, Texas, <http://www.srh.noaa.gov/ewx/html/climate.htm>.
- Nees.utexas.edu, (2005).
- Reese, L. C., Cox, W. R. and, Koop, F. D. (1974), "Analysis of Laterally Loaded Piles in Sand," *Proceedings*, Offshore Technology Conference, Houston, Texas, Vol. II, Paper No. 2080, pp. 473-484
- Reese, L. C., Wang, S. T., Isenhower, W. M., Arrellaga, J. A. (2004) *Computer Program LPile Plus Version 5.0 Technical Manual*. Austin, TX

## VITA

Joshua S. Black was born in Murray, Utah on January 1, 1978 to David J. and Mary W. Black. He graduated from Murray High School in 1996 and attended Utah State University for one year before serving as a missionary for two years in La Paz, Bolivia for the LDS church. Upon returning he resumed his studies and graduated Suma Cum Laude from Utah State University with a degree in Civil Engineering. Prior to pursuing his master's degree at the University of Texas at Austin, he completed internships with Paulsen Construction, a general contractor in the Salt Lake City area, and Shiner Moseley and Associates, a structural and coastal design firm in Corpus Christi, TX.

Permanent Address: 862 W. Germania Ave  
Murray, UT 84123

This thesis was typed by the author.